Regulation of stimulatory dendritic cells through tumor matrix remodeling

By:

Athanasios Papadas

A dissertation submitted in partial fulfillment of the requirements for the degree of

Doctor of Philosophy
(Cellular and Molecular Pathology)

at the
University of Wisconsin-Madison
2021

Date of final oral examination: 5/25/2021

The dissertation is approved by the following members of the Final Oral committee:

Fotis Asimakopoulos, Associate Professor, Medicine, and Clinical Adjunct Associate Professor, Medicine
Christian Capitini (Chair), Associate Professor, Pediatrics
Dustin Deming, Associate Professor, Medicine
Peiman Hematti, Professor, Medicine
Mario Otto, Associate Professor, Pediatrics

TABLE OF CONTENTS

LIST OF FIGURES and TABLES

Abstract:

Immunotherapeutic interventions are effective across a wide range of cancer types, but only a small subset of patients shows clinical response to therapy. Response to immunotherapy has been linked to the presence of a pre-existing ‘’inflamed’’ tumor microenvironment. The contribution of the tumor matrix to the inflamed tumor microenvironment has not been adequately studied. Dendritic cells (DCs) are a heterogeneous population of immune cells that are recognized as key initiators and regulators of T-cell-mediated immunity. Conventional type 1 DCs (cDC1) othwerwise known as Batf3-DC, excel in the activation of cytotoxic lymphocytes including $CD8^+$ T cells (CTLs), as well as innate cells such as NK cells, which are all critical effector cell types in antitumor immunity. Tumor-resident Batf3-lineage dendritic cells (cDC1), although very sparse, are critical for spontaneous anti-tumor responses as well as immunotherapy efficacy. Here we report that versikine, a bioactive proteolytic fragment (matrikine) arising from site-specific N-terminal cleavage of the large matrix proteoglygan versican (VCAN), regulates intratumoral Batf3-DC abundance and function. This observation is consistent with our published reports linking N-terminal VCAN proteolysis with human tumor CD8+ infiltration. Intriguingly, stromal, non-proteolyzed VCAN accumulation is associated with T-cell exclusion, suggesting dichotomous roles between parental VCAN and versikine in T-cell inflammation. To model VCAN proteolysis in the preclinical setting, I use a system of versikine overexpression in tumor cells, showing that versikine localizes in the pericellular matrix, mirroring thus the physiologic site of proteolysis in the human. In this thesis, I demonstrate that versikine modifies the immune milieu of the tumor by boosting Batf3-DC in both solid and hematopoietic tumors. It does not alter tumor-seeding pre-DC differentiation despite robust intratumoral IRF8 induction. Instead, versikine expands and engages an atypical NK subset expressing cytotoxicity receptors, low IFNγ and high GM-CSF, essential for Batf3-DC survival. Versikine elicits a unique co-stimulatory transcriptional program, distinct from TLR-signatures, that promotes antigen presentation *in vitro* and *in vivo*. Moreover, versikine signatures correlate with lung cancer TCGA CD8+ scores. From a translational perspective, versikine synergizes with intratumoral STING agonist therapy and thus, lowers the therapeutic threshold to STING activation in a Batf3-dependent fashion. My results in this Thesis demonstrate tumor T-cell inflammation regulation through matrix remodeling that can be therapeutically exploited.

Acknowledgements:

I would like to extend my most sincere thanks to all of the members of the Asimakopoulos Lab: Gauri Deb, Garrett Arauz, Alex Cicala, Josh Wiesner, Varun Bansal and Dr. Fotis. I would also like to thank my former lab members that I worked with and they helped me to complete my project, Chelsea Hope, Adam Pagenkopf, Evan Flietner and Zachary Morrow. I am deeply indebted to Chelsea for all her help and guidance in the beginning of my scientific career, when she taught me research methodology, various bench techniques including FACS analysis, which was later proven to be one the most important tools in my research project.

I would like also to thank Adam Officer from Dr. Harismendy's lab for his crtitical contributions to the bioinformatics analysis of my project. I am extending also my gratitude to Dr. Gutkind and members of his lab for collaborating with me, providing useful input to my project, and sharing their research equipment.

One of the most crucial contributions in completing my research project was made by Gauri. I would like to express my sincere gratitude to Gauri for her continuous help and support in compiling figures, analyzing data and putting the paper together as I was still running experiments.

Also, my mentee, Alex Cicala cannot go without mention. Alex came in the lab as an undergraduate and he was extremely passionate about learning about tumor immunology and getting actively involved in my research project. He helped me in numerous experiments and assays during those 4 years, contributing maximally to the completion of the story. Also, special mention to my second mentee, Josh Wiesner, for his work on the project, support, humor and friendship. Josh came with the lab to San Diego and his help with unpacking 133 boxes of laboratory stuff was life-saving!

I would like to thank also the members of my PhD committee: Dr. Christian Capitini, Dr. Dustin Deming, Dr. Peiman Hematti and Dr. Mario Otto for their continuous support, mentoring and for having an important role in my scientific training as a young physician-scientist.

Most importantly, there is one person that I will be forever thankful to, Dr. Fotis Asimakopoulos. Fotis not only inspired me to pursue a career as a physician-scientist but he went above and beyond to support me in my decision to pursue a PhD and an academic career in Hematology/Oncology. He will always serve as my inspirational model and I was lucky to have him as my mentor in my early scientific career.

Finally, I would like to thank my family and friends for their encouragement and support and dedicate this thesis to my dad, an ENT professor and my first role model as a young doctor, whom I unfortunately lost suddenly and he didn't have the chance to see my Thesis defense and my Match into residency.

CHAPTER ONE:

Introduction and Background

Structure, isoforms and key inter-molecular interactions

Versican is a chondroitin sulfate (CS) matrix proteoglycan with crucial, non-redundant roles in organ development and disease [1]. In humans it is encoded from a single locus on chromosome 15q14.3 [2]. Its amino-acid sequence is 89% identical between mouse and human [3] highlighting the highly conserved nature of this proteoglycan. The locus encoding versican (*VCAN, CSPG2*) comprises 15 exons, which are arrayed over 90 kb of contiguous genomic DNA. Versican core protein consists of an N-terminal G1 domain, a C-terminal G3 domain and CS chain-binding regions (Fig. 1). The G1 domain is composed of an immunoglobulin (Ig)-like module, followed by two hyaluronan (HA)-binding domains (link modules). The G3 domain of versican consists of two epidermal growth factor (EGF)-like repeats, a carbohydrate recognition (lectin-like, CRD) domain and a complement binding protein (CBP)-like motif [4]. The expression of versican gene is regulated by a promoter that harbors a typical TATA box. Successful cloning of the gene in man, mouse, cow and chicken has revealed the existence of at least four splice variants of versican, which differ in the size of the core protein and the number of glycosaminoglycan (GAG) chains. The central, glucosaminoglycan (GAG)-bearing domain of the versican core protein is coded by two large exons, GAG-α and GAG-β, which can be alternately spliced at exon 7 (which codes for the GAG-α region) and exon 8 (which codes for the GAG-β) region. When both exons 7 and 8 are present and no splicing occurs, versican V0 isoform is formed. When exon 7 is spliced out, versican V1 is generated. When exon 8 is spliced out, versican V2 is formed. When both exons 7 and 8 are spliced out, versican V3 is formed. Since V3 contains no GAG (CS) chains and is solely composed of the G1 and G3 domains, it cannot be considered a proteoglycan, but it is frequently grouped with proteoglycans and characterized as such [1, 5].

Versican is a crucial partner in extracellular matrix (ECM) assembly through key protein-protein or protein-carbohydrate interactions. One of the most studied interactions is between the amino-terminal domain of versican (G1 domain) to HA, mediated through link modules [5]. Versican interacts with diverse ECM components that are important in inflammation, such as TNF-stimulated gene-6 (TSG-6), fibulins and fibrillin, inter-alpha-trypsin inhibitor (IαI), fibronectin, and tenascin-R and -C. Tenascin-R binds to versican at its C-terminal lectin-like domain (CRD)

through protein-protein interactions [6]. Versican binds to fibulin-2 and fibrillin-1 through its C-terminal lectin-like domain in a calcium-dependent manner [7, 8]. Fibulin also may serve as a bridge between versican and fibrillin, forming highly ordered multimolecular structures important in the assembly of elastic fibers [1]. Versican also interacts with fibronectin, as well as collagen type I [9, 10]. Moreover, versican G3 domain can form complexes with fibronectin and vascular endothelial growth factor (VEGF). This complex was found to stimulate endothelial cell adhesion, proliferation and migration. Disrupting the complex through anti-fibronectin antibody reversed G3's enhancing effects on endothelial cell activities [11]. Finally, versican binds to adhesion molecules on the surface of inflammatory leukocytes such as L- and P-selectins through oversulfated sequences [12, 13].

Versican and versican proteolysis in embryonic development

Versican has been implicated in cardiovascular morphogenesis, neural crest cell migration, and skeletal development. The ADAMTS protease family includes several versican-degrading members (versicanases) that are active during remodeling of the embryonic provisional matrix, especially during sculpting of versican-rich tissues [14]. Versican is cleaved at specific peptide bonds by ADAMTS proteases, and the proteolytic products are detectable by neo-epitope antibodies. The developmental significance of versican's proteolytic processing has been elucidated at the sites of the most dramatic shaping of the provisional matrix such as interdigital webs, sculpting, redirection and migration of the secondary palate shelves prior to their midline fusion, resorption of cardiac jelly during myocardial compaction, and remodeling of endocardial cushions to form mature heart valve leaflets. Collectively, several studies have illustrated how proteolysis of versican deposited early in the embryo could be a regulator of morphogenetic processes during subsequent development ([15-18]).

In cardiac development, versican is essential to the formation of endocardial cushion mesenchyme by epithelial-mesenchymal transformation (EMT). Versican proteolytic fragments generated through the actions of ADAMTS proteases can be detected in the cardiac cushions [19]. Later in development, endocardial cushions are rapidly remodeled to achieve their mature structure, and cleaved versican is broadly distributed around cushion mesenchyme cells. Congenital valve anomalies associated with accumulation of versican were seen in both *Adamts9*$^{+/-}$ mice

and *Adamts5*$^{-/-}$ mice and were attributed mostly to subtle developmental alterations in extracellular matrix remodeling or defects in adult homeostasis [15, 20].

Versican proteolysis by ADAMTS9 in vascular endothelium and by ADAMTS20 in palate mesenchyme drives palatal shelf sculpting and extension. Co-operation of ADAMTS9 and ADAMTS20 contributes to secondary palate closure [16]. Reduced sculpting of the shelves and decreased growth were accompanied by accumulation of ECM and reduced cell density, with decreased cell proliferation in palate mesenchyme of the *Adamts9*$^{+/-}$ *and Adamts20*$^{bt/bt}$ mutant mice. Moreover, the palates of these embryos showed a clear reduction of processed versican as evident from reduced anti-DPEAAE staining (a neo-epitope generated by cleavage of V1-versican) [16]. *Vcan* haploinsufficiency in the *Adamts20*$^{bt/bt}$, background also led to cleft palate, demonstrating that versican was a necessary partner of ADAMTS proteases during palate closure, possibly by providing a bioactive fragment, versikine [16]

Versikine, a bioactive N-terminal fragment generated by V1-versican cleavage, is implicated in induction of apoptosis in the context of web regression. Specifically, when affigel beads were soaked in conditioned medium from HEK293 cells stably overexpressing versikine, they could induce apoptosis in ADAMTS-deficient interdigital tissues [18]. Thus, versican itself and its proteolytic derivative are essential for web regression.

Versican in tissue inflammation and immunity

Versican is a major component of the inflammatory response cascade. Its production is highly regulated by inflammatory cytokine networks and in turn, regulates downstream inflammatory mediators to amplify the response [21]. Upon extravasation in the subendothelium, leukocytes encounter ECM structures enriched in versican and HA that act as scaffold for leukocytes having an impact on their cell adhesion and subsequent retention and activation [22]. Versican interacts with receptors on the surface of leukocytes such as P and L selectins and then provides intrinsic signals that influence immune and inflammatory phenotypes [4, 12, 13, 23]. Once bound to the versican-containing ECM, leukocytes degrade the ECM to generate pro-inflammatory fragments, mostly derived from laminin, elastin and IV collagen that further drive the inflammatory response by increasing monocyte/macrophage-dependent secretion of proteases and pro-inflammatory cytokines [24-27]. Versican, which binds to HA, can also bind to CD44 via chondroitin sulfate (CS) GAGs [13], suggesting that both versican and HA may strengthen CD44-dependent

interactions and subsequent CD44-dependent signaling in inflammatory cells. On the other hand, versican binding to HA may interfere with the binding of HA to CD44 on immune cells, such as T lymphocytes [28] and attenuate the immune response. Versican proteolysis can also drive new blood vessel formation as part of inflammatory events associated with tissue repair. For instance injection of an adenoviral vector expressing $VEGF_{164}$ into the skin induces a robust angiogenic response by increasing ADAMTS-1 and versican's proteolytic fragment, versikine [29].

Versican appears to have a role in monocyte adhesion. ECMs that did not support monocyte adhesion were deficient in versican but enriched in HA. In support of this notion, treating a monocyte-attractant ECM with an antibody against the N-terminal region of versican before adding monocytes, blocked monocyte adhesion to that ECM [30]. Versican also controls inflammatory cytokine release by myeloid cells. Versican acts as a danger-associated molecular pattern (DAMP) molecule that interacts with toll-like receptors (TLRs), such as TLR2 on alveolar macrophages, to promote production of inflammatory cytokines, including tumor necrosis factor-α (TNFα), IL-6, and other pro-inflammatory cytokines [31-34].

A major source of versican production in the inflammatory milieu is macrophages. Versican gene is differentially expressed in M1 macrophages, as opposed to M2 macrophages. Matrix metalloproteinases (MMP) degrade ECM proteins [35-37], however ECM degradation is neither the sole, nor predominant function of these enzymes. Versican produced by macrophages can form complexes with MMPs [38], such as MMP-9, implying possible roles for versican in controlling the activity of matrix-degrading enzymes. Such activity suggests that versican could assist myeloid cells in shaping their own microenvironment [22]. Versican can also alter the inflammatory milieu through chemokine regulation. Versican expression is elevated in CD14+ monocytes isolated from patients with systemic sclerosis and this elevated expression is accompanied by increased expression of CCL2 [39]. Earlier studies had also shown that CCL2 binds to versican and impacts inflammation in a model of neuronal inflammation hyperalgesia [40]. In the setting of lung infection, versican and hyaluronan are increased in the lung during acute inflammation associated with *E. coli* pneumonia. Bacterial activation of TLR4 led to synthesis of versican which can itself interact with TLR4 to further modulate the inflammatory response [41].

Versican is also a crucial mediator of chronic inflammation. Versican accumulates in chronic lung diseases that involve persistent inflammation such as pulmonary fibrosis, acute respiratory distress

syndrome, asthma and chronic obstructive pulmonary disease [42-45]. Versican, which is mainly secreted by fibroblasts throughout the airway tree, contributes to airway remodeling in asthma, leading to to persistent airway obstruction and subsequent decline in lung function [46]. Altered deposition of proteoglycan in the asthmatic lung seems to vary between asthma phenotypes and severities [47, 48]. Interestingly, fibroblasts isolated from bronchial biopsies from asthmatic patients with the greatest degree of hyperresponsiveness produced larger amounts of versican [49]. Patients with fatal asthma had increased versican content in the internal area of large and small airways compared with controls [50]. Versican is also implicated in chronic obstructive pulmonary disease (COPD), a chronic lung condition characterized by loss of elastic fibers from small airways and alveolar walls. Fibroblasts in distal airways from COPD patients bear modifications in proteoglycan production that may contribute to disease development: there is an imbalance with a higher rate of versican production/accumulation compared to degradation [51]. Versican in the alveolar wall is also negatively correlated to elastin and elastin-binding protein (EBP), a molecular chaperone important in processing of elastin [52]. In versican-rich microenvironment, new formation of elastic fibers is hampered. The association between elastic fibers loss and accumulation of versican suggests that modulation of versican influences elastic fiber deposition [53, 54].

In a seminal study by the Stambas group, versican was implicated in regulation of antigen-specific, adaptive immunity. Accumulation of versican in *Adamts5*-knockout mice, which lack ADAMTS5 versicanase, causes impaired influenza virus clearance and prevents CD8+ T cell egress, leading to compromised anti-viral immunity. However, when *Adamts5*$^{-/-}$*Vcan*$^{+/hdf}$ (versican-haploinsufficient) mice were infected with influenza virus, T cell function was restored. The authors showed that V0/V1 versican accumulation impedes migration of CD8+ T cells from draining lymph nodes to the periphery, which is critically important for the establishment of full effector function and eventual clearance of the viral pathogen [55].

Versican in cancer

Versican is of central relevance to several hallmarks of cancer [56] and plays important roles in both malignant transformation and tumor progression (Fig. 2). Increased versican expression has been observed in a wide range of malignant tumors and has been associated with both cancer relapse and poor patient outcomes.

A. Source of versican production in the tumor bed

There are at least four major sources of versican production in the tumor bed: the tumor cells, the stromal cells, the tumor-associated myeloid cells and the tumor-infiltrating lymphoid cells. Versican sources are often context-specific and not necessarily mutually exclusive.

In lung cancer, versican's main source of secretion is the tumor cell. Versican secretion by the experimental lung cancer model Lewis lung carcinoma (LLC) is necessary for metastatic spread to lung, liver and adrenal gland, a process that depends on TLR2-mediated myeloid cell activation and TNF-α production [57]. Tumor cells show also an elevated expression of versican in ovarian cancer [58], leiomyosarcoma [59], hepatocellular carcinoma [60], colon carcinoma [61], glioma [62] and bladder cancer [63]. Several of these studies find a direct correlation between tumor versican expression and tumor grade.

In other contexts, stromal cells constitute the main source of versican production, such as in breast cancer [64-67], colon cancer [68], pharyngeal cancer [69], ovarian cancer [70] and prostate cancer [71-73]. Stromal versican is often accompanied by increased hyaluronan (HA) in the tumor bed. The increased amounts of versican and associated polysaccharide (HA) expand pericellular matrix volume and as a result distend the ECM [1]. Peritumoral versican expression is induced in stromal cells by factors secreted by carcinoma cells [66, 72, 74]. Versican, which is not expressed in normal breast tissue, gets upregulated with progressive pre-malignancy and frank malignancy [64]. Strong versican expression was also observed in primary pharyngeal tumors whereas in metastatic tumors, stromal versican staining in the metastatic site was found to be significantly more intense compared to the primary tumor [69]. TGF-β has been found to induce strong stromal versican expression in breast cancer [75] as well as other types of cancer [76]. Intriguingly, TGF-β can also induce the production of versican by the tumor cells themselves, e.g., in prostate cancer [77]. In some cancers, such as endometrial and cervical cancers, tumor and stromal cells can both be the source of versican production. The combination of tumor and stromal expression of versican correlates with shortened disease-free survival and overall survival [78].

Myeloid cells are a major source of versican production in the tumor microenvironment in certain cancer types. Studying spontaneous breast cancer murine models, Gao and colleagues showed that a $CD11b^{+}Ly6C^{high}$ monocytic fraction of the myeloid cells (but not the tumor cells or other stromal cells) produces versican that subsequently promotes mesenchymal to epithelial transition and metastasis [79]. Likewise, in breast cancer, versican derived from myeloid cells is crucial for tumor

metastatic potential [80]. Interestingly, co-culture of myeloid cells with bladder carcinoma cells *in vitro* results in upregulation of versican in the myeloid cells, suggesting that the source of versican in cancerous tumors includes myeloid cells associated with the tumor [63]. Finally, in patients with acute myeloid leukemia (AML) post-cord blood stem transplantation, macrophages were the major versican-producing cells in the bone marrow (BM) [81]. Consistent with the latter observation in the hematopoietic context, our group has demonstrated that macrophages are the major source of versican in the bone marrow of patients with multiple myeloma [82].

B. Role of versican in cancer

B. 1. Tumor cell proliferation and self-renewal

Versican is a crucial mediator of tumor cell proliferation and in some cases, proliferation of crucial tumor-accessory components. Versican enhanced proliferation rate of melanoma cells [9]. The G1 domain of versican is thought to stimulate proliferation by destabilizing cell adhesion [83], while the G3 domain mediates proliferation through two EGF-like motifs, which play a role in stimulating cell growth [84-86]. The EGF-motifs were also shown to mediate breast cancer cell self-renewal [87]. Overexpression of the versican G3 domain enhanced breast cancer self-renewal through EGFR/Akt/GSK-3β signaling and conferred enhanced resistance to chemotherapeutic drugs. Of interest, primary tumor tissues of versican G3-overexpressing mice not only showed high levels of 4B6, pEGFR, pAKT, and GSK-3β (S9P), all of which were related with tumor invasiveness, but also expressed high levels of tumor stem cell markers Sox2, Sca-1, and ALDH1 [87]. Finally, siRNA against versican isoform V1 decreased tumor cell proliferation in human glioma cells [76].

Versican also regulates the proliferation of crucial tumor-accessory components. For example, platelet-derived growth factor (PDGF) upregulates versican expression in arterial smooth muscle cells and promotes the expansion of the pericellular ECM, which is required for the proliferation and migration of these cells [88-90].

B. 2. Tumor cell survival and apoptosis

Genetic or epigenetic modifications in tumor apoptotic signaling machinery facilitate tumor cell survival [91]. V1-versican overexpression has been reported to cause either selective apoptotic resistance or selective apoptotic sensitization. This combination of selective apoptotic resistance and sensitivity is often seen in cancer cells. Intriguingly, murine NIH 3T3 fibroblasts

overexpressing V1 versican (V1-cells) were shown to have concurrent high resting levels of p53, which confers apoptotic sensitivity and Mdm2, which is a crucial negative regulator of p53 [92]. Expression of the G1 and G3 domains of versican protects cells from apoptosis induced by death receptor ligands or cytotoxic drugs [93]. The G3 domain of versican interacts also with beta (β1) integrin and protects glioma cells against free radical-induced apoptosis [94]. Furthermore, versican protects cells from oxidative stress-induced apoptosis through an enhancement of cell-matrix interactions and increased cell attachment and expression of beta1 integrin and fibronectin [95]. However, versican has also been implicated in pro-apoptotic signaling. siRNA-mediated versican knockdown prevented G3-modulated cell apoptosis in human breast cancer cell lines. . The somewhat contradictory roles of versican in modulating cancer cell survival and apoptosis, underscores the complexity of apoptosis regulation in tumor development and progression.

B. 3. Tumor angiogenesis

Angiogenesis is the creation of new blood vessels from the branching of pre-existing ones. Tumor neo-angiogenesis provides nascent tumors with adequate oxygen and nutrients. A recent study illustrated the impact of stroma-derived versican in tumor growth and vascularization [96]. The investigators showed that the major source of versican production was the tumor stroma in B16F10 (melanoma) and LLC tumors and compared vasculature density of B16F10 tumors in *Vcan* $^{hdf/+}$ mice (haploinsufficient for versican) and wild-type littermates. A significant reduction of tumor volume, as well as capillary formation in the *Vcan* $^{hdf/+}$ mice at 10 days and 13 days post-tumor inoculation compared to wild-type mice was observed [96]. Thus, genetically-manipulated reduction of versican attenuates tumor angiogenesis by impairing vascular invasion into the tumor core, at the same time as exerting cell-autonomous growth-regulatory effects on tumor cells [96]. In the context of the well-vascularized tumor glioblastoma, versican appears to exert a pro-angiogenic effect. The versican G3 domain enhanced angiogenesis both *in vitro* and *in vivo*. G3-expressing cells and tumors formed by these cells expressed very high levels of fibronectin and VEGF. Furthermore, the G3 domain directly interacted with fibronectin and formed a complex together with VEGF. This complex promoted angiogenesis-associated activities in endothelial cells and its disruption inhibited these processes [97]. Consistent with the observation that G3 domain binds fibronectin, the V2-versican isoform promoted extensive vasculature formation by up-regulating and binding to fibronectin [98]. Silencing fibronectin expression by siRNA abolished V2-versican's effect in enhancing vascular tube-like structure formation [98].

Pericytes also participate in normal and tumoral angiogenesis. Type-2 pericytes in particular have been shown to possess angiogenic potential and play an important role in stabilizing blood vessels in the microvaculature [99]. RT-PCR has demonstrated abundant versican message in cultured pericytes in vitro [100]. Thus, type 2 pericyte-derived versican might participate in new blood vessel formation during tumor angiogenesis.

B. 4. Tumor cell motility and local invasion

Versican is associated with local tumor invasion [101]. Elevated levels of versican in pericellular stroma is an indicator for disease relapse following surgery for clinically localized prostate cancer [71, 102, 103] and breast cancer [66, 104]. Versican has been shown to impede cell adhesion to ECM substratum and this activity is attributed to the G1 domain: for example, versican enhances locomotion and reduces cell adhesion of astrocytoma cells through the binding of its G1 domain to hyaluronan and link protein [83, 105]. More recent studies have demonstrated that purified versican from cultured human prostatic fibroblasts inhibited adhesion of prostate cancer cells to a fibronectin substratum in vitro, highlighting the key anti-adhesive regulatory role of versican in prostate cancer [73]. Moreover, the formation of an HA/versican pericellular matrix promoted prostate cancer motility in Boyden chamber motility assays using fibronectin as a chemoattractant. Thus, prostate cancer cells in vitro have the ability to recruit versican produced by prostatic stromal cells to promote their motility [106]. These findings suggest that the formation of a pericellular sheath in vivo by prostate cancer cells utilizing versican laid down by prostate stromal cells may contribute to the development of locally invasive disease.

Silencing versican by a specific siRNA against isoform V1, but not V3, significantly decreased migration in human glioma cell lines and primary cultures in vitro [76]. Induction of stromal versican expression correlated with higher tumor grade and invasiveness in carcinomas and was associated with tumor progression [107, 108]. Elevated versican expression in the tumor-associated stroma resulted in reduced numbers of intraepithelial CD8-positive T cells and enhanced cancer cell local invasion in cervical cancer [109], whereas increased expression of CD44 and versican was associated with loss of expression of both progesterone receptor (PR) and E-cadherin [110]. Moreover, in vitro silencing of V0/V1 versican caused increased adhesion to type I collagen, laminin and fibronectin. This was coupled with reduced cell migration in both wound healing assays and transwell chamber assays [111].

Ovarian cancer cells have the ability to recruit stromal ECM components such as versican and HA to form a pericellular matrix which in turn promotes ovarian cancer cell motility and invasion. By using modified chemotaxis assays, it was found that treatment with versican in vitro promotes ovarian cancer cell motility and invasion and enhances their migratory potential. However, HA oligomers (6–10 disaccharides) were able to significantly block formation of pericellular matrix by ovarian cells, as well as the increased motility and invasion induced by recombinant versican. Thus, HA oligomers could be a promising adjuvant treatment tool, administered intra-peritoneally together with chemotherapy drugs to ovarian cancer patients following debulking surgery, to inhibit residual ovarian cancer cells from repopulating and invading peritoneal sites [112].

B. 5. Tumor systemic metastasis

Versican accumulation has been associated with tumor metastasis to distant organs. Versican expression was upregulated in patients with clear cell renal carcinoma (ccRCC) and this upregulation was associated with poor prognosis and high rate of metastasis [113]. In a study of eighty-four matched sporadic ccRCC and normal renal tissues, patients with high versican expression had a significantly worse 5-year OS (overall survival) (p-value=0.007) and a higher rate of systemic metastasis than those with low versican expression (p-value= 0.0139). Mechanistically, versican promoted ccRCC cell migration and invasion via MMP7 and CXCR4 [113]. In breast cancer, versican derived from CD11b+ Ly6C^{high} myeloid cells is critical in promoting metastasis to the lung in a TGFβ-dependent manner [79].

Karin and colleagues showed that versican binds TLR2 and its co-receptors TLR6 and CD14 on myeloid cells in a highly metastatic lung cancer model (Lewis Lung carcinoma, LLC). Upon activating TLR2:TLR6 complexes and inducing TNF-α secretion by myeloid cells, versican strongly enhanced LLC metastatic growth. TLR2 was absolutely necessary for metastatic growth, since no metastatic enhancement was seen in WT/TLR2$^{-/-}$ mice [57]. On the other hand, TNF-α is one of the major pro-metastatic factors produced by host myeloid cells. TNF-α can suppress the apoptosis of cancer cells and stimulate their proliferation through NF-κB activation [114]. In addition, by increasing vascular permeability [115], TNF-α can enhance recruitment of leukocytes as well as intravasation and extravasation of cancer cells. Since TLR2 is absolutely necessary for versican to exert its metastasis-enhancing abilities and TNF-α is the product of activated myeloid cells after interacting with versican, either or both of these targets could provide a useful point for anti-metastatic intervention.

B. 6. Interplay between versican and immune cells in the tumor microenvironment (TME)

Dendritic cells (DCs) play a crucial role in the regulation of the balance between CD8+ T cell immunity vs. tolerance to tumor antigens. Cross-priming, a process which DCs activate CD8+ T cells by cross-presenting exogenous antigens, plays a critical role in generating anti-tumor CD8+ T cell immunity [116]. However, DC-mediated cross-presentation of tumor antigens in tumor-bearing hosts often induces T cell tolerance instead of immunity. There is accumulated evidence that the TME modulates tumor-infiltrating DCs and other antigen-presenting cells such as macrophages, leading to impairment of their function in initiating potent anti-tumor immunity and even promotion of tumor progression [117, 118].

Importantly, tumor-derived versican leads to DC dysfunction through TLR2 activation. TLR2 ligation not only stimulated secretion of autocrine IL-10 and IL-6 but also led to sustained elevation of the cell-surface receptors for these cytokines, which decreased the threshold concentration required to activate STAT3. This amplification loop reprogrammed DCs to produce high amounts of IL-10 rather than IL-12 and IL-1β when stimulated with LPS, a classic pro-inflammatory stimulus. Thus versican impeded immunogenic DC activation and conceivably downstream Th and cytotoxic lymphocyte (CTL) differentiation [119, 120]. In multiple myeloma, versican is abundantly expressed and processed in the bone marrow [82]. We have previously proposed a model in which versican activates myeloma-associated monocytes/macrophages through TLR2/6 signaling, thus generating trophic IL-1β and IL-6 induction [82]. The significance of versican pathway for human myeloma is further underscored by two recent reports: the first high-resolution analysis of the human immune microenvironment in MM showing that myeloid-derived versican transcription was very strongly associated with MM progression and loss of protective T cell stem-like (Tcf1+) memory in favor of dysfunctional/ exhausted T effectors [121]; second, the demonstration that immunosuppressive macrophages (expressing versican, ENTPD1 and STAB1) were associated with persistence of minimal residual disease post-autologous stem cell transplant for myeloma, thus promoting relapse [122].

In the setting of mesothelioma, tumor-derived versican promotes tumor progression by shaping a tumor-conducive inflammatory milieu, mainly by blunting macrophage anti-tumor activities [123]. Mice harboring versican-deficient tumors presented fewer tumor/pleural macrophages and neutrophils, and fewer pleural T-regulatory cells, compared to the control animals. Moreover,

macrophages co-cultured with versican-deficient mesothelioma cells were polarized towards M1 anti-tumor phenotype and demonstrated increased tumor cell phagocytic capacity, compared to macrophages co-cultured with control tumor cells [123]. Overall, the critical crosstalk created by versican among different type of immune cells, leads to an immunosuppressive TME that promotes cancer progression and metastasis.

Versican proteolysis and versican-derived matrikines in inflammation and cancer

Regulated proteolysis of versican by ADAMTS proteases at the Glu^{441}-Ala^{442} bond of the V1-isoform is associated with robust CD8+ infiltration in MM BM [124, 125] as well as solid tumors [126]. This proteolytic event is predicted to release a 441-aa long N-terminal fragment, *versikine* **(**Fig. 1 and 3). We previously showed that versikine induces IRF8-dependent interferon-stimulated genes [125]. Versikine promotes IRF8-dependent Batf3-DC [127, 128] generation from Flt3L-mobilized BM *in vitro* [126] and Batf3-DC density *in vivo* (see unpublished data in Chapters Three and Four). Enhanced Batf3-DC at the tumor site could provide a conceptual link between versikine and CD8+ infiltration because Batf3-DC, in addition to their role in cross-presenting tumor antigen for priming CD8+ effectors, orchestrate chemokine networks that enhance intratumoral CD8+ infiltration [116] .

Versican: potential for cancer biomarker discovery

Versican expression correlates with poor prognosis, disease progression, metastasis and drug resistance in cancer. The prognostic role of versican expression is tissue-specific. Versican is considered an independent and adverse prognostic marker in oral squamous cell cancer: high stromal versican expression correlates with both increased risk for disease recurrence and shortened survival this cancer [129]. On the other hand, versican expression in the primary tumor is not an independent prognostic factor in pharyngeal squamous cell carcinoma (PSCC), although versican is more strongly expressed in the stroma of local metastases and in the earlier stages of disease in PSCC [69]. In hepatocellular carcinoma (HCC), versican expression correlates with poor prognosis, increased intratumoral macrophage infiltration, poor tumor differentiation and a higher tumor-grade metastasis (TNM stage) [60, 130]. In colon cancer, versican expression by RT-PCR is significantly up-regulated (3-fold) compared to normal tissues [131]. High stromal versican expression is associated with reduced 5-year survival rates of ovarian cancer patients (44% versus 32%) [132]. Versican is upregulated in chemoresistant ovarian cancer compared to chemosensitive ovarian cancer [133]. In multiple myeloma, we recently presented the first set of data ascribing

prognostic significance to the versican proteolysis immunoregulatory pathway [124]. We observed the somewhat paradoxical association between intense versican proteolysis and high CD8+ T cell infiltration with poor post- autologous stem cell transplant (ASCT) survival. Patients with low versican proteolysis compared to moderate/high versican proteolysis had better 2-year PFS (72% vs. 29%, p=0.018) and 2-year OS (83% vs. 35%, p=0.006) [124]. Thus, versican expression and/or proteolysis detection may generate powerful prognostic and in certain cases predictive (e.g., association of versican proteolysis with CD8+ T cell infiltration), cancer biomarkers [134].

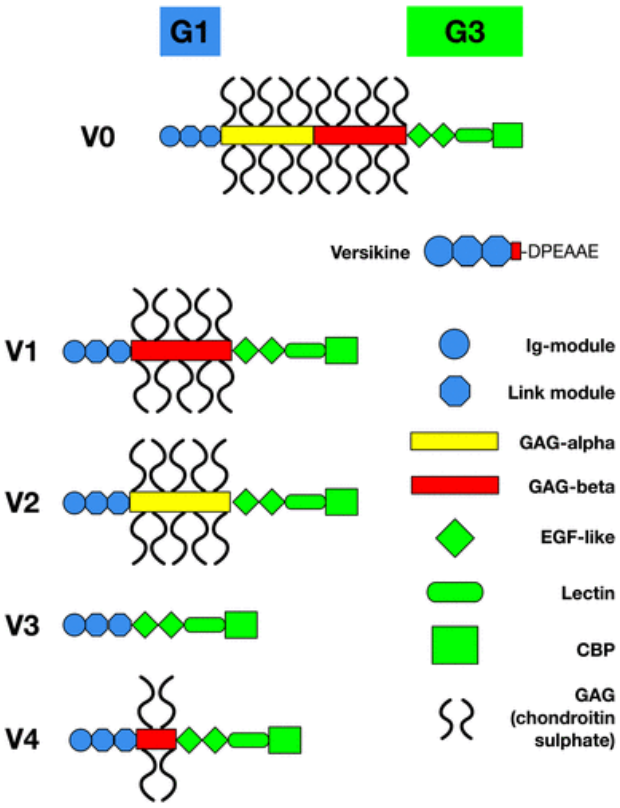

Figure 1. Structure of versican, its isoforms, and its proteolytic product, versikine

Ig immunoglobulin, GAG glycosaminoglycan, EGF epidermal growth factor, CBP complement-binding protein

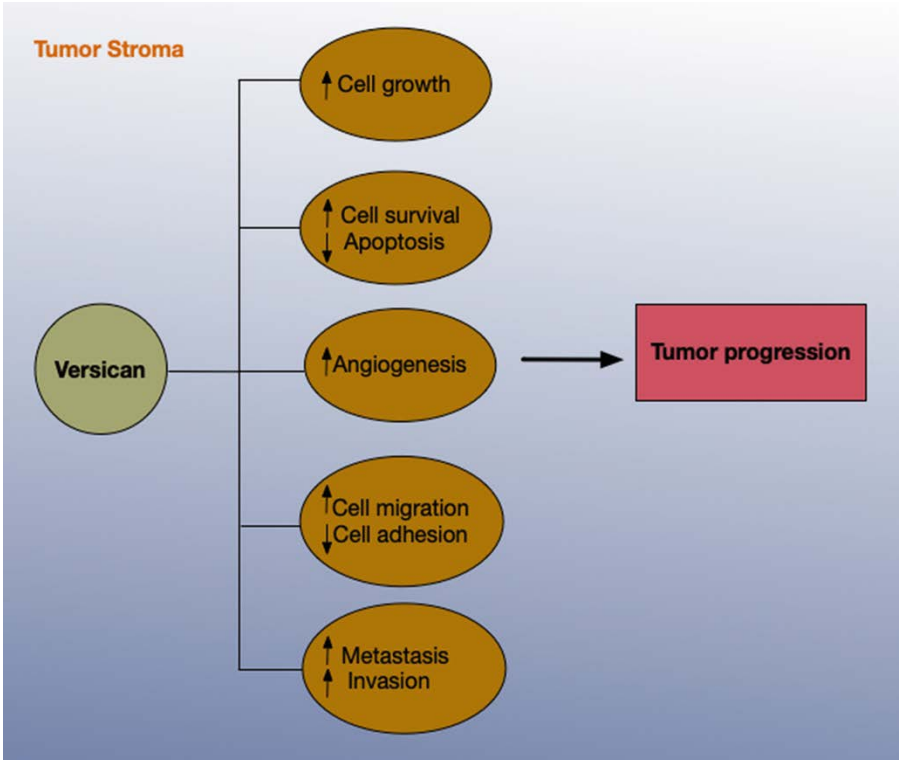

Figure 2. Synopsis of the actions of versican on tumor progression

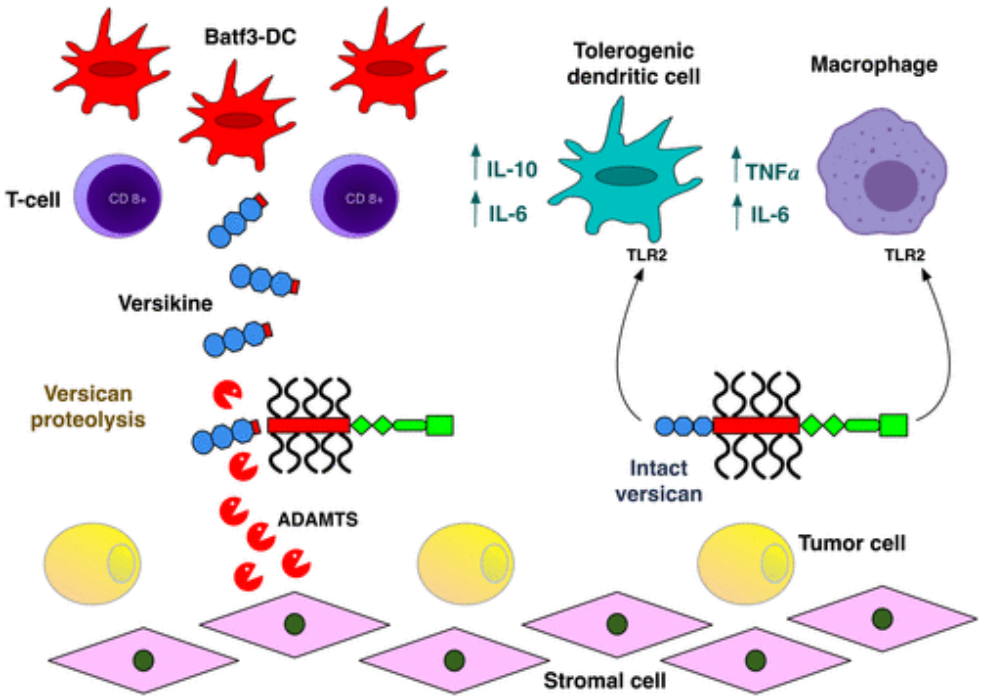

Figure 3. **Concerted actions of versican and its proteolytic product, versikine, in tumor-immune cell cross-talk.** Intact versican acts through TLR2 on antigen-presenting and other tumor-associated myeloid cells to influence their polarization toward protumoral roles. Versican's proteolytic product, versikine, promotes Batf3-DC in the tumor bed and thus could act to mitigate the detrimental effects of parental versican in antitumor immunity. Versican proteolysis is associated with T-cell infiltration in many cancers, both solid and hematopoietic. For simplicity, only the versican V1 isoform is depicted. Abbreviations: ADAMTS, a disintegrin and metalloproteinase with thrombospondin motifs; DC, dendritic cell; IL, interleukin; TNF-α, tumor necrosis factor-a; TLR2, toll-like receptor 2 [135].

CHAPTER TWO:

Versican-derived matrikines boost the generation of CD103+ cDC (Batf3-DC) *in vitro* and promote T-cell infiltration in colorectal cancer

Abstract:

Proteolysis of the tolerogenic matrix proteoglycan versican (VCAN) strongly correlated with CD8+ T-cell infiltration in colorectal cancer, regardless of mismatch-repair status. Tumors displaying active VCAN proteolysis and low total VCAN were associated with robust (10-fold) CD8+ T-cell infiltration. In addition to regulating VCAN levels at the tumor site, VCAN proteolysis results in the generation of bioactive fragments with novel functions (VCAN-derived matrikines). The VCAN-derived matrikine, versikine, enhanced the generation of CD103+CD11c^{hi}MHCII^{hi} conventional dendritic cells (cDC) (homologous to Batf3-DC/ CD8α+ DC/ CD103+ DC/ cDC1 subset/ intratumoral DC2) from Flt3L-mobilized primary bone marrow-derived progenitors, suggesting that VCAN proteolysis may promote differentiation of tumor-seeding DC precursors towards IRF8- and BATF3-expressing cDC. Intratumoral BATF3-dependent DC are critical determinants for T-cell anti-tumor immunity, effector T cell trafficking to the tumor site and response to immunotherapies. Our findings provide a rationale for testing VCAN proteolysis as a predictive and/or prognostic biomarker.

Introduction:

Versican (VCAN) is an extracellular matrix proteoglycan with non-redundant functional roles in diverse biological and cellular processes, ranging from embryonic development to inflammation and cancer. Matrix proteolytic processing generates bioactive fragments (''matrikines'') that activate pathways not triggered by their full-size parent macromolecules [136-138]. VCAN-V1 isoform undergoes ADAMTS-mediated extracellular proteolysis at Glu^{441}-Ala^{442} to release a bioactive 441 aa-long N-terminal fragment, versikine [125]. Although intact versican promotes DC dysfunction through TLR2 mediated IL-6 and IL-10 upregulation [120], versikine does not induce IL-10 and induces IL-6 only weakly [125]. In contrast, versikine induces IRF8-dependent transcripts. Our previous work has demonstrated that versican accumulates in the extracellular matrix of multiple myeloma tumors and in addition versican proteolysis correlates with CD8+ infiltration, as observed in core biopsies obtained from multiple myeloma patients[125]. However, it is unclear whether VCAN-dependent immunoregulatory mechanisms are operative in non-myeloma, or indeed non-hematopoietic, settings. We chose to investigate colorectal cancer because both myeloma and colorectal cancer are driven by chronic inflammatory networks [139] and because better understanding of CRC immunosurveillance mechanisms will likely result in improved outcomes for large patient populations. Here we demonstrate that VCAN proteolysis correlates with CD8+ T-cell infiltration in CRC, regardless of mismatch-repair status. Mechanistically, we propose that the VCAN-derived matrikine, versikine, promotes T-cell infiltration through regulation of Batf3-dependent dendritic cells.

Results:

"VCAN proteolysis-predominant" tumors show robust CD8+ T-cell infiltration. Given the immunosuppressive properties of VCAN and immunostimulatory properties of its proteolytic product, versikine [125], we hypothesized that VCAN proteolysis-predominant tumors are primed for immune infiltration. To determine whether VCAN processing correlated with CD8+ T-cell infiltration, the tissue microarray (TMA) was stained for the effector T-cell marker, CD8, and correlated with the VCAN proteolysis classification. We detected a statistically significant correlation between proteolysis-predominant status and CD8+ T-cell infiltration. CD8+ scores in "proteolysis-predominant" tumors were on average 10-fold higher than "proteolysis-weak" tumors (mean of 22 CD8+ T-cells per HPF versus 2, respectively; Wilcoxon rank sum test, $p<0.001$; Fig. 1A-B). Across tumors with robust CD8+ T-cell infiltration (defined by $\geq$15 CD8+ TILs per HPF), 77% of the CD8+ T-cells were in the epithelial compartment of the tumors.

CD8+ T-cell infiltration was highest in tumors that displayed intense VCAN proteolysis together with low amounts of total VCAN (Fig. 1C). This finding suggests that low VCAN accumulation may not adequately promote T-cell infiltration unless VCAN is actively processed to generate proteolytic fragments. This observation is consistent with our hypothesis that VCAN proteolysis generates bioactive fragments with novel activities. Conversely, in tumors with high total VCAN, CD8+ T-cell infiltration may be impeded through an unfavorable stoichiometry between intact VCAN and VCAN fragments. In summary, these data suggest that VCAN proteolytic fragments are not mere markers of VCAN turnover but are endowed with important novel immunomodulatory activities.

CD8+ T-cell infiltration correlates with VCAN proteolysis regardless of MMR status.

Deficient mismatch repair (dMMR) is observed in 15% of localized CRCs and 3-4% of metastatic cases [140-142]. MLH1 and MSH2 are the most commonly lost MMR proteins. These proteins can be lost secondary to somatic or germline mutations or epigenetic silencing. dMMR status has been associated with an improved prognosis and increased response to immune checkpoint blockade [140-142]. Since dMMR is one of the strongest predictors of CD8+ T-cell infiltration, we next examined the potential for a correlation between VCAN proteolysis and MMR status. Immunohistochemistry (IHC) staining for the MMR proteins MLH1, MSH2, PMS2 and MSH6 was performed to determine MMR status. Consistent with prior reports, CD8+ T-cell infiltration

was increased in dMMR tumors (Wilcoxon rank sum test, $p<0.001$; Fig. 2A). MMR status was then correlated with VCAN and αDPEAAE staining. We observed all potential staining combinations in both pMMR and dMMR cancers (Fig. 2B). A trend towards increased intensity of VCAN staining in pMMR cancers was observed. No significant differences were observed in the proportions of tumors staining for VCAN and αDPEAAE across dMMR cancers (Fig. 2B). The correlation between VCAN proteolysis and CD8+ T-cell infiltration was maintained in both pMMR and dMMR (Fig. 2C). In both pMMR and dMMR, those tumors staining for the VCAN proteolysis-predominant classification had the greatest degree of CD8+ T-cell infiltration (Wilcoxon rank sum tests: pMMR $p=0.006$; dMMR $p=0.03$). Among the VCAN proteolysis-predominant tumors there was a greater degree of CD8+ T cell infiltration in the dMMR cancers compared to pMMR cancers (35 versus 14.8 TILs per HPF, Wilcoxon rank sum test, $p=0.04$).

Versikine promotes the generation of CD103+ cDC (Batf3-DC) from Flt3L-mobilized primary bone marrow cultures.

VCAN proteolysis may impact tumor immune contexture through regulation of intact VCAN bioavailability and/or the generation of novel bioactive fragments (matrikines). We have previously shown that versikine, a matrikine generated through VCAN proteolysis at the Glu^{440}-Ala^{442} bond, activates an IRF8-dependent transcriptional program in macrophage-like cells [125]. IRF8 is a terminal selector for Batf3-DC [variably referred to as cDC1 subset/ CD8α/CD103+ cDC/ intratumoral DC2) [143], a DC subset with crucial roles in T-cell-mediated immunosurveillance [144-151].

Flt3L-mobilized BM cultures have long provided a faithful *ex vivo* model of DC differentiation [152]. Addition of recombinant versikine at the onset of culture (together with Flt3L) consistently and reproducibly promoted expansion of the CD103+$CD11c^{hi}MHCII^{hi}$ DC at both early and late culture timepoints (Fig. 3A, 3B). These cells were $SIRP\alpha^{lo}$, $CD11b^{lo\text{-}int}$ and $SiglecH^{lo}$ confirming their identity as CD103+ conventional DC (cDC). There was no difference in the prevalence of $CD11c^{int}SiglecH^{hi}$ plasmacytoid dendritic cells (pDC) at Day #4, but $CD11c^{int}SiglecH^{hi}$ pDC were reduced in the presence of versikine by Day #9 (Fig. 3C). Addition of the TLR2/6 ligand FSL-1 (Pam2CGDPKHPKSF) together with Flt3L, at the onset of culture, conferred a disadvantage to CD103+ DC development (Fig. 3D). Because intact VCAN is thought to act through TLR2/6 heterodimers [57], these results suggest that versikine may signal through pathways other than

those triggered by intact VCAN. They also suggest that intact VCAN may exert tolerogenic actions by preventing Batf3-DC differentiation. Taken together, our data suggest that tumor-seeding, bone-marrow-derived DC precursors may preferentially develop into immunogenic Batf3-DC in tumor microenvironments undergoing active VCAN proteolysis.

Versikine promotes the expansion of IRF8- and BATF3-expressing DC

Versikine-treated, Flt3L-mobilized cultures displayed increased expression of Irf8 and Batf3 at Day #9 (Fig. 4A). To more precisely map versikine's effects on DC development, we added versikine in Flt3L supplemented cultures either at Day #0 (culture initiation day) or on both Day #0 and Day #6. The latter timepoint was chosen because pre-DC in Flt3L-mobilized cultures have been shown to peak at Day #6 [153]. Versikine added at Day #0 likely acts on pre-DC already present within the explanted bone marrow. Addition of versikine at both timepoints further increased Batf3-DC generation compared to single administration at Day #0 (Fig.4B). These data provide indirect support to the hypothesis that versikine acts on pre-DC to favor Batf3-DC differentiation. Because Batf3-DC are extremely sparse [149] but critical for several aspects of T-cell-mediated immunity, even modest expansions at the tumor site may have profound consequences for T-cell anti-tumor immunity [144]. We wanted to know whether the increase in total Irf8 expression reflected an expansion of Irf8-expressing Batf3-DC. To this end, we used bone marrow cells derived from *Irf8*-EGFP reporter mice. Indeed, versikine-induced CD103+ cDC uniformly expressed the cDC1 (Batf3-DC) terminal selector, Irf8 (Fig. 4C). Moreover, these results suggest that versikine does not induce CD103 expression in an unrelated cell type but results in expansion of *bona fide* cDC1 subset DCs (Batf3-DC).

Discussion:

Immunotherapeutic interventions are showing effectiveness across a wide range of cancer types, but only a subset of patients shows durable clinical responses to therapy. Colorectal cancer remains a challenging problem with significant impact for the general population. Recent advances in immunotherapy of solid tumors previously thought to be non-immunogenic, such as lung cancer, raised hopes that CRC patients might also benefit. However, CRC responses to novel immunotherapy modalities have been modest at best, with the exception of a small number of patients with mismatch repair-deficient CRC. We report here the strong association between VCAN proteolysis and CD8+ T-cell infiltration. At a mechanistic level, proteolysis of intact VCAN can be postulated to produce three alternative consequences, not mutually exclusive: Firstly, proteolysis may regulate the amount and bioavailability of tolerogenic intact VCAN at the tumor site and the resultant degree of DC dysfunction [120]. Secondly, proteolysis may disrupt VCAN's complex interactions with other immunoregulatory matrix components, such as hyaluronan or tenascin C [4]. Thirdly, VCAN proteolysis generates fragments with novel activities. We recently showed that versikine, a bioactive fragment generated through VCAN proteolysis, elicits an IRF8-dependent type-I interferon transcriptional program as well as IL12 but not IL10 production from macrophage-like cells [125]. These actions are predicted to enhance immunogenicity and tumor "sensing" by the immune system. Indeed, in a small myeloma panel, VCAN proteolysis was necessary, albeit not sufficient, for CD8+ T-cell infiltration [125]. In this chapter, we demonstrate that versikine promotes generation of CD103+CD11c^{hi}MHCII^{hi} conventional DC (Batf3-DC) from Flt3L-mobilized BM progenitors. The data support a model in which DC precursors seeding tumor sites undergoing active VCAN proteolysis may preferentially differentiate towards Batf3-DC implicated in T-cell mediated immunosurveillance and response to immunotherapies [144-148, 150, 151]. However, the underlying mechanisms involved in intratumoral DC regulation and its' potential for human translation are unclear.

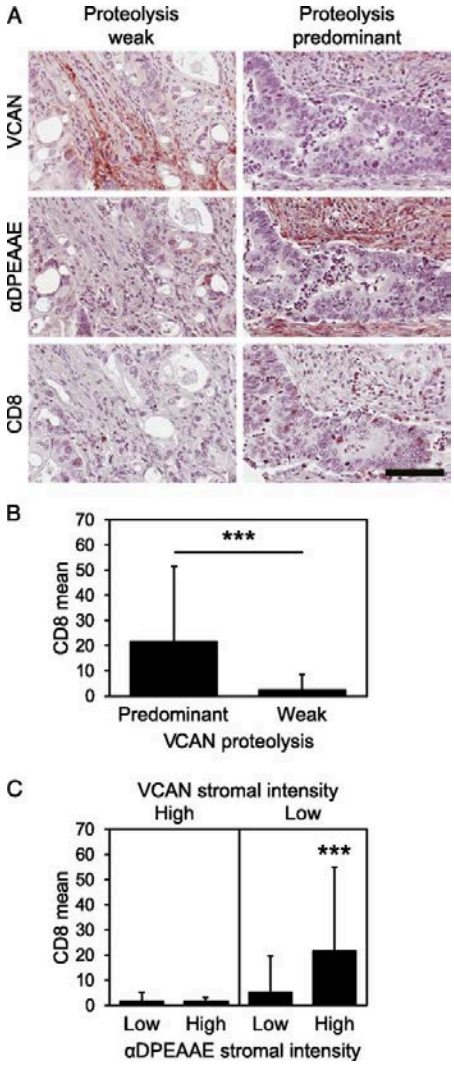

Figure 1. VCAN proteolysis-predominant tumors show robust CD8+ T-cell infiltration

A:Colorectal cancers were classified as "VCAN proteolysis-predominant" if their staining for total VCAN was weak (≤1+) and staining for VCAN proteolysis was strong (αDPEAAE intensity ≥2+). Tumors that did not meet those criteria were classified as "proteolysis-weak" . **B**: Given the immunoregulatory properties of VCAN and the immunostimulatory properties of its proteolytic product, versikine, CD8+ T-cell infiltration was assessed comparing VCAN proteolysis-predominant cancers versus proteolysis-weak cancers. Proteolysis-predominant tumors display 10-fold higher CD8 scores on average than proteolysis-weak tumors (Wilcoxon rank sum test, $p<0.001$; **C**: CD8+ T-cell infiltration was greatest in cancers with intensive VCAN proteolysis and

low total VCAN (Wilcoxon rank sum test, $p<0.001$, C). Scale bar in A = 100µm. (Data generated by Phil Emmerich, Deming lab).

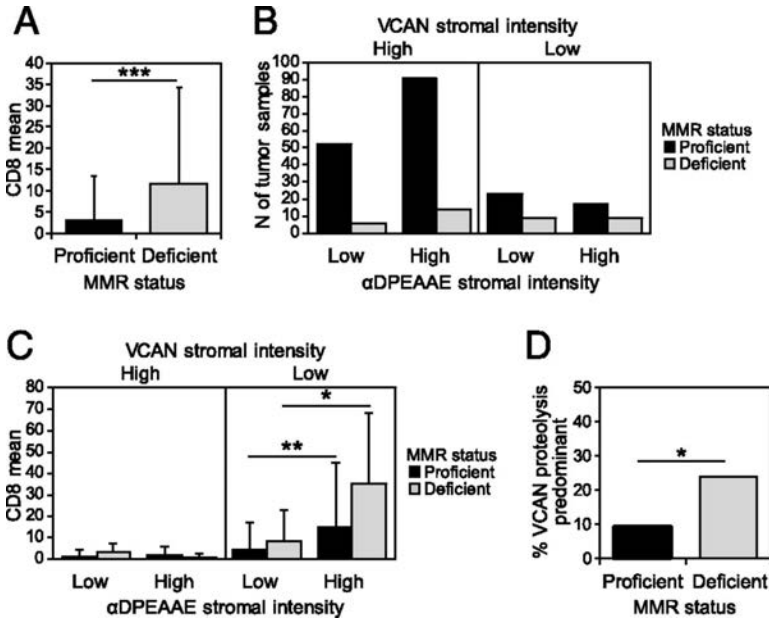

Figure 2. Impact of VCAN proteolysis on CD8+ T-cell infiltration in MMR proficient and deficient cancers Identification of cases within the TMA with MMR deficiency was performed by IHC analysis for MLH1, MSH2, PMS2 and MSH6. Loss of staining for any of these proteins confirmed MMR deficiency. Non-tumor cells were utilized as an internal control. Increased CD8+ T-cell infiltration in dMMR cancers was confirmed in the TMA CRC cores with a mean of 11.7 CD8+ T-cells per HPF in dMMR tumors compared to 3.1 per HPF in pMMR (Wilcoxon rank sum test, $p<0.001$; A). The intensity of staining for both VCAN and αDPEAAE varied across both dMMR and pMMR cancers with a trend toward more intense VCAN stromal staining in pMMR cancers (B). In both pMMR and dMMR cancers, the VCAN proteolysis predominant cancers had the greatest infiltration of CD8+ T-cells (Wilcoxon rank sum test, dMMR $p=0.031$, pMMR $p=0.006$; C). Comparing the VCAN proteolysis-predominant tumors, the dMMR cancers had increased CD8+ T-cell infiltration compared to the pMMR cancers (Wilcoxon rank sum test, $p=0.04$; C). The proportion of VCAN proteolysis predominant tumors varies depending on the MMR status with this being more common in dMMR tumors (Wilcoxon rank sum test, $p=0.01$; D). (Data generated by Phil Emmerich, Deming lab).

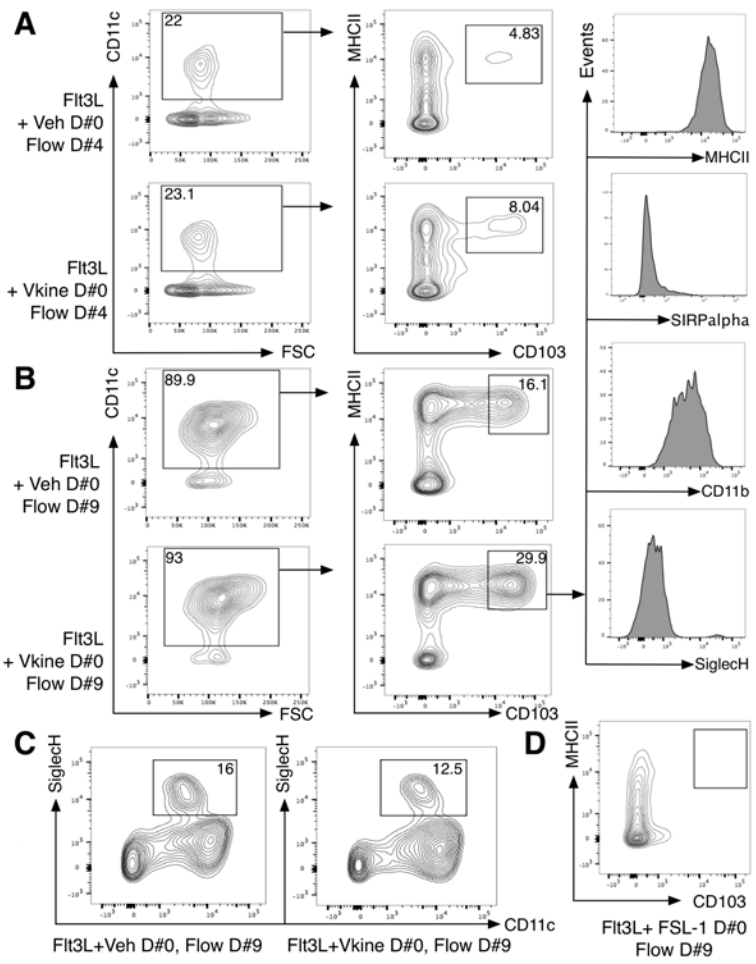

Figure 3. Versikine promotes CD103+CD11c^{hi}MHCII^{hi} DC generation from Flt3L-mobilized bone marrow progenitors

Bone marrow (BM) from C57BL/6J animals was isolated and cultured in the presence of 200 ng/mL Flt3L for 9 days, as previously described [152]. At conclusion of culture, a mixture of DC precursors and mature DC is obtained in this well-characterized system. Addition of versikine (1μM) at Day #0, alongside Flt3L, resulted in reproducible expansion of CD103+CD11c^{hi}MHCII^{hi} DC at both earlier culture timepoints (4 days, **A**) and later culture timepoints (9 days, **B**). CD103+MHCII^{hi} cells were SIRPα^{lo}, CD11b$^{lo\text{-}int}$ and SiglecH^{lo} confirming their identity as CD103+ conventional DC (cDC). Versikine resulted in disadvantage to plasmacytoid DC (pDC) development (CD11c^{int}SiglecH^{hi}) at Day #9 (**C**). Intact VCAN acts through TLR2/6 heterodimers. **D**: Addition of the TLR2/6 ligand, FSL-1, to Flt3L- supplemented cultures results in CD103+MHCII^{hi} differentiation impediment. Veh= vehicle; Vkine= versikine; flow= flow cytometry.

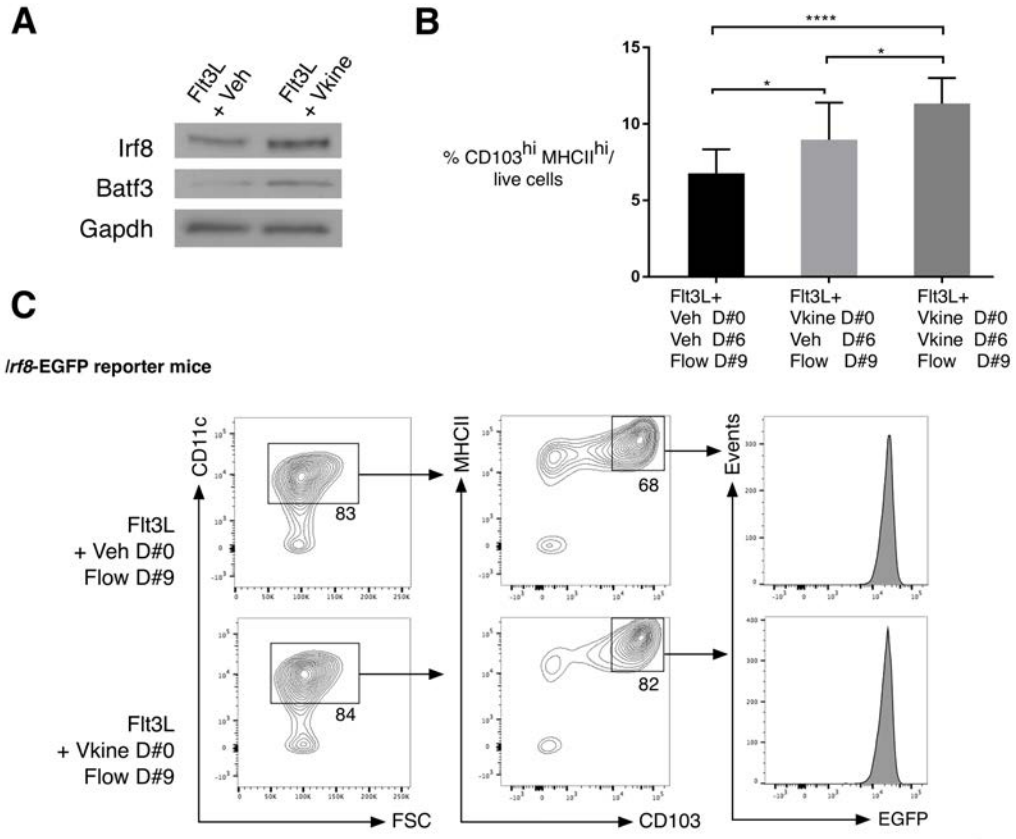

Figure 4. Versikine promotes the expansion of Irf8- and Batf3- expressing DC from Flt3L-mobized bone marrow progenitors

A: Western blot demonstrating that versikine-supplemented Flt3L-mobilized BM cultures demonstrate increased expression of the CD103+ DC terminal selector, Irf8, as well as transcription factor Batf3 at Day #9. **B**: Frequencies of CD103+ DC at Day#0, Day#6 and Day#9 of the 9 day standard Flt3L-supplemented bone marrow cultures with the addition of versikine vs veh. **C**: Versikine-induced, Flt3L- mobilized CD103+ cDC are *bona fide* expressors of the cDC1 (Batf3-DC) terminal selector, *Irf8* (Bone marrow was harvested from *Irf8*-EGFP mice donors) * $p<0.05$; **** $p<0.0001$.Veh= vehicle; Vkine= versikine; flow= flow cytometry.

CHAPTER THREE:

Versikine alters the tumor immune milieu *in vivo*

Abstract:

The impact of tumor matrix remodeling to the generation of an "inflamed" microenvironment that modulates responses to immunotherapy is unclear. We have already demonstrated that versican proteolysis correlates with T-cell infiltration across multiple cancers and that the bioactive cleavage product of versican, versikine, boosts Batf3-DC *in vitro*. Here we show a mechanistic link between the expansion of Batf3-DC and CD8 T- cell recruitment in the tumor bed. Proteolytic N-terminal cleavage product, versikine, which localizes in the pericellular matrix, altered dramatically the immune milieu by boosting Batf3-DC and leading to an expansion of NKp46+ NK1.1+ cells secreting high GM-CSF, an immune modulatory cytokine essential for Batf3-DC survival. However, versikine did not alter tumor-seeding pre-DC differentiation despite robust intratumoral IRF8 induction. Versikine promoted Batf3 DC through NK cells but not through TLR-2. Finally, versikine regulated Batf3-DC activity through non-TLR costimulatory programs.

Introduction:

Efficient innate sensing of tumors and the establishment of an "inflamed" immune microenvironment are essential for productive adaptive anti-tumor immunity and generally associate with improved patient outcomes [154]. Tumor inflammation is also predictive of efficacy of novel immunotherapies [155]. However, the factors regulating innate sensing of cancers are complex and often poorly understood. The crucial role of Batf3-lineage dendritic cells (DC) (hereafter referred to as Batf3-DC, also referred to as cDC1) is undisputed [144, 145, 156-159]. However, the mechanisms underlying homeostatic regulation of Batf3-DC in tumors are only beginning to be understood. Tumor-intrinsic factors, such as mutations controlling Batf3-DC-tropic chemokine networks have been described: for example, activating wnt pathway mutations result in Batf3-DC exclusion through down regulation of CCL3/4 chemokine activity [146]. Tumor-extrinsic factors, such as bi-directional cross-talk between Batf3-DC and NK cells, are increasingly appreciated [160-162]. Batf3-DC support NK activation through mediators such as IL-18 and IL-12 [163]; NK in return support Batf3-DC survival/differentiation through FLT3L [164] and recruitment through XCL1 [165]. Nevertheless, a comprehensive understanding of the essential upstream signals orchestrating and coordinating Batf3-DC/ NK crosstalk has been lacking.

The contribution of tumor matrix and its remodeling to innate sensing of cancer is relatively unexplored [134, 166-170]. The tumor matrisome includes collagens, glycoproteins, and proteoglycans [171], some of them with recognized roles in inflammatory and immune signaling. However, there is significant heterogeneity among tumor and tissue contexts and the core, non-redundant matrix entities that broadly regulate anti-tumor immunity have not been firmly established.

The proteoglycan versican (VCAN) has major and non-redundant roles in embryonic development and tumor formation [14, 22, 172-176]. *Vcan*-null mice are embryonic lethal, demonstrating the crucial role of the proteoglycan in organogenesis of the developing embryo [177]. In the adult, VCAN has been shown to act as an "inflammation amplifier" and as a regulator of aspects of tumor progression, such as cancer cell proliferation, self-renewal, survival/apoptosis, motility/invasion as well as distant metastasis [4, 14, 21, 22, 58, 96, 178-180].

In an early paper by the Karin group, tumor-secreted VCAN was shown to stimulate myeloid inflammatory cells through TLR2 [57]. This axis was shown to be important in the establishment of the pre-metastatic niche [79, 80]. Later, the VCAN-TLR2 pathway was shown to promote tolerogenic polarization of antigen-presenting cells by orchestrating an IL10/IL6 autoregulatory loop [119, 120].

VCAN proteolysis by ADAMTS proteases at Glu^{441}-Ala^{442} bond of the V1 isoform has been associated with CD8+ infiltration in both solid and hematopoietic tissues [82, 126, 181]. This proteolytic event is predicted to release an N-terminal fragment (matrikine), termed *versikine*. Conceptually, VCAN proteolysis could act either through local depletion of non-proteolyzed VCAN (and thus attenuation of non-proteolyzed VCAN signaling, e.g., through TLR2) or through novel actions of versikine. The Apte group demonstrated bioactivity of versikine towards pro-apoptotic activities necessary for tissue sculpting during embryogenesis [18]. Later, our group and others demonstrated that versikine's bioactivity on adult inflammatory cells *in vitro* [125, 182]. We showed that versikine promotes the generation of Batf3-DC from Flt3L-mobilized bone marrow (BM) *in vitro* [126]. However, the precise contribution of versikine to sculpting the immune microenvironment as the result of VCAN proteolysis has remained unknown. This conundrum has been highlighted by our observation that in human colorectal cancer, maximum CD8+ infiltration was associated with the VCAN-proteolysis-predominant (VPP) phenotype: defined as the constellation of intense VCAN proteolysis, non-proteolyzed VCAN substrate depletion *together with* versikine accumulation [126]. These observations suggested that versikine may antagonize the specific activities of non-proteolyzed VCAN.

In this chapter, we delineate a mechanistic framework to understand the complex contribution of versikine, to innate sensing of cancers and the setting of the tumor "immune thermostat".

Results:

Versikine alters tumor immune milieu *in vivo*

ADAMTS versicanases generate versikine in the pericellular matrix (pericellular halo, "glycocalyx") during development [183]. To determine the physiological site of VCAN cleavage in human adult lung cancers, we took avail of a tissue microarray incorporating various non-small cell and small cell histologies. Using an IHC-validated antibody against DPEAAE, an neoepitope generated through VCAN proteolysis at Glu^{441}-Ala^{442} [184](Fig. 1A), we observed frequent pericellular, and to a lesser extent, stromal DPEAAE signal in human lung cancers (Fig. 1A). Across histological subtypes, squamous and small cell lung cancers showed the most intense pericellular staining whereas adenocarcinoma showed staining that, while still consistent, was occasionally more diffuse (Fig. 1A). Examples of negative staining are given in Fig. 1B; staining pattern across 110 human lung cancer cases is summarized in Table 1.

For mechanistic studies, we sought to uncouple versikine from the functional consequences of VCAN depletion. To achieve this aim, we generated LLC cells stably expressing hemagglutinin (HA)-tagged versikine in the WT background . Ectopically expressed versikine was secreted into the pericellular matrix and thus mimicked the localization of endogenously-generated versikine (Fig. 1C). Expression of versikine did not result in grossly visible increase in angiogenesis or hemorrhagic propensity (Fig. 2C). Using an antibody against the HA tag, we determined that ectopically-expressed versikine was readily detectable by western blotting of murine tumors at the expected MW of 75-80 kD (Fig. 1D), whereas background endogenous DPAEEAE proteolysis was weak in both control empty vector- (LLC-EV) and versikine-replete (LLC-Vkine) tumors, when assessed by western blot of total tumor lysates (Fig. 1D). Immunohistochemically as well, endogenous DPEAAE proteolysis was low in both LLC-EV and LLC-Vkine tumors (Fig. 1C). There were no differences in growth rates between LLC-EV and LLC-Vkine tumors (Fig. 2B). We used mass cytometry to analyze immune contexture of LLC-EV vs. LLC-Vkine tumors (Fig. 2D). Ectopic expression of versikine impacted the inflammatory milieu by creating a more immunogenic immune microenvironment.(Fig.2D). In particular, versikine produced an expansion of Batf3-DC, expansion of an innate lymphoid NK1.1+NKp46+ population, a modest increase in intratumoral CD8+ T cells and a depletion of G-MDSC (Fig. 2D). We previously hypothesized an impact of versikine of G-MDSC [125], based on known regulation of this population by versikine's

target, IRF8 [185]. We further delineated DC subsets through 9-color flow cytometry, using the scheme by [150] (Fig 3A). Within the cDC gate, we observed an expansion of Batf3-DC, however there was no change in Mo-DC frequency between LLC-Vkine and LLC-EV tumors (Fig. 3B). To confirm that the observed effects of versikine on Batf3-DC were not peculiar to the non-orthotopic microenvironment of subcutaneous LLC, we injected EV- and versikine-expressing LLC cells intravenously and harvested lungs bearing metastatic nodules at D10 post-analysis, prior to clinical demise (Fig. 3C). We analyzed intratumoral DC through a similar strategy with the minor substitution of CD103 for CD24, with regard to Batf3-DC analysis: we found CD103 to be more consistent in lung tissue. Similar to what we observed in subcutaneous LLC tumors, orthotopic lung LLC-Vkine tumors showed enhanced Batf3-DC frequency (Fig. 3C).

Versikine promoted Batf3-DC in the orthotopic immunocompetent breast Cancer model, 4T1, in the Balb/c background (Fig. 4B). A preponderance of Batf3-DC in the cDC gate was clearly observed in 4T1-Vkine tumors. Growth rates of 4T1 versikine-replete tumors did not differ from those of their EV counterparts (Fig.4A). We earlier reported a role of versikine in altering the bone marrow myeloma microenvironment in human patients [125]. We recently developed the first Ras-driven immunocompetent myeloma model, VQ [186], a model that allows gene transfer into myeloma cells and engraftment into immunocompetent syngeneic recipients in the C57BL6/J background. Versikine-replete myeloma tumors in the VQ myeloma microenvironment also demonstrated enhanced Batf3-DC (Fig. 4C), whereas clinical progression was unaffected by versikine expression alone (Fig. 4D). This result is notable for two reasons: First, it corroborates the notion that versikine's actions are relevant to both solid and liquid tumor contexts. Second, it demonstrates consistent activity of versikine on Batf3-DC homeostasis whether in peripherally-located tumors seeded by hematopoietic cells tumors or within hematopoietic tissue itself. Taken together, the results demonstrate that versikine results in very specific changes in tumor immune contexture in *in vivo* immunocompetent models.

Tumor-seeding pre-DC differentiation is unaffected by versikine despite robust, broad tumor IRF8 induction.

Batf3-DC "signature" transcripts (*Irf8*, *Batf3*, *Cxcl9*, *Cxcl10*) were increased in the bulk transcriptome of versikine-replete (LLC-Vkine) tumors (Fig. 5A). The robust, broad induction of IRF8 is particularly notable because of the central role of this transcription factor in the

development, maintenance and function of lineages that are crucial for adaptive antitumor responses [187] as well as negative regulation of immunosuppressive myeloid cells [185]. Moreover, IRF8 is a "terminal selector" for the Batf3-DC lineage itself [143]. The absolute increase in Batf3-DC caused by versikine could be attributed to enhanced differentiation of tumor seeding pre-DC through an Irf8-mediated mechanism. Indeed, our previous results reported that addition of recombinant versikine to flt3L-mobilized BM cultures, in standard BM DC differentiation assays, promoted generation of Batf3-DC *in vitro* [126]. This observation raised the possibility that versikine may act on immature DC precursors (pre-DC) to promote their differentiation into Batf3-DC soon after seeding the peripheral tumor site. To interrogate this possibility, we sorted CD45.2+ pre-DC precursors from the BM of B16-flt3L- mobilized mice (Fig. 7A). CD45.2+ pre-DC were adoptively-transferred intratumorally into subcutaneous LLC-EV and LLC-Vkine tumors implanted in CD45.1 mice (Fig. 6A). 72 hours post-adoptive transfer, tumors were dissociated and CD45.2+, as well as endogenous CD45.1+, DC fractions were enumerated and characterized by flow cytometry. The CD45.1+ endogenous frequency served as an internal control for the experiment. As expected, CD45.1+ endogenous Batf3-DC were increased in LLC-Vkine tumors (Fig. 6B). By contrast, CD45.2+ Batf3-DC and cDC2 did not differ between LLC-Vkine and -EV controls (Fig. 6C). Thus, versikine does not appear to act by forcing the differentiation of pre-DC that seed peripheral tumor sites.

Versikine elicits a TLR-distinct transcriptional program in Batf3-DC.

The correlation between VPP phenotype and CD8+ infiltration suggested that versikine may impact the activation state of Batf3-DC. Indeed, recombinant versikine elicits IRF8-dependent type-I IFN transcripts in both cultured and primary macrophages, suggesting a role consistent with DC maturation/activation [125]. To explore versikine-induced activation pathways in Batf3-DC, we took avail of Batf3-DC cell model, MutuDC1940 [188]. These cells have been shown to constitute *bona fide* Batf3-DC equivalents, in terms of immunophenotype, transcriptional factor profile, cytokine secretion and cross-presentation capacity [188]. To explore steady-state changes in MutuDC1940 transcriptome in the presence of versikine, we generated stable MutuDC1940-Vkine cell lines through lentiviral transduction (Fig. 8A). Stable expression of versikine did not alter the baseline growth characteristics of MutuDC1940 cells (not shown). MutuDC1940-versikine cell morphology was not significantly different from MutuDC1940-EV counterparts, albeit with slightly more developed dendritic appearance (Fig. 8B).

Versikine elicited a co-stimulatory transcriptional program in MutuDC1940 cells, distinct from transcriptional programs elicited by TLR4 (LPS)- and TLR2- agonist (FSL-1) (Fig. 8C). Notably, TLR2 is the presumed receptor for non-proteolyzed VCAN [120]. Interestingly, combination of versikine+LPS elicited a transcriptional signature distinct from either stimulus alone, whereas versikine+FSL-1 signature was very similar to FSL-1 signature alone (Fig. 8C). The latter observation is consistent with our finding that VCAN proteolysis has minimal impact on CD8+ accumulation in the presence of non-proteolyzed VCAN accumulation [126]. The overlap of transcriptional signatures is further dissected in the Venn diagrams of Figure 8D.

We subsequently dissected the unique signature of versikine in MutuDC1940 cells (Fig. 9A/B). Examination of the genes and pathways triggered by versikine suggests a clear stimulatory role (Fig. 9A/B). Volcano plot of gene expression changes demonstrates several upregulated genes involved in DC maturation (interferon-stimulated genes such as Ifi209 and Ifi204), chemokines (Ccl7, Ccl2, Cxcl9, Cxcl10) and co-stimulatory ligands (CD80, CD40) (Fig. 9B). Downregulated genes include components of TGFβ signaling and wnt signaling, both associated with immunosuppression [156, 189-192].Gene set enrichment analysis (GSEA) of upregulated and down regulated pathways further suggests that versikine promotes immunogenic polarization of Batf3-DC (Fig. 9C). Several of the top hits were confirmed by RT-PCR and at the protein level, by ELISA (Fig.10). One of the top-induced versikine-signature genes, Ccl7, was recently shown to act as a Batf3-DC chemoattractant [193]. Indeed, bulk LLC-Vkine tumors expressed higher Ccl7 message than LLC-EV tumors (Fig. 11A) as did freshly explanted CD11c+ cells from LLC-Vkine tumors (Fig. 11A). Moreover, freshly explanted CD11c from LLC-Vkine tumors expressed higher levels of T-cell attractants CXCL9/10 as well as NK-regulating IL-23 (a subunit), IL-27 (p28 and EBI3 subunits) and IL-15 [194](Fig. 11B). Liposomal delivery of IL-23 mRNA in tumors was recently shown to promote anti-tumor immune responses through Batf3-DC [195].

Versikine promotes expansion of GM-CSF-expressing NK cells.

Versikine resulted in expansion of a NKp46+NK1.1 innate lymphoid subset (Fig. 2D) and triggered NK-activating cytokine expression in DC cells (Fig. 11B). Previous studies implicated NK-derived differentiation/survival mediator Flt3L as well as chemo-attractants XCL1 and CCL5 in Batf3-DC support [164, 165]. Moreover, NK-derived IFNγ was recently shown to induce IRF8, a Batf3-DC "terminal selector" [196]. To determine whether any of these previously reported

mechanisms were utilized by versikine, we flow-sorted NKp46+NK1.1+ cells from LLC-EV and LLC-Vkine tumors. Surprisingly, NKp46+NK1.1 cells form LLC-Vkine tumors were potent producers of GM-CSF and relatively weak producers of IFNγ compared to LLC-EV-derived cells. Expression of XCL1, FLT3L and CCL5 remained unchanged (Fig. 12). Therefore, versikine results in expansion of an atypical NK subset producing low IFNγ despite cytotoxicity receptors, and GM-CSF, an essential survival factor for Batf3-DC both at steady-state and in the tumor microenvironment [197-199].

Versikine promotes Batf3-DC through NK cells but not through TLR2.

We further sought to determine whether versikine requires innate cells to promote Batf3-DC. We used asialo-GM1 antibody for *in vivo* depletion of NK cells, preferentially over tissue-resident ILC1 [200]. The layout of the experiment is presented in Fig. 13A. NK cell depletion was approximately 70% efficient (Supp. Fig. 13B). NK depletion completely abrogated versikine-mediated enhancement of Batf3-DC (Fig.13C and Fig. 13D).

The versikine receptor is unknown but a major contenders, TLR2, merits interrogation, since it has been directly implicated in VCAN signaling pathway. Parental non-proteolyzed VCAN is thought to act through TLR2 [57, 120] but it is unclear if versikine utilizes TLR2. The transcription profiling of Fig. 8C suggests that versikine does not utilize Tlr2, at least in MutuDC1940 cells. To determine whether versikine-mediated Batf3-DC boost requires TLR2 *in vivo*, we carried out the experiment in *Tlr2*-null recipients. Loss of Tlr2 had no impact on versikine-induced Batf3-DC enhancement (Fig. 14A and Fig.14B). Tumor growth rates were similar between WT- and *Tlr2*-null recipients (Fig. 14C). We conclude that versikine promotes intratumoral Batf3-DC independent from Tlr2-mediated signaling.

Discussion:

The role of tumor matrix in regulating key players in adaptive immunity has not received adequate scrutiny. By contrast, the notion that matrix components and their bioactive fragments can act as endogenous "alarmins" has been firmly established [169]. Small leucine rich proteoglycans were among the prototypes of matrix components acting as danger associated molecular patterns (DAMPs) to activate TLR in settings of inflammatory tissue damage [170]. Large matrix proteoglycans have essential roles in tissue sculpting during embryonic development. Of the large matrix proteoglycans, VCAN is perhaps best studied as a regulator and amplifier of inflammation in the adult [173]. VCAN is a chondroitin sulphate large matrix proteoglycan with pleiotropic roles emanating from diverse signaling motifs embedded in its core protein and potentially, carbohydrate side chains. VCAN signaling through TLR2 is relevant to adaptive immunity, particularly in cancer contexts, as it establishes an autoregulatory IL6/IL10-loop that promotes regulatory DC polarization thus contributing to immunosuppression associated with tumor microenvironments [119]. These observations may provide a mechanistic explanation for early reports showing that reduced VCAN correlated with CD8+ infiltration in cervical cancer biopsies [109]. A report from our group that VCAN proteolysis is associated with CD8+ infiltration in colorectal cancer may be taken to indicate, at face value, that proteolysis results in local reduction of intact VCAN and thus, attenuation of VCAN's immunoregulatory roles [126].

Whereas stromal non-proteolyzed VCAN promotes T-cell exclusion, the bioactive fragment versikine promotes Batf3-DC recruitment, survival and activation across tumor types and genetic backgrounds. Therefore, the stoichiometry between non-proteolyzed VCAN and versikine appear to critically influence the levels of immune infiltration. Here we demonstrate that the bioactive N-terminal fragment, versikine alters the tumor immune compartment by boosting the frequency of Batf3-DC. Enhanced Batf3-DC at the tumor site could provide a conceptual link between versikine and CD8+ infiltration because Batf3-DC, in addition to their role in cross-presenting tumor antigen for priming CD8+ effectors, orchestrate chemokine networks that enhance intratumoral CD8+ infiltration. By further studying that link, we show that versikine acts through NK cells and is associated with expansion of an atypical NKp46+ innate lymphoid subset producing GM-CSF, a regulator of Batf3-DC survival in both steady-state and tumor settings [198,

199]. At cell-autonomous level, versikine promoted immunogenic polarization of Batf3-DC through a transcriptional program distinct from TLR4 or TLR2 agonists. In addition to promoting Batf3-DC survival through NK cells, versikine elicited Ccl7, a newly-characterized player in Batf3-DC chemotaxis [193]. Versikine further reinforces the cross-talk between Batf3-DC and NK by upregulating the levels of expression of IL-15 and IL-23, which are main NK cell activators in the tumor bed. Also, versikine promotes CD8+ T-cell inflammation by augmenting the expression of CXCL9 and CXCL10, which lead to CD8+ T cell influx in the tumor. Therefore, versikine helps sculpt an immune microenvironment where Batf3-DC are encouraged to home in, and whose homeostasis is locally supported. Intriguingly, versikine has no impact on the short-term differentiation of tumor-seeding pre-DC precursors, despite the significant intratumoral IRF8 inducation. However, the observed reduction in G-MDSC in versikine replete tumors might be a result of the robust IRF8 induction, since IRF8 inversly controls the MDSC burden in the tumor and particularly the G-MDSC [201]. Finally, versikine does not mediate its activity on increasing the in-vivo density of Batf3-DC through Tlr2, implying thus that it be might involved in a different signaling pathway than the parent macromolecule, VCAN.

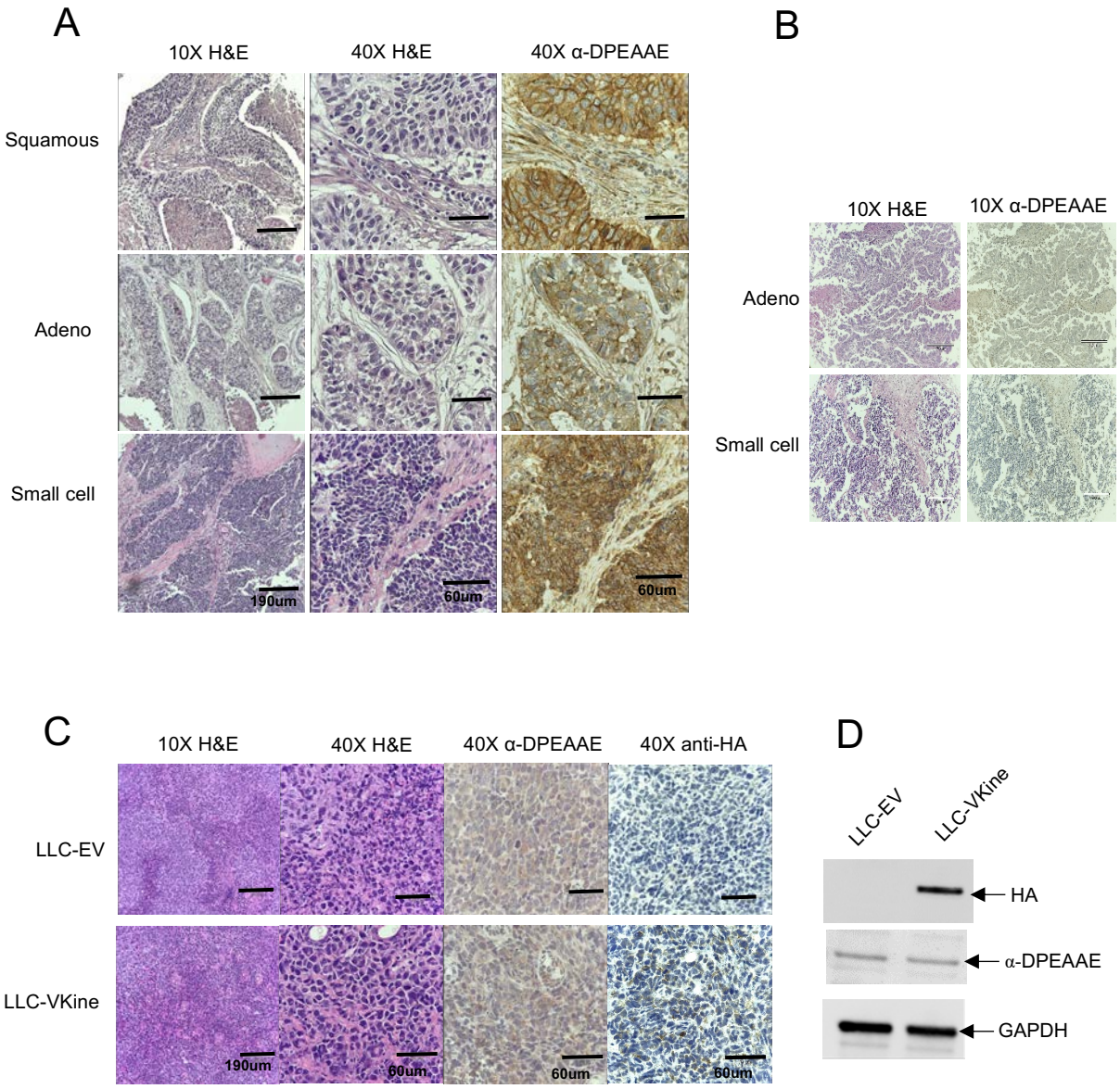

Figure 1. **Detection of VCAN proteolysis and ectopic expression of versikine in human lung cancer and murine LLC cells, respectively**

A: Pericellular and stromal distribution of aDPEAAE immunohistochemical staining in lung cancers of various histologies. DPEAAE constitutes the C-terminus of versikine (DAB, counterstain hematoxylin). **B**: Examples of negative DPEAAE staining in major human lung cancer histologies. **C**: LLC engineered to express HA-tagged versikine (LLC-Vkine) and empty vector controls (LLC-EV). Endogenous DPEAAE proteolysis is low-level and similar between LLC-EV and LLC-Vkine. Anti-HA staining localizes in the pericellular halo in LLC-Vkine tumor cells. **D**: Western blotting demonstrates comparable rates of low-level endogenous DPEAAE

proteolysis between LLC-EV and LLC-Vkine tumors. Anti-HA antibody detects a 75-80kD band in LLC-Vkine tumor lysates, consistent with ectopic versikine.

A

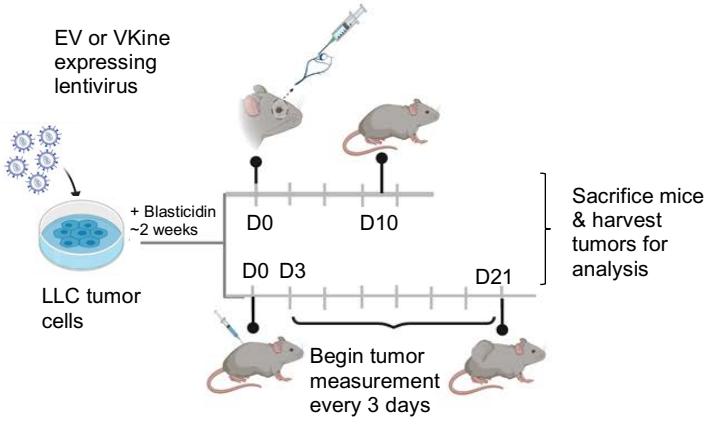
EV or VKine
expressing
lentivirus
+ Blasticidin
~2 weeks
LLC tumor
cells
D0
D10
D0 D3
D21
Sacrifice mice
& harvest
tumors for
analysis
Begin tumor
measurement
every 3 days

B

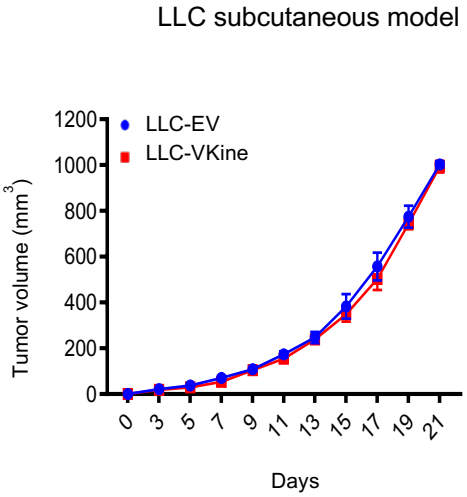
LLC subcutaneous model
LLC-EV
LLC-VKine
Tumor volume (mm3)
1200
1000
800
600
400
200
0
0 3 5 7 9 11 13 15 17 19 21
Days

C

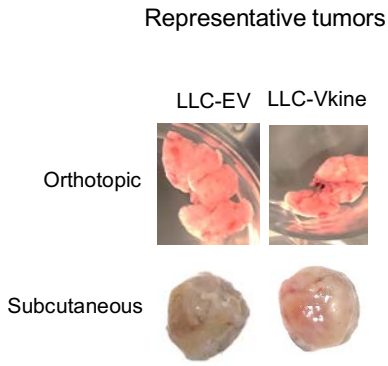

D

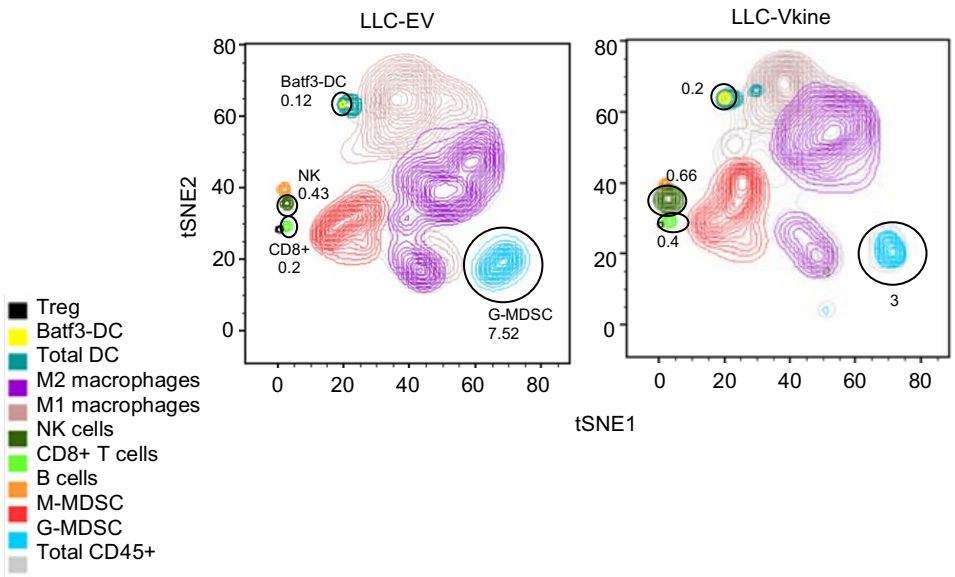

Figure 2. Versikine alters the immune infiltrate contexture (CD45+) in LLC-EV and LLC-Vkine tumors

A: Experimental layout for LLC model. **B**: Growth rates for subcutaneous LLC-EV and LLC-Vkine tumors. **C**: Gross morphology of orthotopic (top) and subcutaneous (bottom) LLC tumors. **D**: Comparison of immune infiltrate contexture (CD45+ cells) in LLC-EV and LLC-Vkine tumors by 31-marker mass cytometry.

A

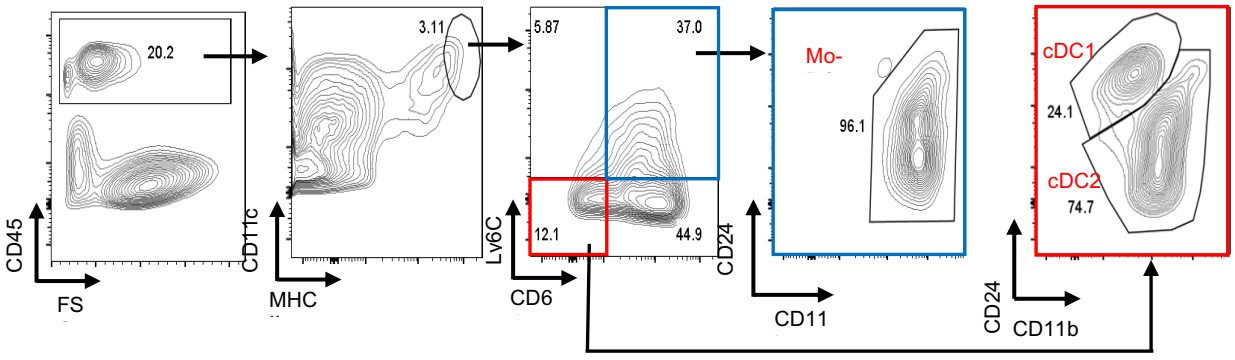

cDC1: live, CD11c^{high} MHCII^{high} Ly6C^{low} CD64^{low} CD24^{high}CD11b^{low}
cDC2: live, CD11c^{high} MHCII^{high} Ly6C^{low} CD64^{low} CD24^{low} CD11b^{high}
Mo-DC:live, CD11c^{high} MHCII^{high} Ly6C^{high}CD64^{high} CD24^{int} CD11b^{high}

B

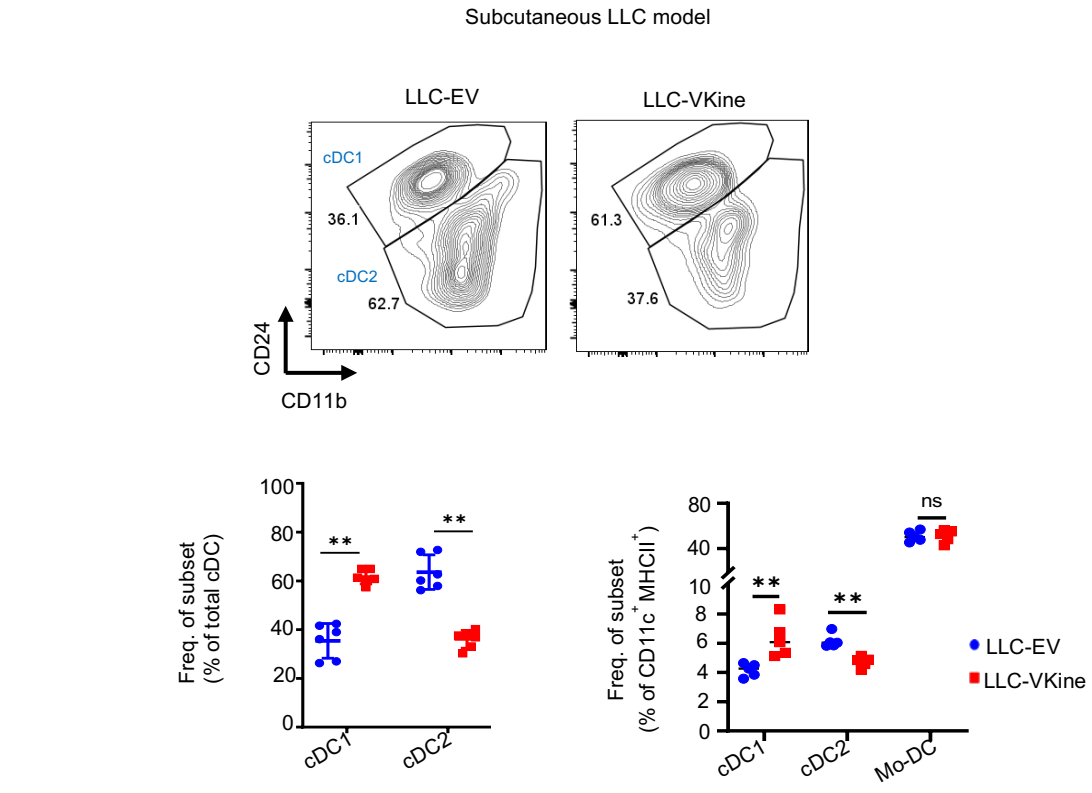

C

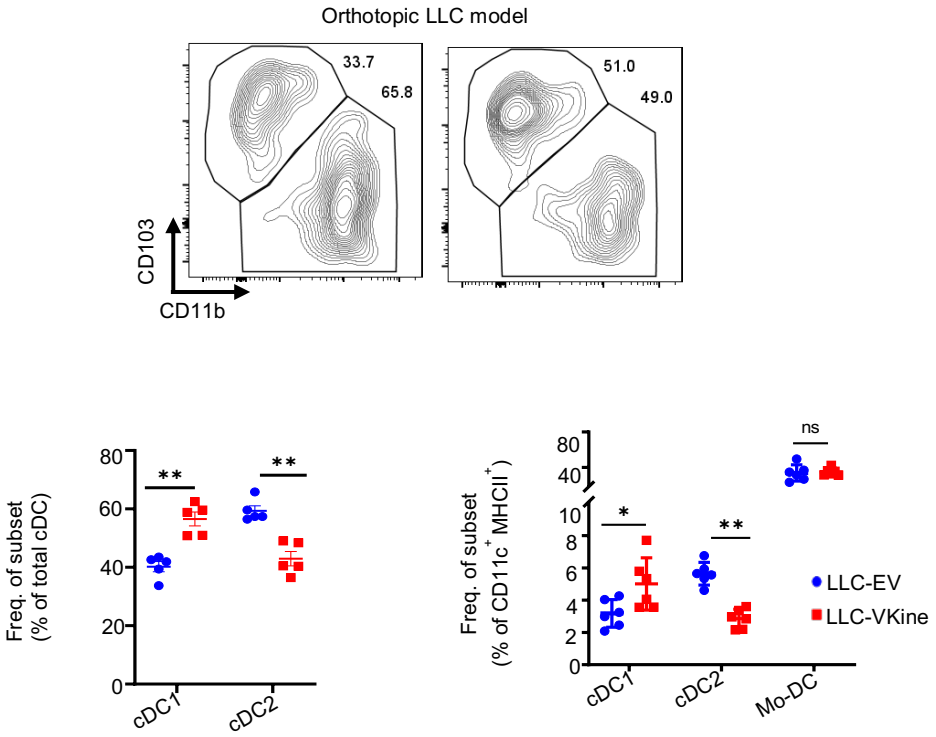

Figure 3. Versikine promotes Bat3-DC in the orthotopic and subcutaneous LLC models

A: Gating strategy to delineate tumor-associated dendritic cells (TADC) per Ginderachter group [150]. **B**: Flow cytometric analysis of cDC subsets between subcutaneous LLC-EV and LLC-Vkine tumors. Gating strategy as delineated above. Summary of cDC frequencies depicted to the right **C**: Flow cytometric analysis of cDC subsets between orthotopic LLC-EV and LLC-Vkine tumors (lung metastases induced by intravenous injection). Summary of cDC frequencies depicted to the right.

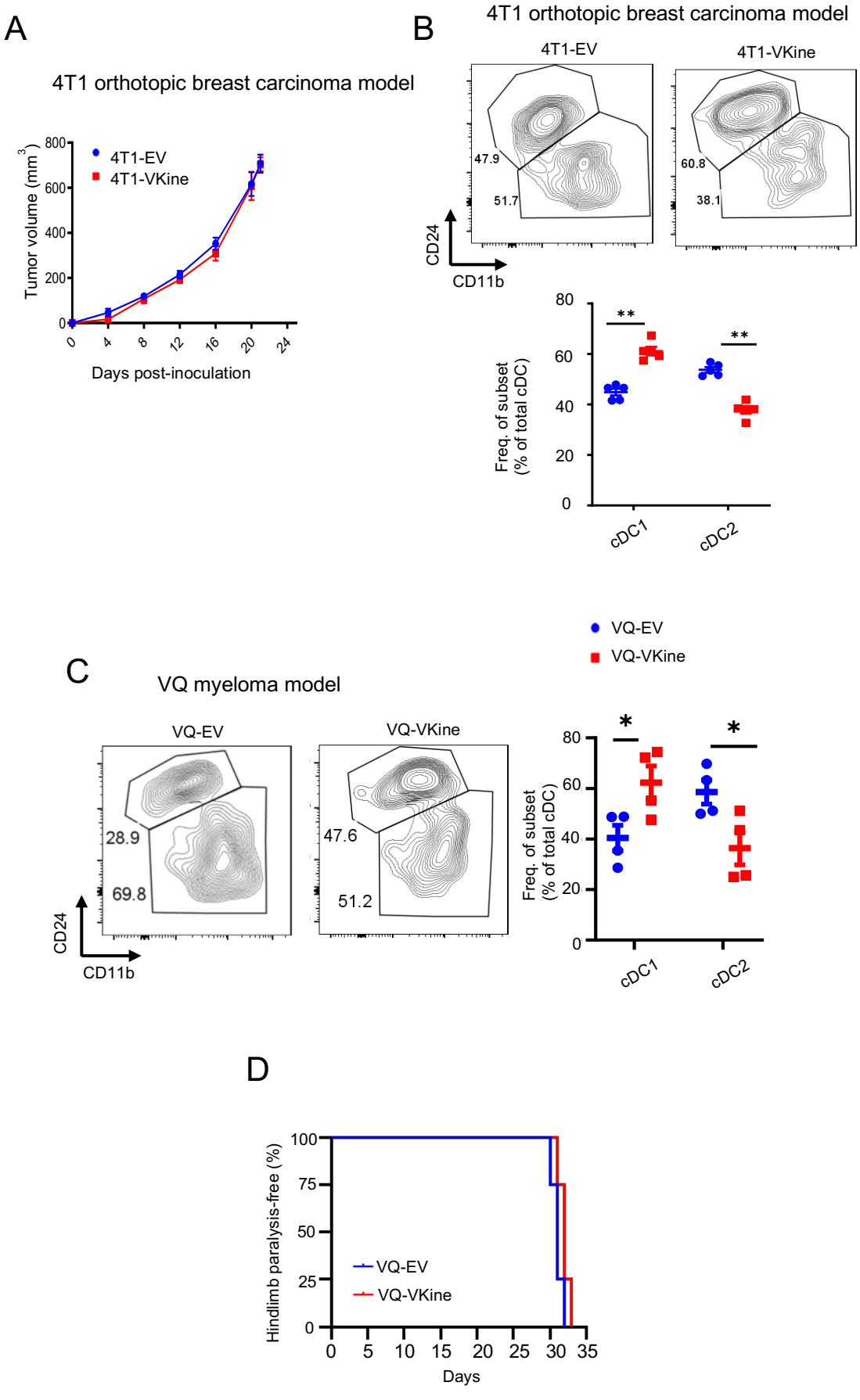
A
4T1 orthotopic breast carcinoma model
Tumor volume (mm3)
4T1-EV
4T1-VKine
Days post-inoculation
B
4T1 orthotopic breast carcinoma model
4T1-EV
4T1-VKine
47.9
51.7
60.8
38.1
CD24
CD11b
Freq. of subset (% of total cDC)
cDC1
cDC2
C
VQ myeloma model
VQ-EV
VQ-VKine
28.9
69.8
47.6
51.2
D
Hindlimb paralysis-free (%)
Days

Figure 4. Versikine promotes Batf3-DC in 4T1 immunocompetent breast carcinoma and Ras-driven VQ multiple myeloma

A: Growth rates of orthotopic 4T1-EV and 4T1-Vkine tumors. **B**: Flow cytometric analysis and cDC subset frequency of 4T1 breast cancer cells orthotopically injected into the cleared fat pad of Balb/c mice, engineered to express empty-vector (4T1-EV) or versikine (4T1-Vkine). **C**: Flow cytometric analysis and cDC subset frequency of VQ myeloma cells engineered to express empty-vector (VQ-EV) or versikine (VQ-Vkine). **D**:Kaplan-Meir curves depicting time-to-hindlimb paralysis (a clinical sequela of myeloma progression) in VQ-EV vs. VQ-Vkine myeloma tumors

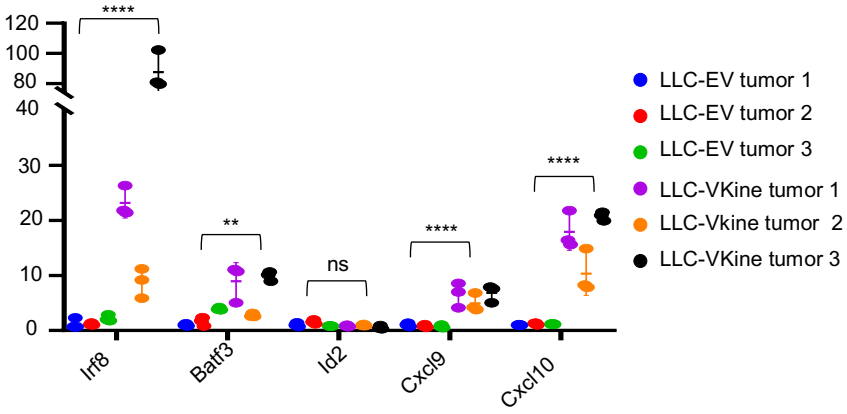

Figure 5. Batf3-DC "signature" transcripts (*Irf8*, *Batf3*, *Cxcl9*, *Cxcl10*) are increased in the bulk transcriptome of versikine-replete (LLC-Vkine) tumors

RT-PCR analysis for Batf3-DC "signature" genes in bulk LLC-EV and LLC-Vkine tumor mRNA.

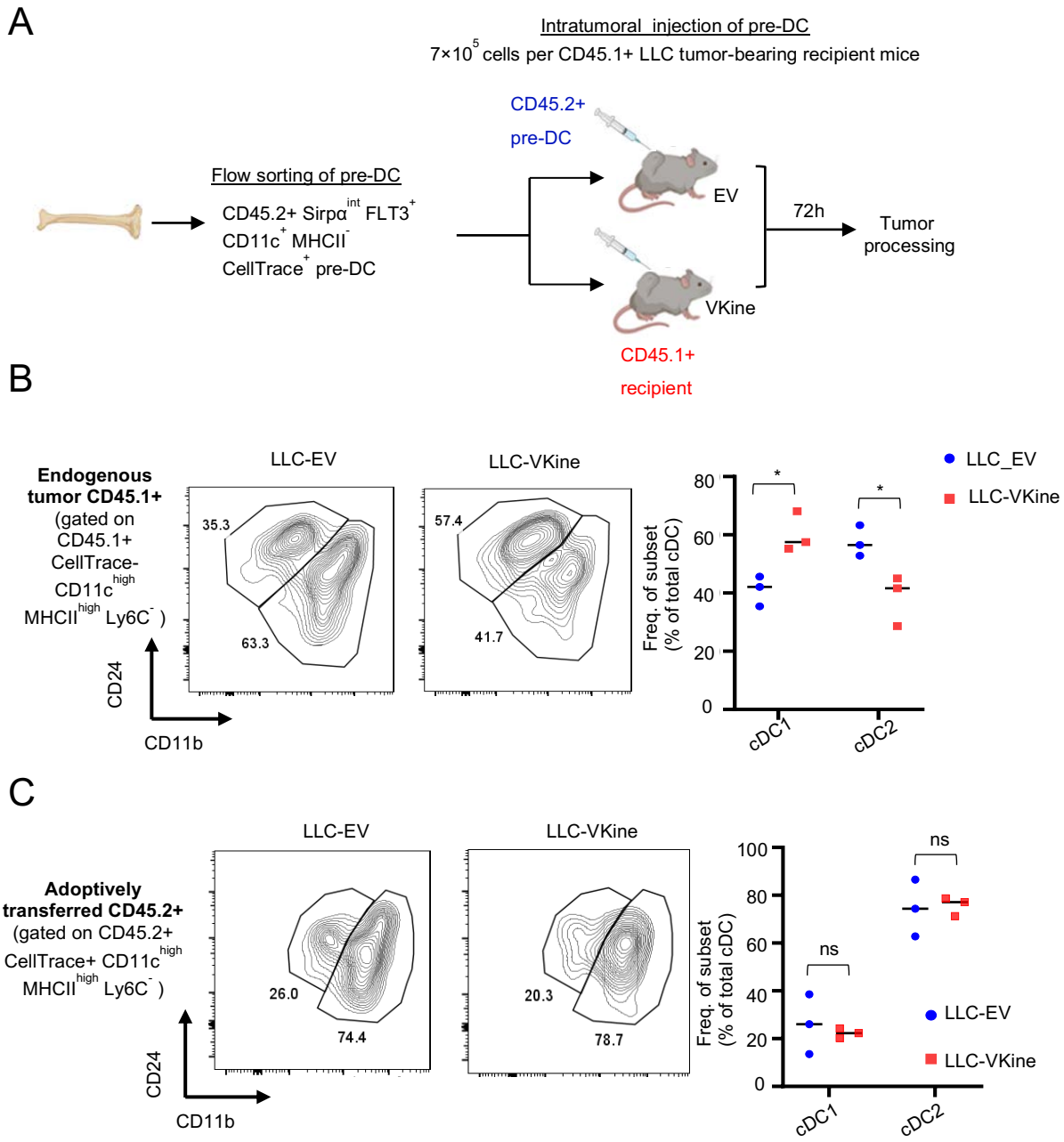

Figure 6. Pre-DC differentiation in versikine-replete tumor microenvironments

A: Schematic layout of the experiment. Pre-DC were harvested from BM of Flt3L-mobilized mice and adoptively transferred into LLC-EV or LLC-Vkine tumors implanted in CD45.1 recipients. **B**: 72 hours post adoptive transfer, CD45.1+ endogenous cDC subsets were analyzed by flow cytometry. CD45.1+ endogenous cDC subset frequencies depicted to the right. **C**: 72 hours post

adoptive transfer, CD45.2+ adoptively transferred cDC were analyzed by flow cytometry. CD45.2+ adoptively-transferred cDC frequencies depicted to the right.

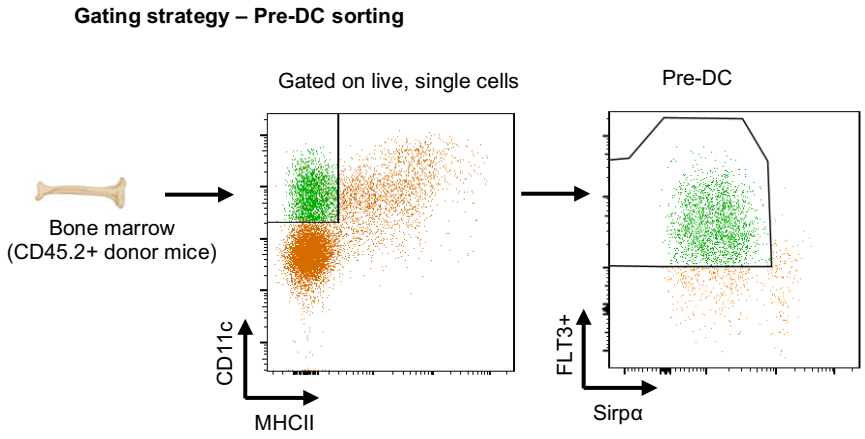

Figure 7. Gating strategy for flow sorting pre-DC from Flt3L-mobilized donors prior to adoptive transfer into CD45.1 recipients

Gating strategy for flow sorting pre-DC from Flt3L-mobilized donors, per the schema of Van Ginderachter [150]. DC were mobilized *in vivo* in donor mice bearing B16-Flt3L-secreting tumor cells.

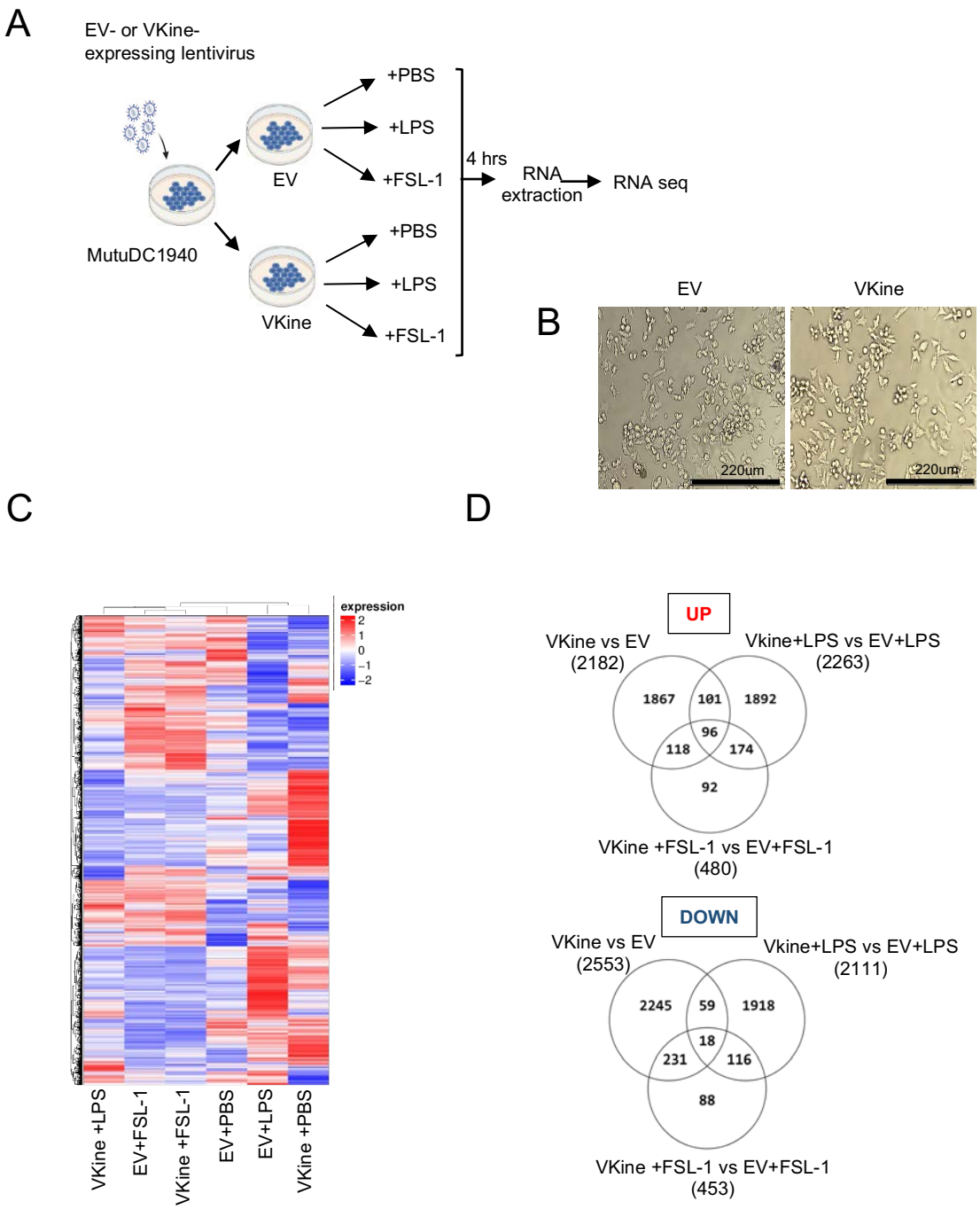

Figure 8. Versikine elicits a TLR-distinct transcriptional program in Batf3-DC

A: A: Schematic layout of experiments. B: Gross morphology of MutuDC1940 cells engineered to express versikine or empty vector (EV). Phase contrast, 10X magnification. C: Hierarchical clustering of transcriptomic profiles by RNAseq analysis of MutuDC1940 cells transduced with EV or versikine (Vkine) and additionally stimulated with TLR4 agonist lipopolysaccharide (LPS)

or TLR2 agonist FSL-1 or vehicle (PBS). D: Venn diagrams of differentially expressed genes between each condition.

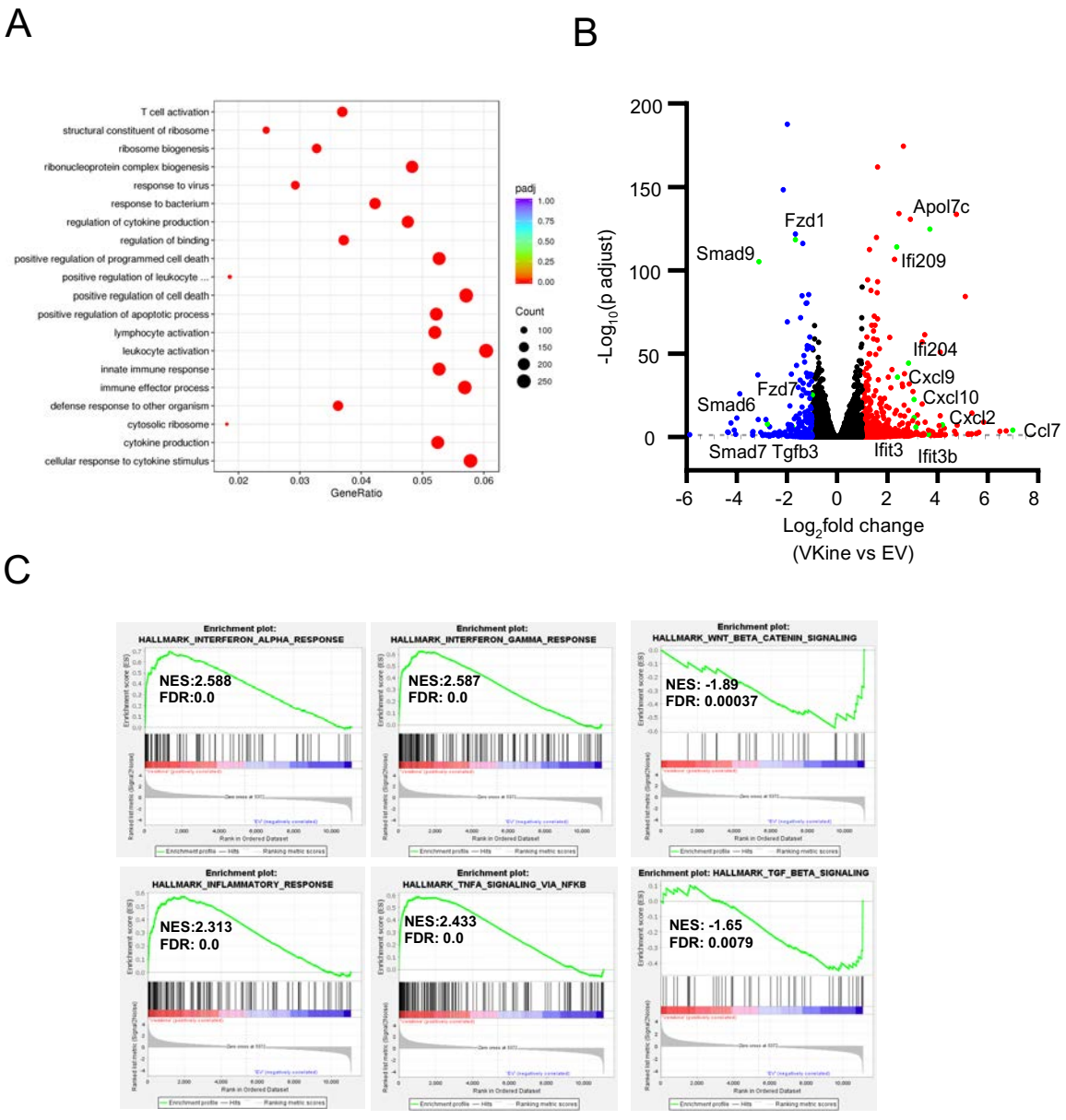

Figure 9. Identification of key differentially expressed genes and pathways in Vkine vs EV

A: Gene ontology pathway analysis of MutuDC1940-Vkine vs. -EV transcriptome. **B:** Volcano plot highlighting key differentially expressed genes in Vkine vs. EV MutuDC1940 cells. **C**: GSEA analysis of significantly upregulated (left, middle column) and downregulated (right column) pathways in MutuDC1940-Vkine vs. -EV cells.

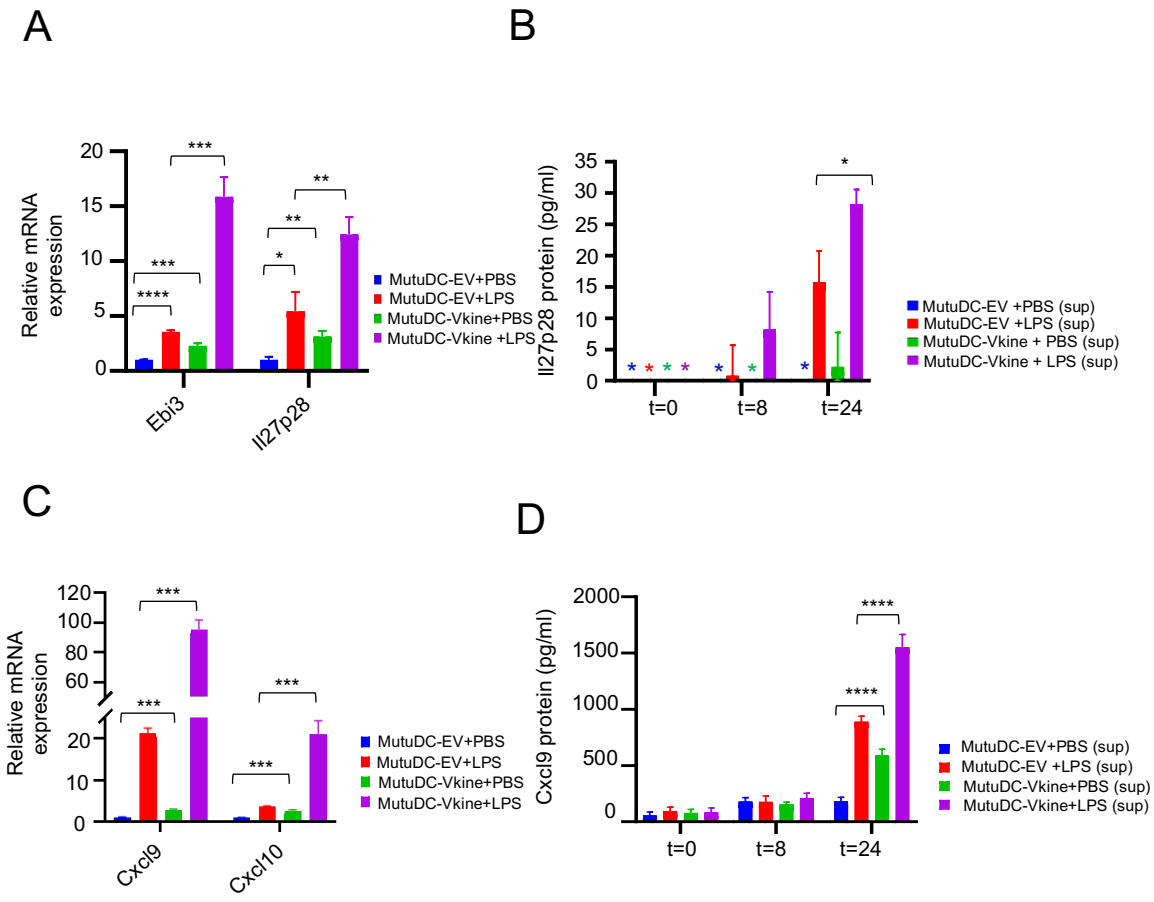

Figure 10. Versikine promotes immunogenic polarization of Batf3-DC

A: RT-PCR for Il27p28 and Ebi3 message in MutuDC1940-EV-vs. -Vkine stimulated with LPS or vehicle (PBS). **B**: ELISA detection of secreted Il27p28 by MutuDC1940-EV- and MutuDC1940-Vkine stimulated with LPS or vehicle (PBS) plotted against time (hours) **C**: RT-PCR of Cxcl9/10 in MutuDC1940-EV vs. MutuDC1940-Vkine stimulated with LPS or vehicle (PBS). **D**: ELISA detection of secreted Cxcl9 by MutuDC1940-EV- and MutuDC1940-Vkine stimulated with LPS or vehicle (PBS) plotted against time (hours).

A

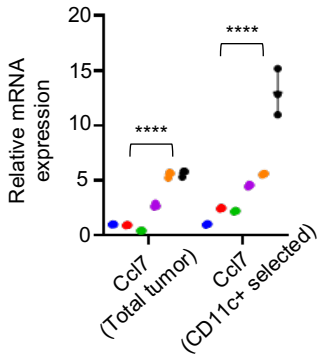

B

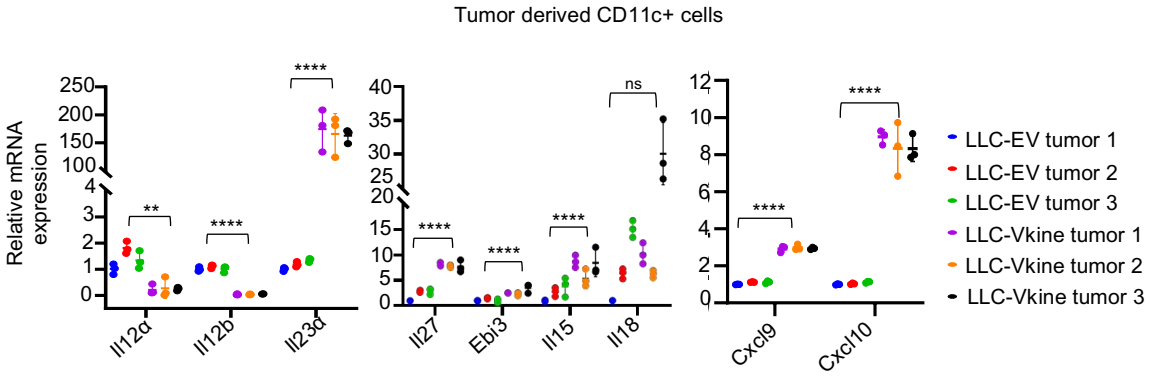

Figure 11. Ccl7, a major Batf3-DC chemoattractant, as well as NK-activating cytokines, are highly expressed in LLC-Vkine tumors

A: RT-PCR analysis for *Ccl7* message in bulk LLC-EV and LLC-Vkine tumor mRNA (left) and CD11c+-selected RNA (right). **B**: RNA from ex vivo-explanted CD11c+ cells from LLC-EV and LLC-Vkine tumors was subjected to RT-PCR to quantitative relative expression of NK-activating cytokines as well as Cxcl9 and Cxcl10, as shown.

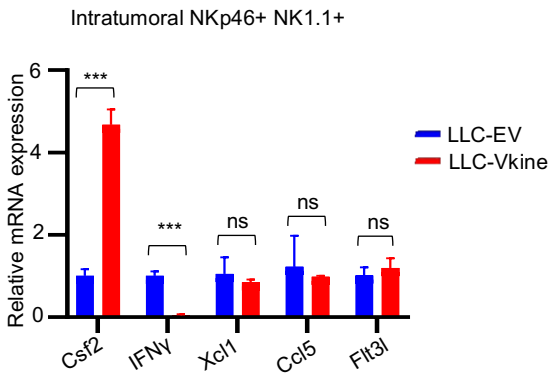

Figure 12. Versikine promotes the expansion of GM-CSF-expressing NK cells

Profiling of NKp46+ NK1.1+ cells in versikine-replete tumors. RNA from flow-sorted NKp46+NK1.1+ cells explanted from LLC-EV and LLC-Vkine tumors was subjected to RT-PCR using gene primers, as shown.

A

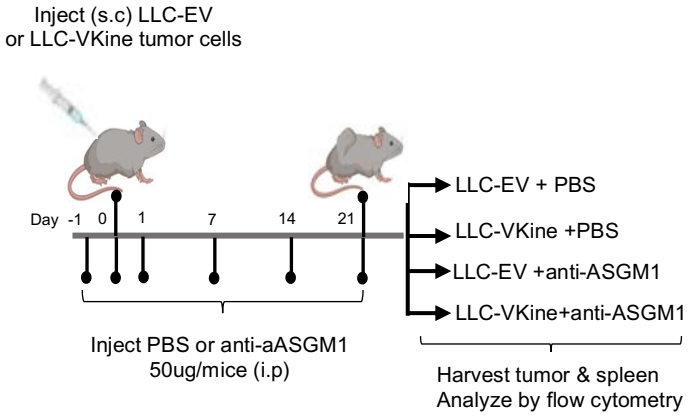
Inject (s.c) LLC-EV
or LLC-VKine tumor cells
Day -1 0 1 7 14 21
LLC-EV + PBS
LLC-VKine +PBS
LLC-EV +anti-ASGM1
LLC-VKine+anti-ASGM1
Inject PBS or anti-aASGM1
50ug/mice (i.p)
Harvest tumor & spleen
Analyze by flow cytometry

B

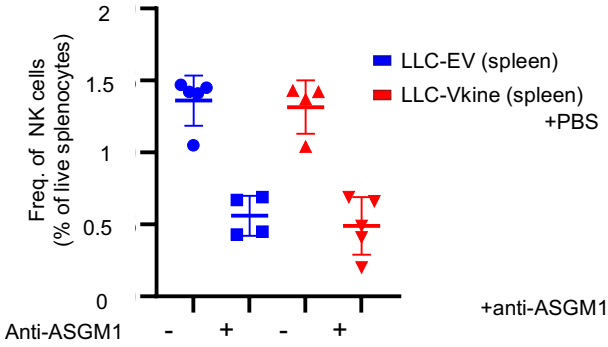
Freq. of NK cells
(% of live splenocytes)
2
1.5
1
0.5
0
LLC-EV (spleen)
LLC-Vkine (spleen)
Anti-ASGM1 - + - +

C

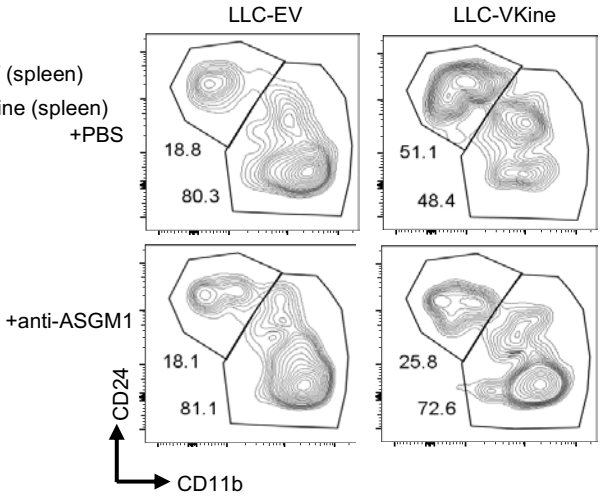
LLC-EV
LLC-VKine
+PBS
+anti-ASGM1
18.8
80.3
51.1
48.4
18.1
81.1
25.8
72.6
CD24
CD11b

D

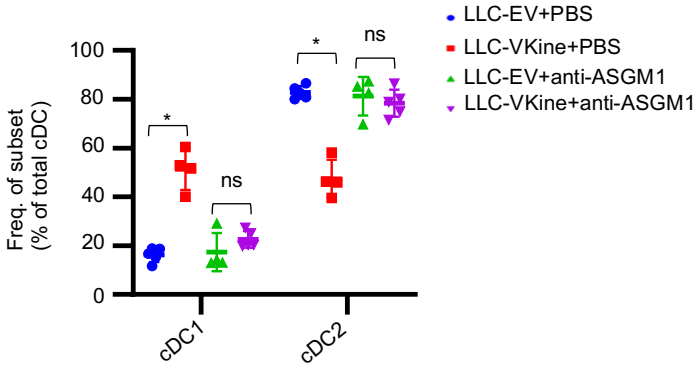
Freq. of subset
(% of total cDC)
100
80
60
40
20
0
*
ns
*
ns
cDC1
cDC2
LLC-EV+PBS
LLC-VKine+PBS
LLC-EV+anti-ASGM1
LLC-VKine+anti-ASGM1

Figure 13. Versikine promotes Batf3-DC through NK cells

A: Schematic layout of NK-depletion. **B**:Validation of splenic NK depletion following anti-ASGM1 treatment. **C**: Flow cytometric analysis of cDC subsets in LLC-EV vs. LLC-Vkine tumors following treatment with NK-depleting antibody (anti-ASGM1) or vehicle (PBS) **D**: Summary of cDC subset frequency by flow cytometric analysis in LLC-EV vs. LLC-Vkine tumors following treatment with NK-depleting antibody (anti-ASGM1) or vehicle (PBS).

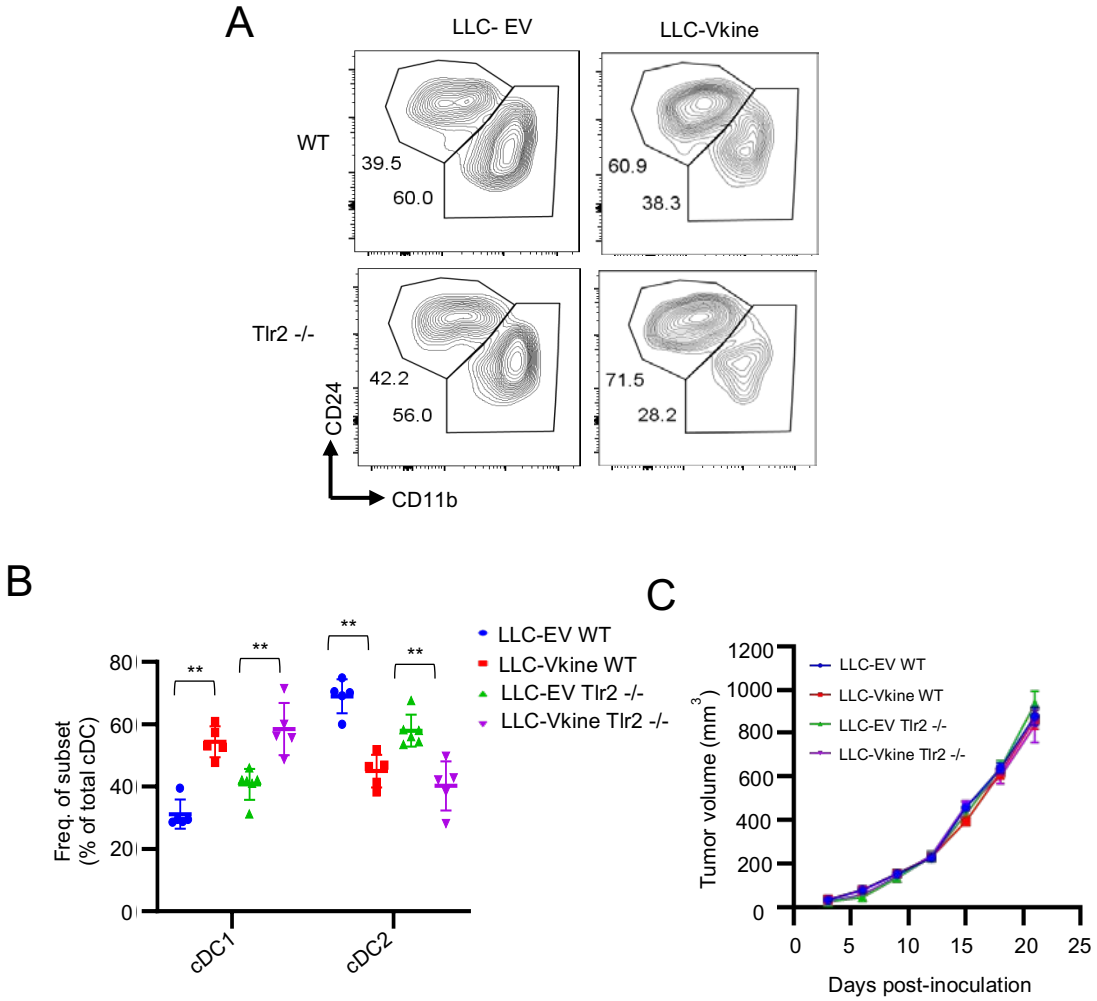

Figure 14. Versikine boosts Batf3-DC in the tumor in a Tlr2-independent manner

A: Flow cytometric analysis of cDC subsets in LLC-EV vs. LLC-Vkine tumors implanted in WT or *Tlr2-/-* recipients. **B**: Summary of cDC subset frequency by flow cytometric analysis in LLC-EV vs. LLC-Vkine tumors implanted in WT or *Tlr2-/-* recipients. **C**: Growth rates of LLC-EV and LLC-Vkine tumors in WT vs. *Tlr2-/-* background.

Table 1. TMA Scoring Table

	Total	Primarily Pericellular (Moderate/Strong)	Primarily Stromal (Moderate/Strong)	Both (Moderate/Strong)	Negative/Weak	Uninterpretable
Squamous Cell Carcinoma	40	4	4	10	19	3
Adenocarcinoma	47	1	4	18	24	0
Small Cell Carcinoma	8	1	0	5	2	0
Adenosquamous Carcinoma	3	0	0	1	2	0
Mucinous Adenocarcinoma	4	1	0	2	0	1
Papillary Adenocarcinoma	1	0	1	0	0	0
Large Cell Carcinoma	3	0	1	1	1	0
Atypical Carcinoid	3	3	0	0	0	0
Carcinoid	1	1	0	0	0	0
Total	110					

Table 2. Cytof counts (% of total CD45+ cells)

Cell counts (% out of total CD45+)

Manually gated population	WT LLC-EV	WT LLC-Vkine
Tregs	12 (0.18)	6 (0.09)
Batf3 DCs	8 (0.12)	13 (0.2)
Total DCs	82 (1.26)	83 (1.28)
M2 macrophages	3621 (55.71)	2491 (38.32)
M1 macrophages	229 (3.52)	1147 (17.65)
NK/ILC1 cells	28 (0.43)	43 (0.66)
CD8+ cells	13 (0.20)	26 (0.40)
B cells	25 (0.38)	12 (0.18)
M-MDSC	874 (13.45)	695 (10.69)
G-MDSC	489 (7.52)	195 (3)
Unidentified	1119 (17.21)	1789 (27.52)
Total CD45+	6500 (100)	6500 (100)

CHAPTER FOUR:

Versikine lowers the threshold for STING agonist immunotherapy and promotes antigen specific CD8+ responses *in vivo*

Abstract:

Cancer immunotherapy modulates and leverages the host immune system to treat cancer. The past decade has witnessed historical advancement of cancer immunotherapy. Recently, activation of stimulator of interferon (IFN) genes (STING), an intracellular receptor residing in the endoplasmic reticulum, has shown great potential to enhance antitumor immunity through the induction of a variety of pro-inflammatory cytokines and chemokines, including type I IFNs. In this chapter, I demonstrate that versikine lowers the threshold for STING activation, an effect that is Batf3-DC dependent, in Lewis Lung carcinoma, B16 melanoma and 4T1 breast cancer. Versikine-STING synergy also presents potent abscopal effects, thus generating systemic anti-tumor immunity. Furthermore, versikine synsergizes with STING agonist to augment antigen specific CD8+ responses. I also demonstrate that versikine promotes antigen presentation efficiency and T-cell priming by Batf3-DC. In line with this, versikine's unique transciptomic signature extracted from the 100 up- and down-regulated genes correlates with CD8+ scores in human lung cancer with patient data obtained from adeno-and squamous lung carcinoma.

Introduction:

The tumor intrinsic and extrinsic factors that dictate success to immunotherapies have not been fully elucidated [202]. Cyclic GMP-AMP synthase (cGAS)/Stimulator of interferon genes(STING) pathway has recently emerged as nodal player in cancer immunity and is currently being explored as potential therapeutic target [203]. Cancer specific antigens and endogenous expansion of CD8+ T cells have been implicated in many cancers. Clinical studies indicate spontaneous T cell priming, immune infiltration of T cell recruiting cytokines, and Type I IFN response into tumor sites; a state collectively defined as "T cell inflamed microenvironment". In anti-cancer immune response, the maturation and activation of antigen-presenting dendritic cells (DCs) is a critical step for activating the T-cell response against cancer cells. This is blocked by immunoregulatory cytokines such as IL-10 and TGFβ [204]. Thus, co-stimulatory inflammatory signals are immensely important for T cell activation. Type I IFN response is considered to be a key player in activating T-cell response. Blockade of Type I IFN response in vivo, either by IFN receptor (IFNAR) deletion or treatment with antibody, has been shown to enhance chemically induced tumor formation [205].The induction of tumor-specific CD8+ T cells, leading to immune rejection of tumors, was predominantly mediated by Type I IFN production in dendritic cells (DCs) [116]. In summary, initial activation of anti-tumor innate immune response depends on Type I IFN production by DCs which eventually helps in CD8+ T cell cross priming, followed by tumor cell killing [206].

Results:

Versikine lowers threshold for STING agonist immunotherapy *in vivo* in a Batf3-DC-dependent manner.

The STING pathway has emerged as a central mediator of innate sensing of tumors [207]. There has been significant enthusiasm for the potential of STING agonists as vaccine adjuvants, particularly for *in situ* administration into tumors to generate "living" vaccines. However, some of the initial enthusiasm has been tempered in clinic, in large part due to limiting Batf3-DC abundance in tumors [155]. We hypothesized that versikine may render tumors hypersensitive to STING agonists through intratumoral enhancement of Batf3-DC. To examine this hypothesis, we performed experiments delineated in Fig. 1A. LLC-EV and LLC-Vkine tumors were challenged with sub-therapeutic doses of STING agonist DMXAA (150-200 mcg) or vehicle (NaHCO3). Notably, Gajewski and colleagues established dose-response relationships for intratumoral DMXAA- the MTD was 500 mcg, as unacceptable toxicity was observed at 600 mcg [203]. Tumor response curves are shown in Fig. 1B and survival plots (Kaplan-Meier) in Fig. 1C. EV-tumors did not appreciably respond to vehicle or subtherapeutic STING agonist. By contrast, versikine lowered the therapeutic threshold of DMXAA so that versikine-replete tumors demonstrated a consistent response to single doses of subtherapeutic DMXAA. Several versikine-replete tumors developed necrotic eschars by 24 hours after subtherapeutic DMXAA injection (Fig. 2A). By contrast, none of the control mice developed an eschar in that time frame. To determine whether versikine reduced therapeutic threshold through a classical type I-IFN response to DMXAA, we harvested tumors for RNA extraction at 2 hours post-DMXAA. Versikine-replete tumors demonstrated several-fold increase in interferon-α transcripts (particularly IFNα2 and IFNα4), and to a lesser degree IFNβ1 transcription (Fig. 2B). A fuller list of up- and down-regulated genes in this experiment is provided in Table 1. These results demonstrate that versikine lowered the threshold for a classical STING agonist response.

To determine whether versikine-STING synergy could produce an abscopal effect, we studied mice bearing tumors inoculated in both flanks. The treated side was inoculated with EV or versikine-expressing LLC cells; the contralateral non-treated side was inoculated with unmanipulated LLC cells. Notably, versikine is tightly bound in the pericellular halo (glycocalyx) (Fig. 1C/Chapter 3) and does not circulate. We observed a consistent abscopal effect when

versikine-replete tumors where injected with 200 mcg DMXAA (Fig. 3A/B). EV- tumors treated with the same subtherapeutic dose failed to elicit any response, either on the treatment or contralateral sides. Importantly, versikine-DMXAA synergy produced a significant survival benefit (Fig. 3C). Versikine-DMXAA synergy produced consistent primary tumor and abscopal effects across genetic backgrounds and as we observed tumor responses and survival benefit in the breast carcinoma 4T1 orthotopic model (Fig. 4A/B/C).

Our hypothesis that versikine-DMXAA synergy is Batf3-DC-dependent would predict that the combination would be ineffective in *Batf3*-null mice. To test this hypothesis, we repeated the experiment (as delineated in Fig. 1A) in *Batf3*-null recipients. As shown in Fig. 5A, versikine was ineffective in the *Batf3*-null background and survival benefit from versikine was lost (Fig. 5B). To confirm that Batf3-DC mediated the effects of versikine (rather than another Batf3-expressing lineage), we attempted to rescue the null phenotype with intratumoral adoptive transfer of iCD103, BM-derived primary Batf3-DC-equivalents generated in culture using the protocol by [153] (Fig.6A). We confirmed iCD103 to have a consistent Batf3-DC-like phenotype in our hands (Fig. 7). Adoptive transfer of iCD103 concurrently with subtherapeutic STING agonist in *Batf3*-null mice restored versikine's efficacy (Fig. 6B). iCD103 adoptive transfer restored a survival benefit (Fig. 6C). To confirm the findings in a different C57BL6/J model, we chose B16 melanoma (4T1 model could not be used as *Batf3*-null animals were maintained in a C57BL6/J background). B16 tumors respond to subtherapeutic dose of DMXAA in the presence of versikine but not EV (Fig. 1D/E). Versikine lost efficacy in the *Batf3*-null background (Fig. 6D) but synergy with STING agonists was restored, at least in a subset of mice, when iCD103 were adoptively transferred (Fig. 6E). Notably, we speculate that adoptive transfer of iCD103 was less consistent in B16 (compared to LLC) due to the immune infiltrate paucity in B16 (B16 are "cold" tumors). Our results demonstrate that versikine-STING agonist synergy is Batf3-DC dependent.

Versikine promotes antigen presentation efficiency and T-cell priming by Batf3-DC

Versikine upregulated co-stimulatory receptors (B7, CD40) as well as co-stimulatory cytokines in MutuDC1940 either alone or in association with TLR4 agonist, LPS (Fig. 9/chapter 2). These results raised the possibility that versikine, alone or in combination with other maturation signals, promoted antigen-presenting efficiency of Batf3-DC. To test this hypothesis, we carried out antigen-presentation assays using the OVA (ovalbumin) antigen system in conjunction with T-cell

receptor engineered OT-I cells (Fig. 8A). Versikine-expressing and EV- MutuDC1940 cells were pulsed with SIINFEKL peptides and co-cultured with OT-I cells. The results are shown in Fig. 8B/C. Versikine alone more than doubled the percentage of primed OT-I cells secreting IFNγ and IL-2 by flow cytometry. Priming was confirmed through ELISA of the culture supernatant for IFNγ (Fig. 8C). Providing both versikine and LPS maximized T-cell activation (Fig. 9). These results raise the possibility that versikine can synergize with endogenous immunogenic DAMPs to maximize stimulatory DC antigen presentation and T-cell priming.

Versikine promotes antigen-specific CD8+ responses *in vivo*

Versikine lowered the threshold for response to STING agonists (Fig. 1). We sought to further determine whether the synergy would result in enhanced generation of antigen-specific effector responses *in vivo*. To test this hypothesis, we employed the ovalbumin (OVA) system as an *in vivo* model antigen (Fig. 10A). EV- and versikine-expressing LLC cells were engineered to express full-length OVA (LLC-OVA). EV- or versikine-replete LLC-OVA tumors were challenged with therapeutic dose of DMXAA (500 mcg). Three weeks after challenge, spleens were harvested and analyzed by flow cytometry for antigen-specific effector responses using an antigen-specific tetramer assay. Challenge of versikine-replete tumors more than doubled the magnitude of the antigen-specific response in the CD8+ compartment as determined MHCI:SIINFEKL-tetramer staining (Fig. 10B). Moreover, spleens contained a larger proportion of CD62LCD44- CD8+ cells with a central memory phenotype (Fig.10C).

Versikine signature correlates with CD8+ scores in human lung cancer.

We earlier laid out the hypothesis that N-terminal VCAN proteolysis results in CD8+ infiltration through both local depletion of non-proteolyzed VCAN and generation of novel versikine activities. To interrogate a specific contribution by versikine, we generated a unique versikine signature comprising the top 100 up- and down-regulated genes in MutuDC1940 cells (Fig. 9/chapter 2). We then correlated this signature to CD8+ scores deduced from TCGA data for 1017 lung cancers (see Materials and Methods for details). The results are shown in Fig.11. We observed a significant, albeit weak, correlation between versikine signature and CD8+ scores. Despite the inherent limitations of the analysis (application of an *in vitro* generated signature to primary bulk human tumor data), the results are consistent with a direct role for versikine in T-cell inflammation.

Discussion:

A decade following the initial reports of checkpoint inhibitor efficacy in common cancer types, most patients are still refractory [208-210]. Early attempts at elucidating the molecular and physiologic underpinnings of response pointed to the importance of an "inflamed' immune microenvironment, i.e., evidence of pre-existing adaptive anti-tumor immunity that could be potentiated through immunotherapy [155]. In this context, Batf3-lineage DC have been identified as key regulators of the tumor immune "thermostat" [202, 211, 212]. This crucial DC lineage regulates two essential aspects of the "cancer-immunity cycle" [213, 214]: first, Batf3-DC are extremely efficient in cross-presenting tumor antigens picked up at the tumor site and transported to the lymph node. Batf3-DC also critically regulate the last leg of the tumor-immunity cycle: infiltration of immune effector cells into tumor cites through control of critical chemokine networks, namely CXCL9 and CXCL10. It is therefore not surprising that they have been shown to be essential for *in situ* vaccination (e.g., with STING agonists), checkpoint inhibitor efficacy and engineered immune effector cell infiltration [215, 216].

STING pathway has emerged as a central mechanism of innate sensing of tumors. *In situ* vaccination of human tumors with STING agonists has had mixed success to date, in large part due to Batf3-DC paucity limiting success of these agents. By contrast, versikine-replete tumors responded to *subtherapeutic* doses of STING agonists, whether on the "warm" (LLC, 4T1) and "cold" (B16) end of immune spectrum and across genetic backgrounds. Versikine-STING synergy elicited type I-interferon-dependent inflammatory responses and was entirely dependent on Batf3-DC. The results suggest that versikine may be useful in up-dialing the immunogenicity of a given tumor, towards a more inflamed "hot" set point thus lowering threshold for immunotherapy efficacy. Versikine-STING agonist synergy not only produced locally robust inflammatory responses but also translated into enhanced antigen-specific CD8+ responses. Thus, versikine could be a useful agonist in *in situ* vaccination approaches either alone or in combination with locally administered immunotherapy.

Finally, the versikine transcriptomic signature showed a direct correlation to CD8+ scores deduced from TCGA data for 1017 squamous lung and lung adenocarcinomas, results that implicate versikine in T-cell influx in the tumor.

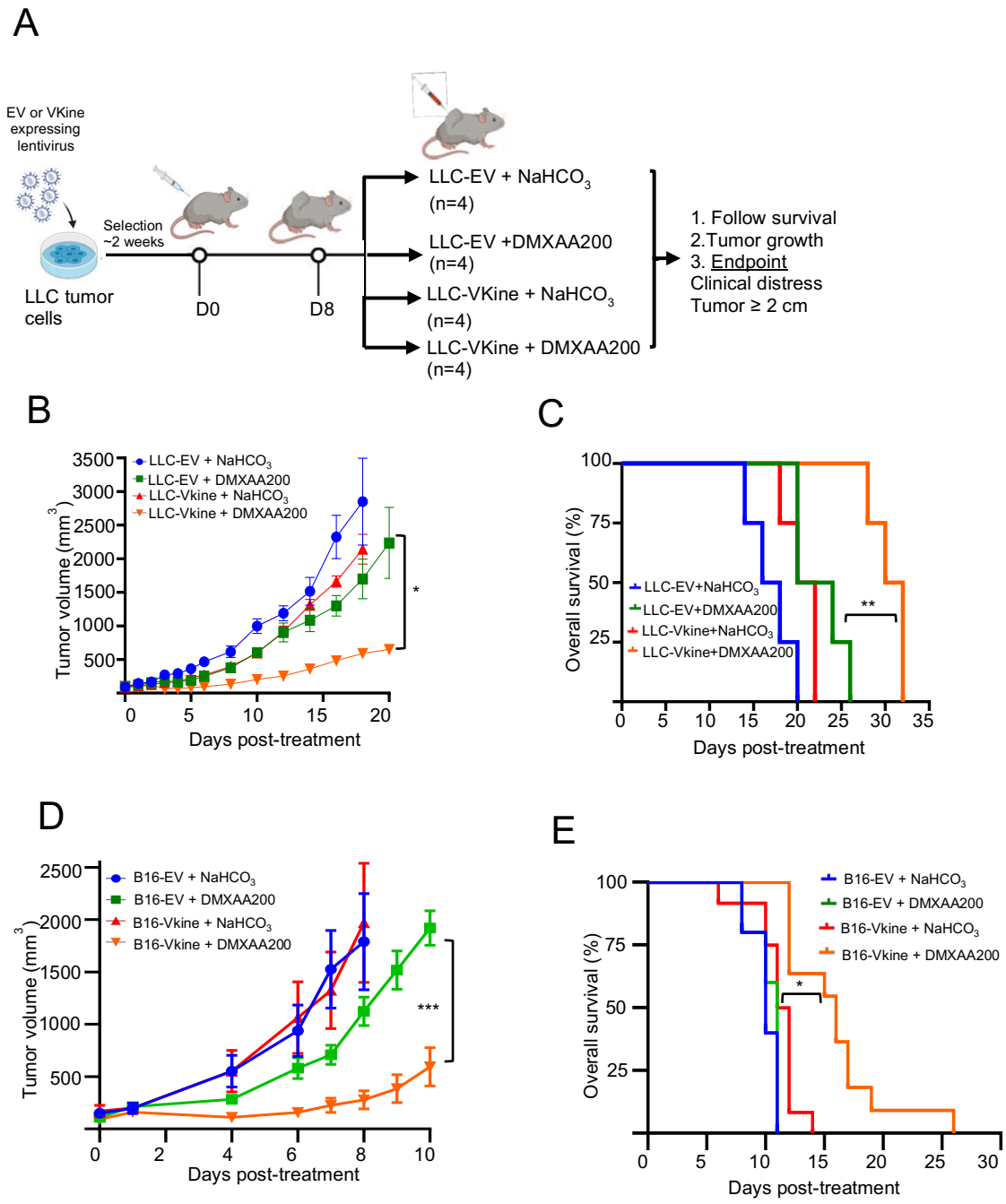

Figure 1. Versikine sensitizes LLC tumors to subtherapeutic doses of STING agonist

A. Schematic layout of the experiments. **B**: Growth curves of LLC-EV and LLC-Vkine tumors challenged with a single subtherapeutic dose (200 mcg) of IT DMXAA on Day 0 (DMXAA200) or vehicle (NaHCO3). **C**: Kaplan-Meir survival curves for the experiment in (B), **=p<0.01 by

log-rank test. **D**: Growth curves of B16-EV and B16-Vkine tumors challenged with a single subtherapeutic dose (200 mcg) of IT DMXAA on Day 0 (DMXAA200) or vehicle ($NaHCO_3$). **E**: Kaplan-Meir survival curves for the experiment in panel 3D, *=$p<0.05$ by log-rank test

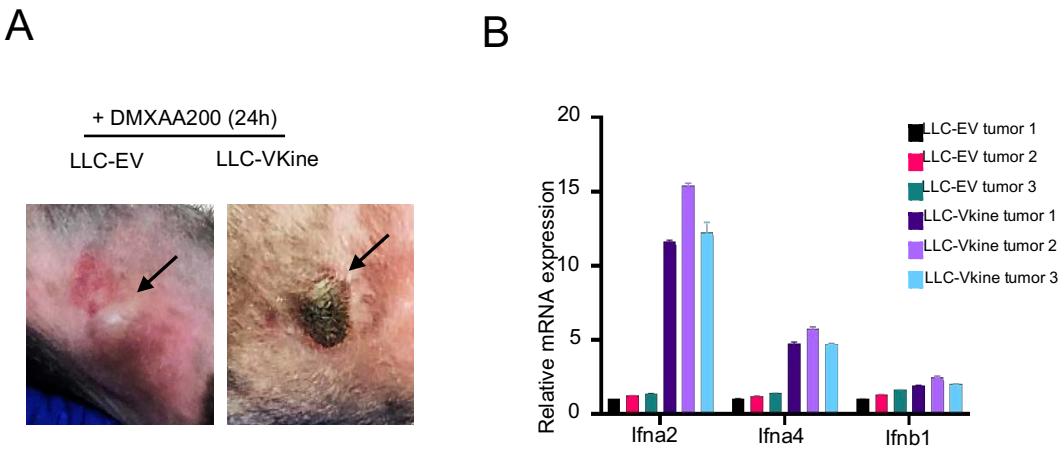

Figure 2. Transcriptomic profiling of DMXAA-response in Vkine- vs EV- LLC tumors

A: Development of hemorrhagic necrosis and a necrotic eschar in LLC-Vkine, but not LLC-EV tumors, at 24 hours post-IT DMXAA200. **B**: Transcriptomic analysis of LLC-EV and LLC-Vkine tumors harvested at 2 hours post-IT DMXAA200.

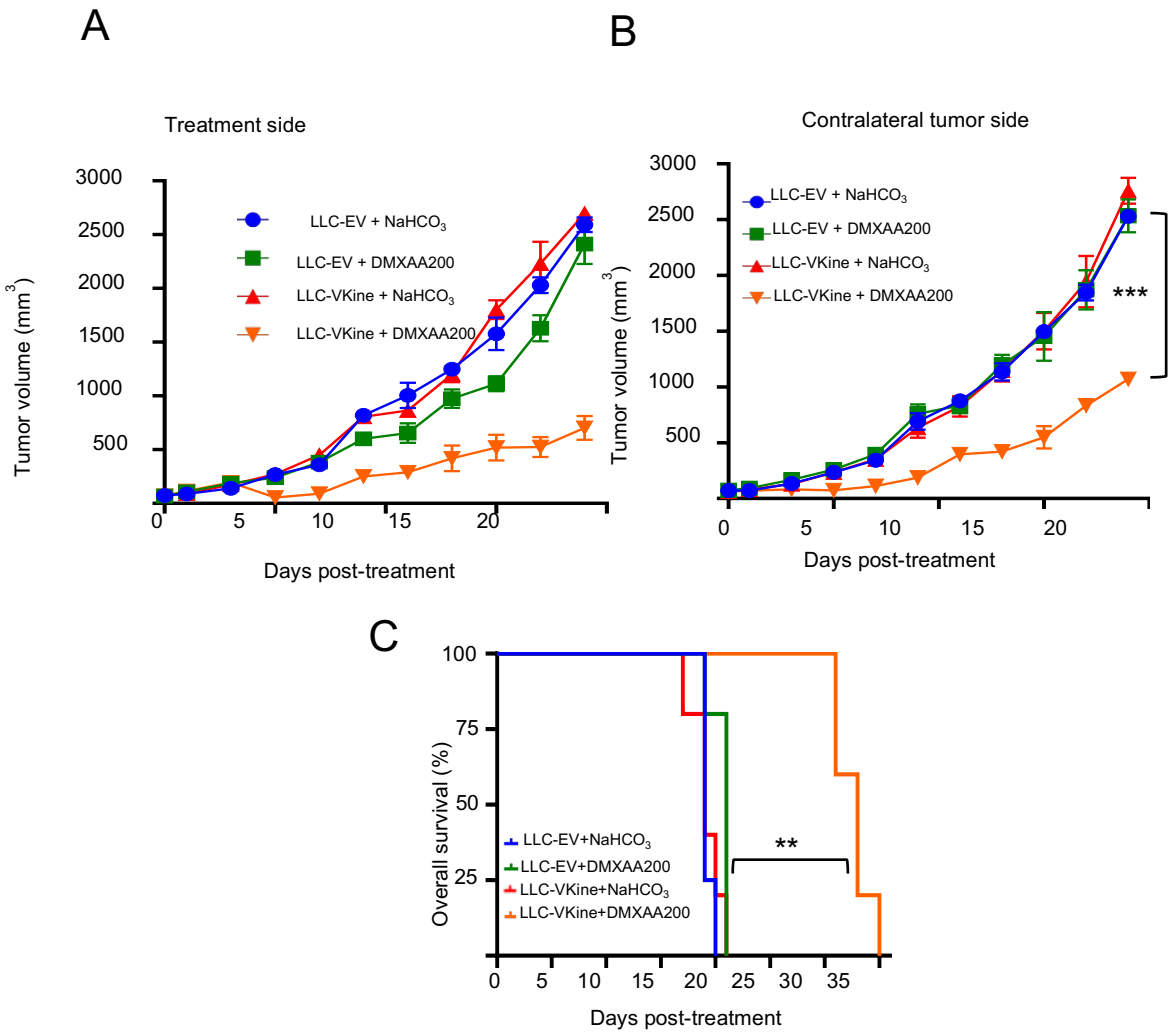

Figure 3. Versikine-STING agonist synergy generates potent abscopal effects in LLC tumors

A: Versikine-DMXAA synergy generates an abscopal effect in LLC tumors. Growth curves of treatment-side LLC-EV and LLC-Vkine tumors challenged with a single subtherapeutic dose (200 mcg) of IT DMXAA on Day 0 (DMXAA200) or vehicle (NaHCO3). **B**: Growth curves of contralateral side unmanipulated LLC tumors, according to corresponding treatment side configuration (treatment as in Panel A). **C**: Versikine-induced abscopal effect is accompanied by a survival advantage. **=p<0.01 by log-rank test.

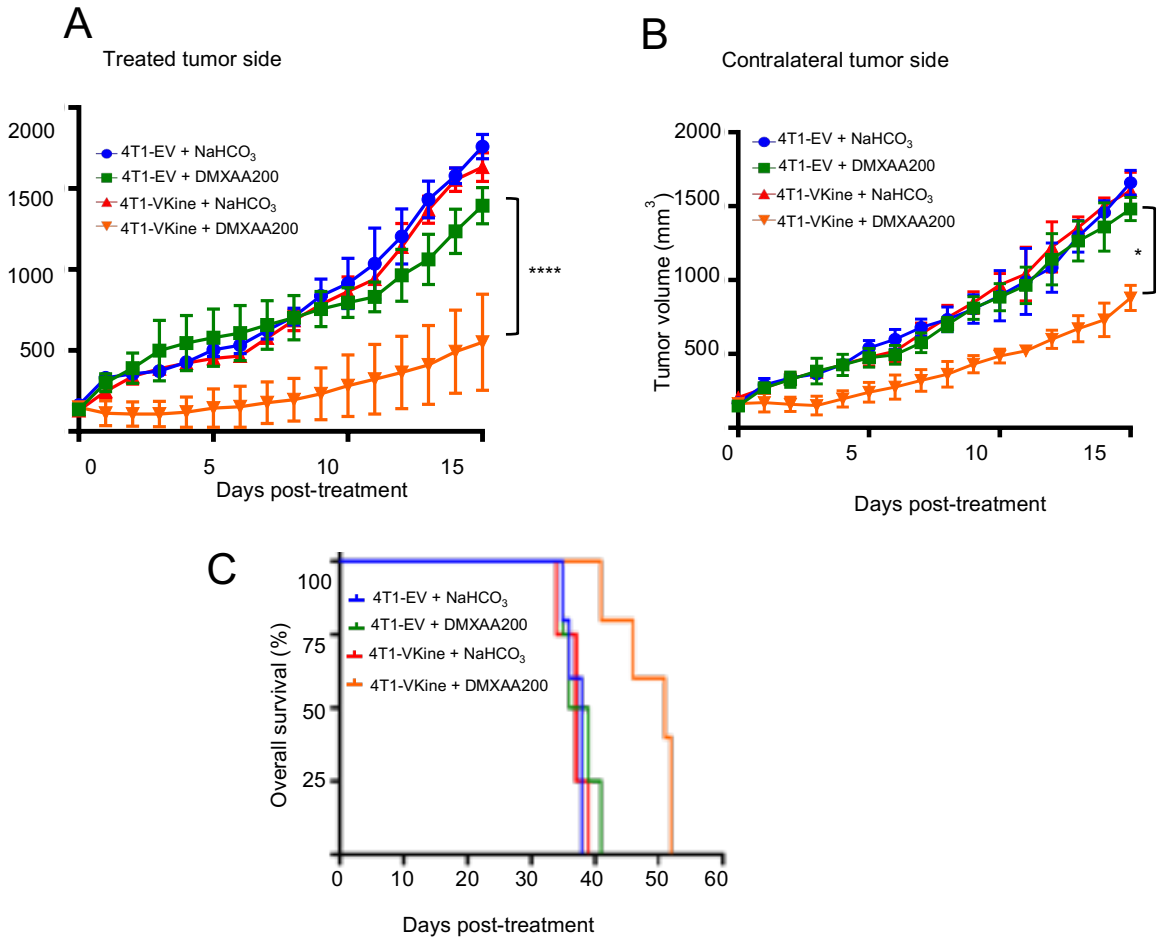

Figure 4. Versikine-STING agonist synergy promotes abscopal responses in orthotopic 4T1 breast carcinoma

A: Versikine-DMXAA synergy generates an abscopal effect in 4T1 tumors. Growth curves of treatment-side 4T1-EV and 4T1-Vkine tumors challenged with a single subtherapeutic dose (200 mcg) of IT DMXAA on Day 0 (DMXAA200) or vehicle (NaHCO3). **B**: Growth curves of contralateral side unmanipulated 4T1 tumors, according to corresponding treatment side configuration (treatment as in Panel 4A). **C**: Versikine-induced abscopal effect is accompanied by a survival advantage in 4T1 tumors. **=p<0.01 by log-rank test.

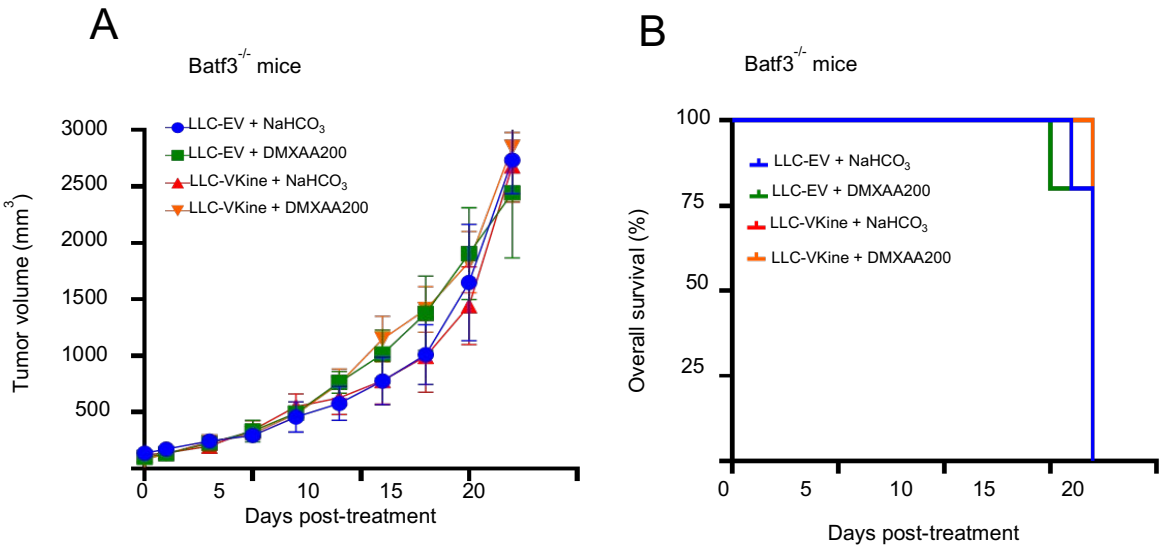

Figure 5. Versikine-STING agonist synergy is mediated by Batf3-DC

A: Response to DMXAA200 is lost in *Batf3*-/- recipients. Growth curves of LLC-EV and LLC-Vkine tumors challenged with a single subtherapeutic dose (200 mcg) of IT DMXAA on Day 0 (DMXAA200) or vehicle (NaHCO3) in *Batf3*-/- recipients. **B**: *Batf3*-loss abrogates the survival advantage seen in WT type (panel 3C).

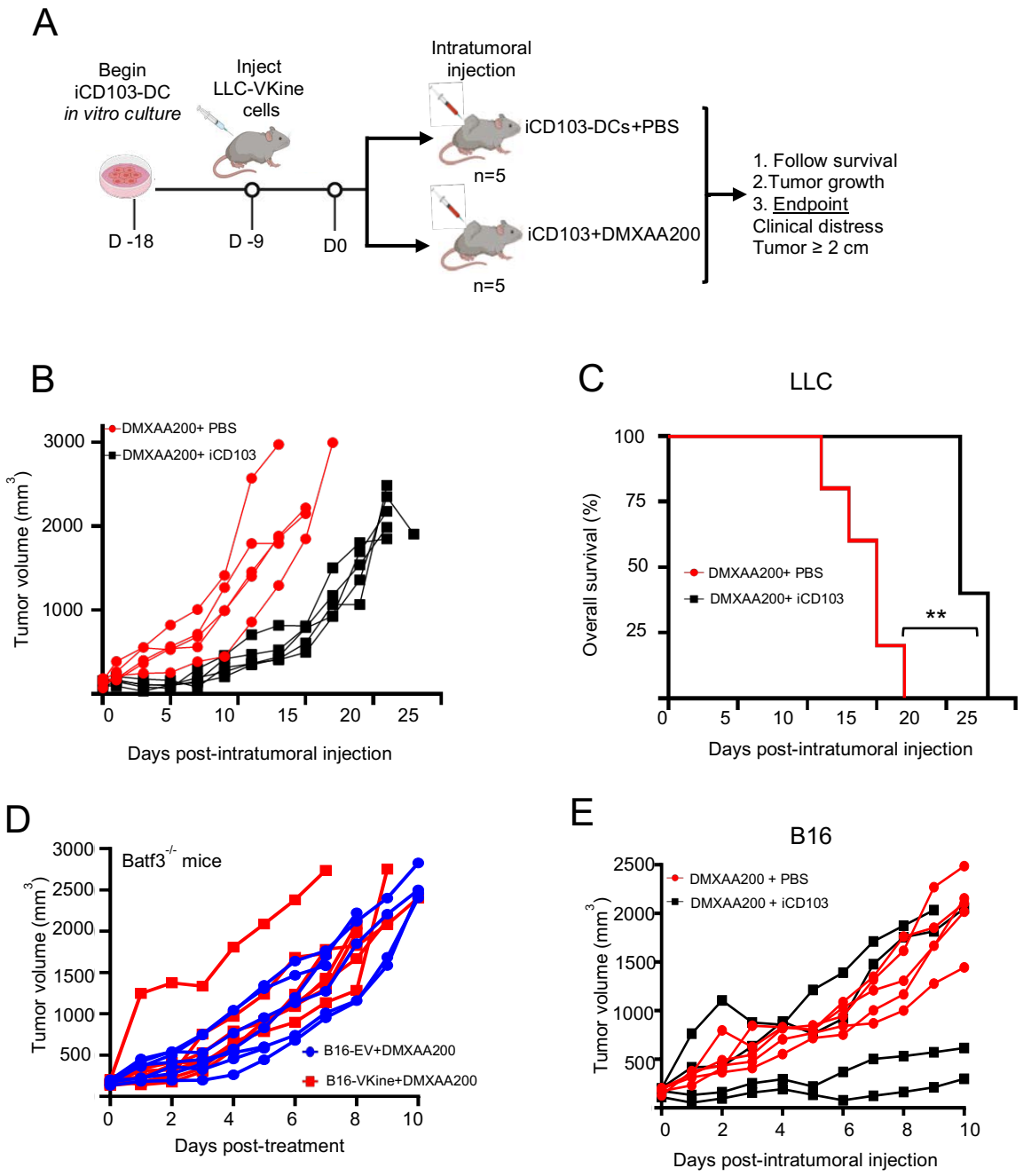

Figure 6. Add-back of Batf3-DC restores sensitivity of versikine replete tumors to STING-agonist

A: Schematic layout of iCD103 adoptive transfer experiments **B**: Efficacy of DMXAA200 in LLC-Vkine tumors implanted in *Batf3*-/- recipients is restored following adoptive transfer of iCD103. **C**: Adoptive transfer of iCD103 in LLC-Vkine tumors implanted in *Batf3*-/- recipients restores

survival advantage of mice treated with DMXAA200. **=p<0.01 by log-rank test. **D**: Response to DMXAA200 is lost in B16-Vkine tumors implanted in *Batf3*-/- recipients, **(E):** however it is restored following adoptive transfer of iCD103. A subset of animals did not respond, likely due to poor engraftment of iCD103 in the pauci-cellular immune environment of B16 tumors.

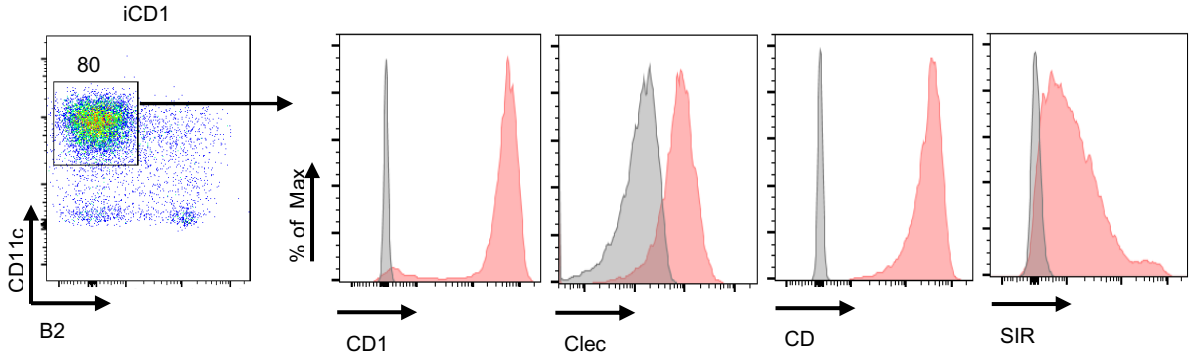

Figure 7. Generation of Batf3-DC (iCD103) *in vitro*

Flow-cytometric validation of the iCD103 cells, generated as described in [153], using standard Batf3-DC markers.

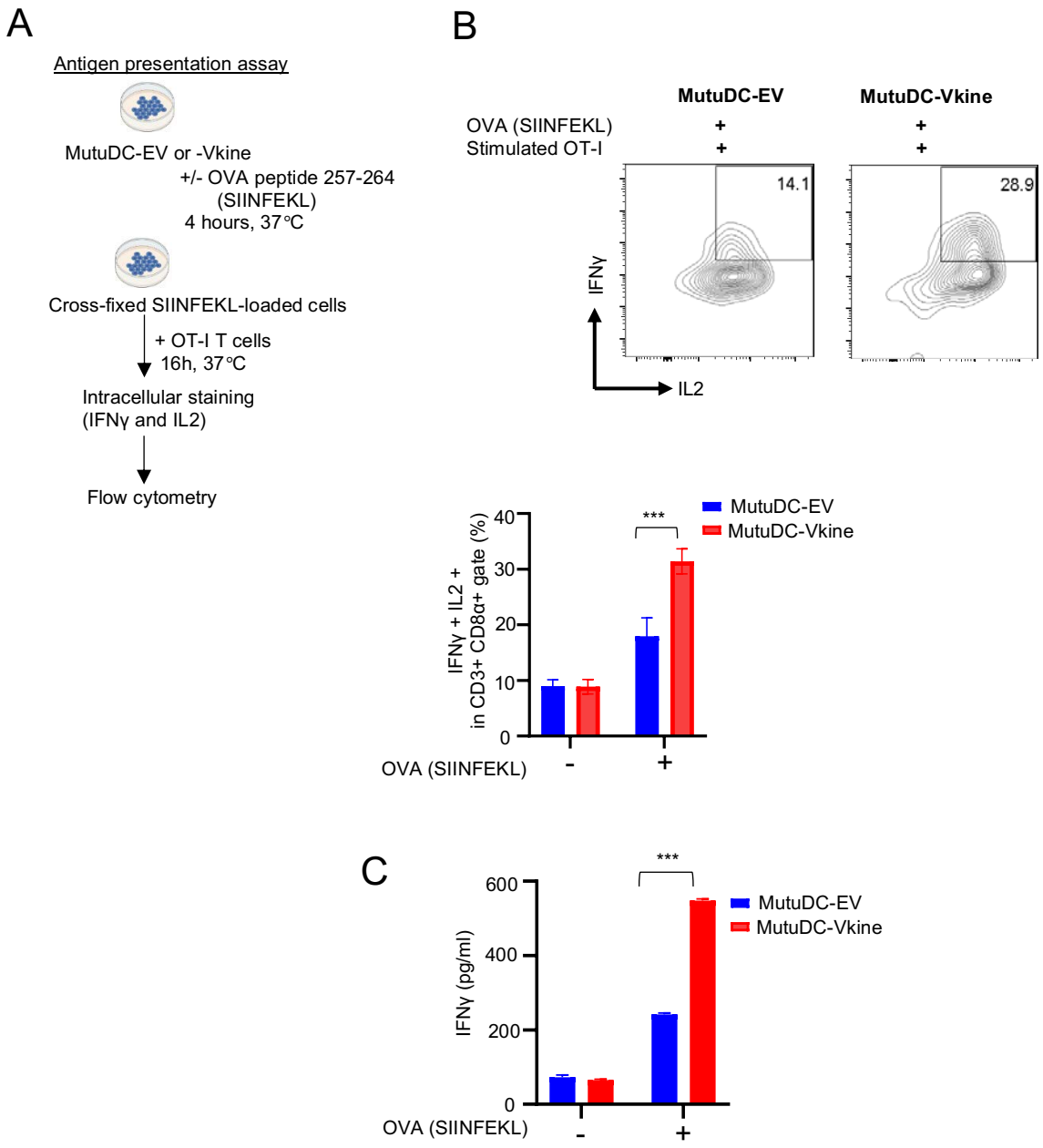

Figure 8. Versikine promotes antigen-specific CD8+ responses *in vitro*

A: A: Schematic layout of antigen-presentation experiment. **B**: Flow cytometry for endogenous IFNγ and IL2 of OT-I CD8+ T cells co-cultured with SIINFEKL-loaded MutuDC1940, either -EV or -Vkine. **C**: IFNγ by ELISA in supernatants from OT-I+ MutuDC1940:SIINFEKL co-cultures in the antigen presentation assa

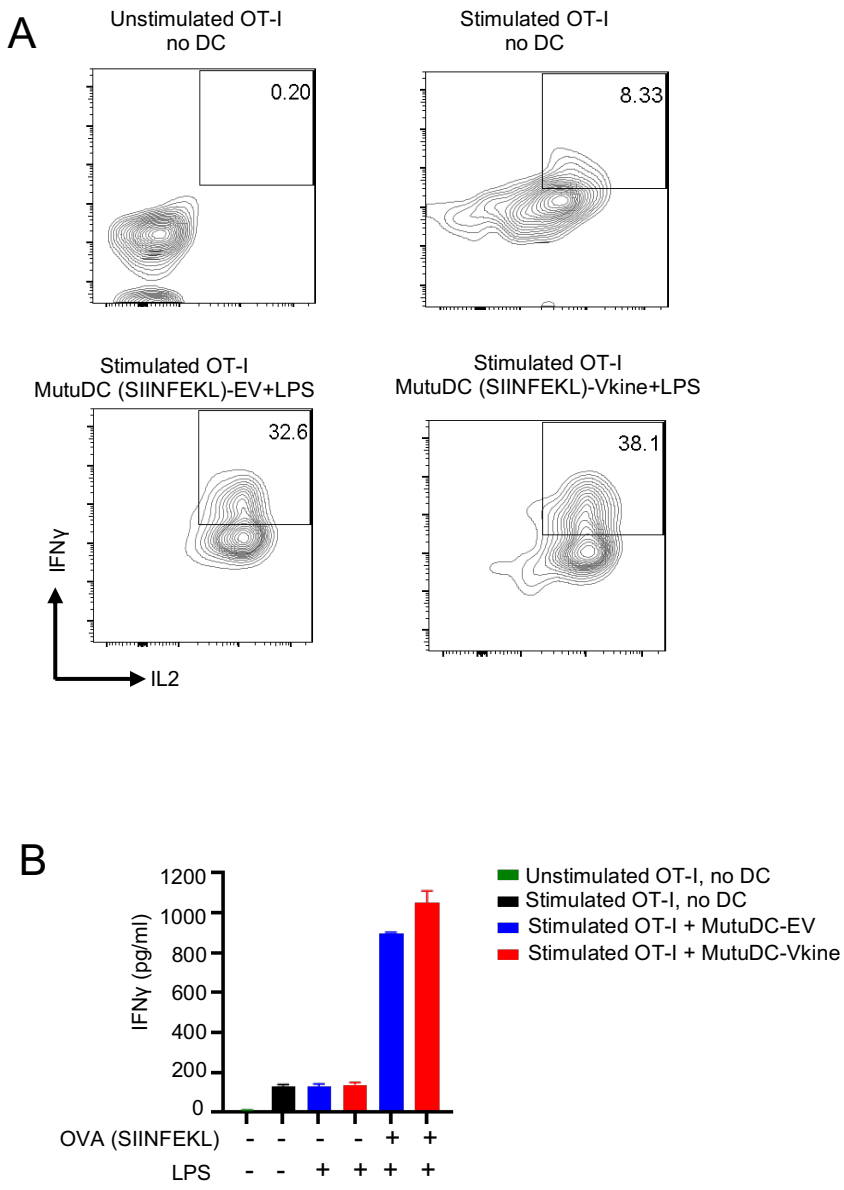

Figure 9. Versikine synergizes with LPS to maximize T-cell activation

A: Flow cytometry for endogenous IFNγ and IL-2 of OT-I CD8+ T cells at baseline (top left), PMA-stimulated (top right) or co-cultured with SIINFEKL-loaded MutuDC1940, either -EV (bottom left) or -Vkine (bottom right) matured with LPS. **B**: IFNγ by ELISA in supernatants from OT-I+ MutuDC1940:SIINFEKL co-cultures in the antigen presentation assay of panel 9A.

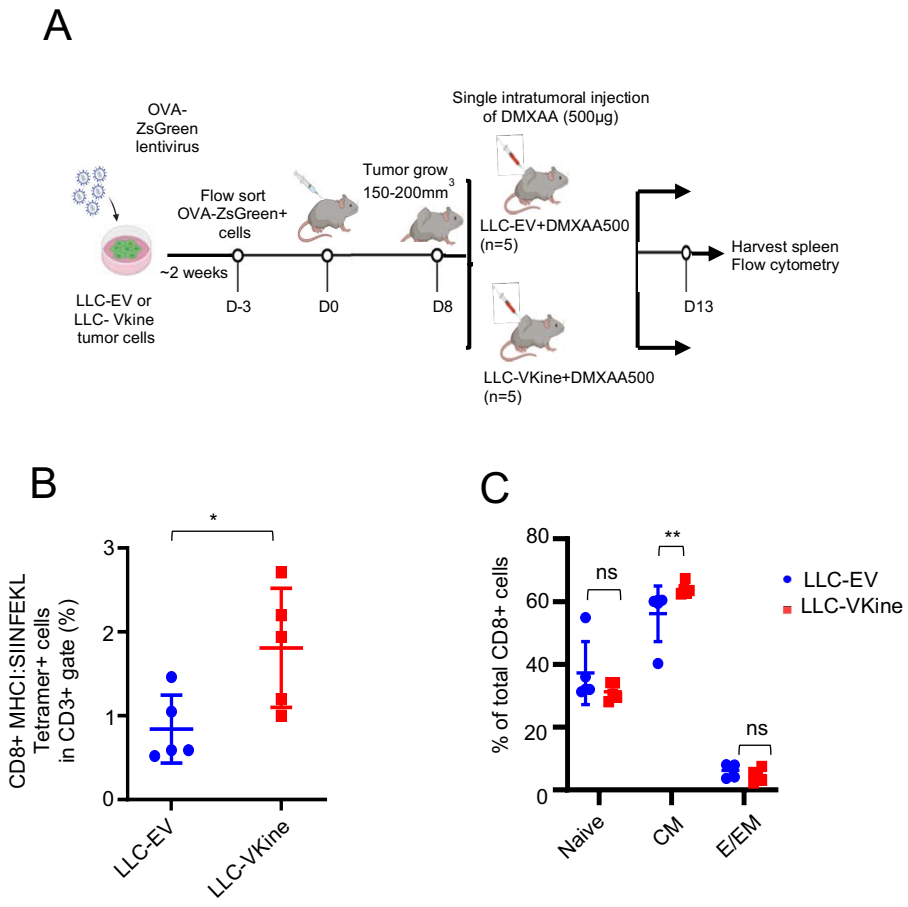

Figure 10. Versikine promotes antigen-specific CD8+ responses *in vivo*

A: Schematic layout of the *in vivo* antigen-specific response experiment. **B**: Frequency of MHCI:SIINFEKL tetramer+ splenocytes in mice bearing LLC-EV vs. LLC-Vkine tumors at 8 days post-challenge with therapeutic dose of STING agonist (DMXAA500). **C**: CD8+ subset frequency in the spleen of mice treated as in panel

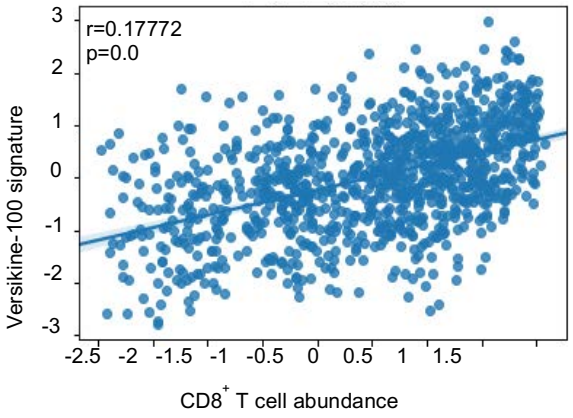

Figure 11. Versikine signature correlates with CD8+ scores in human lung cancer

Correlation of versikine-100 signature with CD8+ infiltration in human lung cancer (Data generated by Adam Officer, UCSD Oncogenomics Lab, Moores Cancer Center).

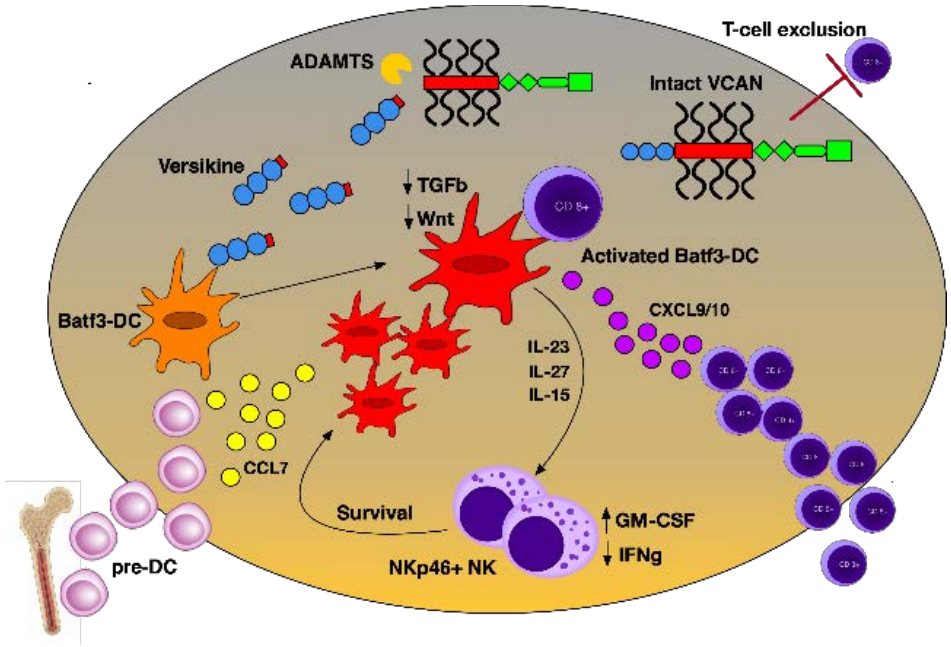

Figure 12. Proposed model for T-cell inflammation by VCAN remodeling

Gene Symbol	Fold Regulation
Il20	56.88
Il3	50
Gdf5	49.06
Il17b	47.12
Bmp5	46.84
Il25	37.95
Il17a	35.37
Il9	33.23
Il23a	32.16
Il21	30.57
Gdf2	30.5
Il5	29.42
Il2	28.67
Lta	28.51
Il17c	27.13
Scgb3a1	26.07
Tnfsf18	25.63
Il7	25.06
Il19	25
Il13	22.92
Il24	22.7
Tnfsf8	21.63
Mstn	20.5
Bmp6	19.33
Il4	17.82
Thpo	16.38
Cd40lg	16.12
Ifna2	16.07
Tnfsf4	15.35
Inha	15.34
Ltb	14.33
Tnfsf15	12.66
Gdf9	12.12
Tnfsf11	10.71
Il10	10.56
Bmp7	10.45
Tnfrsf11b	9.25
Tnfsf13b	9.16
Il16	8.87
Tgfb2	8.03
Adipoq	7.77
Cd70	7.01
Osm	6.38
Ifna4	6.17
Tnf	5.25
Tnfsf10	5.16
Cntf	4.64
Il11	4.58
Fasl	4.35
Csf3	4.32
Csf2	3.59
Bmp4	3.4
Il12b	3.37
Tnfsf14	3.06
Il17f	2.37
Inhba	2.3
Ifng	2.23
Mif	2.02
Il1rn	-2.25
Il1b	-2.87
Il6	-2.95
Nampt	-3.38
B2m	-5.78

Fold-Change (2^(-Delta Delta C)) is the normalized gene expression (2^(- Delta C)) in the Versikine Sample divided the normalized gene expression (2^(- Delta C)) in the Empty vector control sample. Fold-change values greater than one indicates a positive- or an up-regulation, and the fold-regulation is equal to the fold-change. Fold-change values less than one indicate a negative or down-regulation, and the fold-regulation is the negative inverse of the fold-change.

Table 1. STING agonist response analysis using RT² Profiler PCR Array

CHAPTER FIVE:

Summary and Future Directions

Despite the fact that immunotherapy has revolutionized cancer care in the last decade, still only a small subset of patients shows long lasting clinical responses. Today immunotherapy for the treatment of a variety of cancers is rapidly evolving from therapies that nonspecifically stimulate the immune system to more targeted ones that activate individual components of the immune system, increasing efficacy of the treatment while decreasing toxicity. Ipilimumab was the first checkpoint inbitor drug that was FDA-approved for the treatment of advanced melanoma with metastatic lung cancer following next.

In addition to checkpoint inhibitors, other types of immunotherapies, such as adoptive transfer therapy and chimeric antigen receptor (CAR-T) therapy have been proven to be effective in some hematopoietic malignancies (B-cell lymphoma, CLL), however they remain unsussessful in most solid tumors in the non-advanced/metastatic setting.

The interaction of the tumor matrix with the immune milieu still remains an understudied facet of tumor immunology. Here, we demonstate that tumor matrix remodeling has a role in the regulation of intratumoral Batf3-DC and thus promoting T cell inflammation in the tumor and sensitizing tumors to immunotherapy. Boosting and/or activating Batf3-DC at the tumor site is a crucial requisite for efficacy of several modern immunotherapy modalities. This thesis delineates a mechanistic framework by which matrix remodeling regulates Batf3-DC cross talk with NK cells in the tumor, leading thus to a T-cell inflamed environment. The N-terminal VCAN fragment, versikine, boosts Batf3-DC abundance in the tumor through an NK-regulated loop, that promotes their survival. Batf3-DC secrete high levels of T cell chemoattractants such as Cxcl9/10, which then recruit CD8+ T cells in the tumor bed. For my translational work, I focused on the challenging to treat solid tumor models (LLC, B16, 4T11). The rationale of my approach to combine versikine with STING agonist is supported by the need to devise new strategies to enhance in situ vaccination.

<u>Future directions include:</u>

1. The identification of versikine's receptor
2. The translational development of versikine. Recombinant versikine protein, versikine-encoding mRNA, versikine-armored immune effectors, versikine-secreting oncolytic

viruses or specific agonists of the yet uncharacterized versikine receptor/s could be used to promote a “hot” tumor immune microenvironment. Thus versikine could synergize with STING agonists, tumor vaccines, checkpoint inhibitors or engineered immune effector therapies to alter the immune “thermostat” of the tumor and boost endogenous responses, particularly in the challenging setting of solid tumors.

CHAPTER SIX:

Materials and Methods

Mice and regulatory approvals

C57BL6/J (aka B6, JAX stock 000664), BALB/cJ (aka BALBc, JAX stock 000651), B6.129 (Cg)-*Cd44*^{tm1Hbg}/J (aka CD44 KO, JAX stock 005085), B6.129S(C)-*Batf3*^{tm1Kmm}/J (aka Batf3^{-}, JAX stock 013755), B6.129-*Tlr2*^{tm1Kir}/J (aka Tlr2 KO, JAX stock 004650) mice were housed, cared for, and used in accordance with the *Guide for Care and Use of Laboratory Animals (NIH Publication 86-23)* under IACUC-approved protocols #M5476 and #S19109 in the University of Wisconsin , Madison and University of California, San Diego respectively.

Cell lines and primary cell culture

Lewis Lung Carcinoma (LLC, ATCC CRL-1642) and B16F10 melanoma (ATCC CRL-6322) were cultured in complete DMEM medium (10-013 CV Corning DMEM with 10% fetal calf serum, 50μM 2-mercaptoethanol, 100U/ml Penicillin, 100μg/ml Streptomycin, 292ng/ml L-Glutamine). 4T1 breast cancer cell line (CRL-2359) was cultured in complete RPMI (10-040 CV Corning RPMI 1640 with 10% Fetal calf serum, 50μM 2-mercaptoethanol, 100U/ml Penicillin, 100μg/ml Streptomycin, 10mM non-essential amino acids and 1M HEPES buffer). VQ4935 cells (Wen et al, 2020) were cultured in suspension in Iscove's DMEM medium (10-016-CV Corning Iscove's DMEM supplemented with 10% Fetal calf serum, 50μM 2-mercaptoethanol, 100U/ml Penicillin, 100μg/ml Streptomycin, 10mM non-essential amino acids and 10ng/mL IL-6, 200-06 Peprotech). Immortalized mouse dendritic cells (MutuDC1940, Applied Biological Materials Inc. #T0528) were cultured in Iscove's DMEM medium supplemented with 10% Fetal Calf serum, 292ng/ml L-Glutamine, 50μM 2-mercaptoethanoland, 1% of 7.5% sodium bicarbonate (w/v). CD103^{+} cDC1 *in vitro* differentiation was performed using bone marrow cells from female C57BL/6 mice at 6-12 weeks of age according to the induced CD103 DC protocol (Mayer et al., 2014). 15-16 days after the start of the culture, DCs were harvested and used for experiments.

Plasmids

pLenti6-UbC-VKine-HA and pLenti6-UbC-VKine-Myc has been previously described (Hope et al 2016, McCulloch et al , 2009). OVA was PCR amplified from pcDNA3-OVA (addgene #64599) and cloned into pHIV-Luc-ZsGreen backbone (addgene #39196). All lentiviral constructs were transformed into NEB 5-alpha competent cells (#C2987U) for propagation of plasmid DNA. All plasmids were prepped and purified using Macharey-Nagel NucleoBond Xtra Maxi kit (# 740414.50).

Lentiviral transduction

293 cells were transfected with a mixture of ps-PAX2 (packaging plasmid) and pVSV-G (envelope plasmid), and a plasmid coding for the desired protein or empty as control. On Day 2 post-transfection, the pseudotyped virus-containing culture medium was harvested, filtered, supplemented with 7.5 µg/ml polybrene (Sigma-Aldrich), and immediately applied to target cells for spinfection by centrifugation (90min, 2500xg at room temperature). After the incubation, the medium was exchanged for fresh complete RPMI1640 medium. Target cells were passaged at least three times after retroviral transduction and assayed for HA expression as a read out for transduction efficiency.

Generation of HA tagged -Versikine and OVA-ZsGreen expressing tumor cell lines

LLC, 4T1, B16F10 melanoma and MutuDC1940 cells were transduced with HA tagged EV or VKine expressing lentivirus as detailed above. The cells were selected with 10µg/ml Blasticidin for 2 weeks. The versikine expression was confirmed by western blotting using anti-HA antibody. LLC EV or VKine cell lines were transduced with pHIV-Luc-OVA-ZsGreen lentivirus. LLC-OVA expressing cells were FACS-sorted based on ZsGreen expression to ensure equal levels of transduction between different cell lines.

Tumor cell injections

Cells were harvested by trypsinization and washed in PBS. Mice were under isoflurane anesthesia during the tumor injections. $5x10^5$ LLC cells were injected subcutaneously (s.c.) in 100µl endotoxin-free PBS on the flank of recipient mice. 10^5 4T1 cells were injected orthotopically in the mammary fat pad of the mice. Tumor growth was measured using a digital caliper. Tumor volumes were measured bi-weekly and estimated by using the formula: Tumor volume= $(\text{length} \times \text{width})^2$ divided by 2, where length represents the largest tumor diameter and width

represents the perpendicular tumor diameter. Intratumoral injections were performed using a 28G insuilin syringe, when tumors had reached 100-150 mm^3, using surgical forceps to hold the tumor constantly.

For the intravenous (i.v) injections, we followed the retro-orbital approach. Mice were anesthetized using inhaled isoflurane in a chamber. The mouse's eye was partially protruded from the socket by applying downward pressure to the skin dorsal and ventral to the eye. Injections were performed by placing the needle, so the bevel faces down, in order to decrease the likelihood of damaging the eyeball. Once the injection is complete, the needle is slowly and smoothly withdrawn. Triple antibiotic ophthalmic ointment is then applied to the eye.

Intraperitoneal injection was performed using an insulin syringe gauge 28.5 with the head of the mouse tilted down. The needle was inserted at a 30° angle in the lower left or right quadrant. Transplantation of myeloma VQ4935 cells was performed via intracardiac injection after the 6-8 weeks old C57BL/6J recipient mice were sub-lethally irradiated at 6.0 Gy using an X-RAD 320 Irradiator. Intracardiac injection was performed by placement of needle in the 4^{th} intercostal space and into the left ventricle. In particular, the needle was inserted at a 90° angle in the middle of the imaginary line connecting the sternal notch and xyphoid process serving as anatomical landmarks, and the needle was inserted slightly left of the sternum.

Processing of tumor tissue

Unless stated otherwise, tumors were excised 21 days after transplantation. For subsequent analysis by flow cytometry, tumors were cut into pieces and digested with Collagenase Ia (1mg/ml) C2674 Sigma Aldrich and Hyaluronidase V (0.1mg/ml) H6254 Sigma Aldrich for 40min at 37°C using gentle MACS dissociator. Tissue was passed through a 70μm cell strainer (Falcon) and washed with FACS buffer (PBS with 1% FCS) before proceeding with antibody mediated staining. For RNA isolation, homogenization was performed in RLT buffer (QIAGEN) facilitated by a closed tissue grinder system (Fischer brand #02-542-09, 15mL).

CyTOF

Tumor tissue was harvested and processed for mass cytometry analyses directly ex vivo using the same protocol as described above for flow cytometry. After single cell suspensions were acquired, cells were washed with PBS, centrifuged at 300-400g for 5 minutes and supernatant was discarded

by aspiration. Cells were resuspended in PBS and Cell-ID Cisplatin (Fluidigm, #201064) was added to a concentration of 5uM. After rigorous mixing, cells were incubated at room temperature for 5 minutes. Cells were then quench stained with MaxPar Cell Staining Buffer (Fluidigm, #201068) using 5x the volume of the cell suspension, centrifuged and supernatant was discarded by aspiration. The process was continued with surface staining. 50ul of the antibody cocktail was added to each tube so the total staining volume was 100ul (50ul of cell suspension+ 50ul antibody cocktail). Cells were stained for an hour at room temperature. All antibodies used for staining were either bought pre-conjugated to metal isotopes or were conjugated using the Maxpar Antibody Labelling Kit (Fluidigm 201160B) (Table 1). Following the incubation, cells were washed by adding 2mL Maxpar Cell Staining Buffer to each tube, then centrifuged at 300xg for 5 minutes and supernatant was removed by aspiration. This step was repeated for a total of 2 washes, and cells were resuspended in residual volume by gently vortexing after final wash/aspiration. Cells were then fixed with 1.6% FA solution and incubated at room temperature for 10 minutes. Finally, cells were labelled with Cell-ID Intercalator-Ir (Fluidigm, #201192A) at a final concentration of 125nM, incubated for an hour at room temperature and then analyzed on a Helios instrument (WB injector). All samples were resuspended in sufficient volume of 0.1 EQ beads (Fluidigm, #201078 by diluting one part beads to 9 parts Maxpar Cell Acquisition (CAS) solution.

Analysis of mass cytometry data using viSNE

To visualize the global structure of myeloid and lymphoid lineages, the immune milieu of the tumor (CD45+) was enriched by manual gating among single events, equally subsampled to 6,000 events, then run through a Barnes Hut implementation of the t-SNE algorithm, viSNE, in the R package ‘Rtsne’, using optimized parameters (iterations:1000, perplexity:30, learning rate:455). All markers listed in table 1 to characterize the myeloid and lymphoid linages were selected for viSNE, excluding CD45.

Flow cytometry and fluorescence activated cell sorting

Flow cytometric analyses were performed using an LSR II, LSR Fortessa X20. Data were analyzed using FlowJo (Tree Star). DAPI (0.5 mg/ml, Sigma-Aldrich) or a Live/Dead fixable cell stain (Ghost 780 Tonbo Biosciences) was used to exclude dead cells in all experiments, and anti-CD16/CD32 antibody (2.4G2) was used to block non-specific binding of antibodies via Fc-receptors. The following antibodies were used for flow cytometry: anti-CD24 (clone M1/69), anti-

CD45 (30-F11), anti-CD11c (N418), anti-CD11b (M1/70), anti-CD64(X54-5/7.1), anti-Ly6C (HK1.4), anti-CD103(2E7), anti-MHC II I-a/I-E (M5/114.15.2), anti-CD135 (A2F10), anti-CD172a (SIRPa) (P84), anti-CD45.1 (A220) anti-CD45.2 (104), anti-Clec9a/DNGR-1 (7H11), anti-Nk1.1 (PK136), anti-CD49b(DX5),anti-CD3e (145/2C11), anti-NKp46 (29A1.4), anti-CD3(17A2), anti-IFNγ (XMG1.2), anti-CD8a (53-6.7), anti-IL-2 (JES6-5H4), anti- H-2k(b) SINFEKL, anti-CD44 (IM7), anti-CD62L (MEL-14) and anti-CD138,Syndecan-1 (281-2). NK cells were identified as live $CD45^{+}NK1.1^{+}CD49b^{+}CD3^{-}MHCII^{-}$ cells. $CD103^{+}$ cDC1 were identified as live $CD45^{+}$ $Cd24^{+}CD103^{+}CD11b^{-}CD11c^{+}MHCII^{+}$ cells. Quantification of total cell numbers by flow cytometry was done using fluorescent beads (Biolegend Precision beads). For intracellular staining of IFNγ and IL-2 *in vitro*, cells were treated with Golgi Plug (Brefeldin A 500x) and were collected 4h later. Intracellular staining was performed in permeabilization buffer (eBioscience) for 30min and cells were subsequently analyzed by flow cytometry. All antibodies were purchased from Biolegend, BD Biosciences. Sorting of tumor cells after retroviral transduction was done using a BD FACSAria or a BD FACSAria Fusion. Purity of cell populations was determined by reanalysis of a fraction of sorted cell samples.

Generation of Batf3 DCs (iCD103) in vitro

For the generation of iCD103-DCs, typically $15x10^{6}$ BM cells were cultured in 10ml RPMI1640 medium supplemented with 10% heat-inactivated FCS (Biochrom), penicillin/streptomycin and 50μM β-mercaptoethanol. Recombinant human FLT3L (300-19, Peprotech) and recombinant murine GMCSF (315-03, Peprotech) were added at d0 of the culture. 5ml complete medium was added between d5 and d6 to minimize apoptosis. Non-adherent cells were harvested on d9, counted and re-plated at $3x10^{6}$cells in 10ml complete medium supplemented with FLT3L and GMCSF as on d0. Non-adherent iCD103-DCs were harvested on d15-16. Cells were then validated by assaying for CD103, CD24, Clec9A, and CD11c by flow cytometry.

Flt3L-mobilized bone marrow derived standard 9-day culture

Bone marrow (BM) cells were harvested from C57BL/6J mice under IACUC-approved protocol M005476. Tissue from *Irf8*-EGFP mice was provided by Dr. Scott Abrams (Roswell Park Cancer Institute, Buffalo, NY). Total BM cells were cultured for 9 days in the presence of 200ng/mL Flt3L, as previously described [152] with the addition of 1μM recombinant versikine or vehicle at

the beginning of culture. Harvested cells were resuspended in FACS buffer (PBS pH7.4, 2mM EDTA, 0.5% BSA). Cell viability was established by Trypan Blue exclusion and $2x10^6$ live cells were stained the following antibodies: anti-CD11c (N418-PE-Cy7, Tonbo); anti-CD103 (2E7-PE, Biolegend); anti-MHCII (M5/114.152-AlexaFluor 700, Biolegend), anti-SiglecH (551-PerCP-Cy5.5, Biolegend) and anti-CD11b (P84-FITC, Biolegend) for 30 minutes on 4°C.

ELISA

Mutu DC cells were left unstimulated or were in vitro stimulated with LPS for 8 or 24 hours at 37°. Cell-free supernatant was assessed for Il27p28 (R and D Quantikine mouse CXCL9 #MCX900) and IL27p28 (R and D Quantikine mouse IL27-p28 #M2728) protein levels by ELISA according to the manufacturer's instructions (R and D). OT-I T cells after being incubated with DCs +/- LPS for 16 hours after DCs were fixed. Cell free supernatants were collected and assessed for IFN- γ levels (R and D Quantikine mouse IFN-γ #P233156).

Immunoblotting

Whole-cell lysates were prepared by boiling cells in Laemmli Sample Buffer (Bio-Rad) supplemented with 100 mM DTT for 10 min at a final concentration of 10^7 cells per milliliter. A total of 10^5 cells or 20 mg protein was resolved by SDS-PAGE and transferred to Immobilon-P PVDF membranes (Millipore). Membranes were blocked in 5% milk in TBS-T (25 mM Tris-HCl [pH 7.4], 0.13 M NaCl, 2.7 mM KCl). Primary Abs (anti-HA [C29F4; Cell Signaling Technologies], anti-IRF8 [D20D8; Cell Signaling Technologies], anti-Batf3 [LS- B12B125; LSBio]) anti-DPEAAE [PA1-1748A; Thermo]) were diluted in 5% milk–TBS-T, and membranes were incubated overnight at 4℃. Secondary Ab–HRP conjugate, as well as anti-GAPDH– HRP conjugate (A00192; GenScript), incubations were carried out for 1 h at room temperature. Signal detection was achieved using Amersham ECL.

Colorectal cancer (CRC) tissue microarray (TMA)

A CRC TMA was created through the University of Wisconsin Carbone Cancer Center Translational Science Biocore Biobank. This TMA contains samples from 122 subjects with colorectal cancer across all stages. For each subject, the TMA contains 2 cores from the primary tumor and 1 core of tumor-associated normal tissue. The tumors utilized in the TMA were selected

for their location and stage, such that an equal distribution of right, left and rectal tumors and stage I through IV cancers were present.

Scoring and analysis of staining patterns

Cytoplasmic and membrane staining of the epithelium and stroma was scored for each core sample by at least three observers including a pathologist (K.A.M.) blinded to clinical parameters. Stained slides were examined using an Olympus BX43 microscope with attached Olympus DP73 digital camera (Olympus Corp, Waltham, MA). Epithelium and stroma were evaluated separately for total VCAN and αDPEAAE staining. Immunostaining for VCAN, αDPEAAE, phosphorylated ERK1/2, and phosphorylated RPS6 was assessed by scoring staining intensity (0 for no staining, 1 for low/weak staining, 2 for moderate staining and 3 for strong/intense staining) and the percentage of cells staining positive (0 for no staining, 1 for >0-10%, 2 for 11-50%, 3 for 51-75% and 4 for >75% staining). For CD8+ detection, the number of tumor infiltrating lymphocytes (TILs) per high-power field (HPF) within the malignant epithelium was calculated using a single area at 400X magnification (ocular 10x with an objective of 40x). Nuclear localization of β-catenin was recorded as present or absent. Tissue cores that were missing, damaged, contained staining artifacts, or had uncertain histology were excluded from the analysis.

Mismatch repair (MMR) analyses

MMR status was determined by IHC for MLH1, MSH6, MSH2, and PMS2. The following prediluted primary antibodies were utilized: MLH1 ((M1) mouse monoclonal, Ventana Medical Systems, Inc, Tucson, AZ); MSH6 ((44) mouse monoclonal, Ventana Medical Systems, Inc); MSH2 ((G219-1129) mouse monoclonal, Ventana Medical Systems, Inc); and PMS2 ((EPR3947) rabbit monoclonal, Ventana Medical Systems, Inc). Staining was performed on a BenchMark ULTRA automated slide staining system and detected using the Opitview DAB IHC detection kit. Absence of staining for these proteins was scored by independent pathology review (K.A.M.). Tumor infiltrating leukocytes were utilized as an internal control.

Immunohistochemistry

Paraffin embedded tumor sections (LLC-EV and LLC-Vkine) and unstained 4-5 μm-thick human lung carcinoma TMA (US Biomax Inc., BC041115e) sections were deparaffinized and rehydrated using standard methods. Antigen retrieval was carried out EDTA buffer (Vector laboratories,

#(CD8 detection) or in citrate buffer, pH 6.0 (Vector laboratories, #H-3300). Primary antibodies included αDPEAAE (PA1-1748A, Thermo Fisher, anti-HA (C29F4, Cell Signaling Technology). The αDPEAAE neoepitope antibody has been previously validated (Foulcer et al, 2015) . Stained slides were examined using an Echo Revolve microscope with attached digital camera. Immunostaining αDPEAAE was assessed by scoring staining intensity (0 for no staining, 1 for low/weak staining, 2 for moderate staining and 3 for strong/intense staining).

RNA isolation and quantitative real-time PCR

RNA was isolated using QIAGEN RNeasy Mini Kit and cDNA was synthesized using the iScript Reverse Transcription Supermix (Biorad). Quantitative real-time (qRT-PCR) analysis was performed using SsoAdvanced Universal SYBR Green Supermix (Biorad) according to the manufacturer's instructions on an CFX96 Touch Real Time PCR detection (Biorad) using the relative standard curve method. The PCR conditions were 2min at 50°C, 10min at 95°C followed by 40 2-step cycles of 15 s at 95°C and 1 min at 60°C. Primers for the targets listed on the table 2 as well as SDHA for normalization control were used to assess relative gene expression.

For necrotic spot analysis, RT² Profiler PCR Array (QIAGEN, Cat. no. PAMM-021Z) was used. In brief, RNA was isolated from tumors and was reverse transcribed using kits mentioned above. cDNA was mixed with RT² SYBR® Green qPCR Mastermix (Cat. no. 330529). The mixture was aliquoted across the RT² Profiler PCR Array (in 96-well format) and was run on the Real Time PCR machine. Data analysis was performed using the online platform for RT² Profiler Data analysis software.

Library preparation for RNA-seq

A total amount of 1 μg RNA per sample was used as input material for the RNA sample preparations. Sequencing libraries were generated using NEBNext® UltraTM RNA Library Prep Kit for Illumina® (NEB, USA) following manufacturer's recommendations and index codes were added to attribute sequences to each sample. Briefly, mRNA was purified from total RNA using poly-T oligo-attached magnetic beads. Fragmentation was carried out using divalent cations under elevated temperature in NEBNext First Strand Synthesis Reaction Buffer (5X). First strand cDNA was synthesized using random hexamer primer and M-MuLV Reverse Transcriptase (RNase H-). Second strand cDNA synthesis was subsequently performed using DNA polymerase I and RNase H. Remaining overhangs were converted into blunt ends via exonuclease/polymerase activities.

After adenylation of 3' ends of DNA fragments, NEBNext Adaptor with hairpin loop structure were ligated to prepare for hybridization. In order to select cDNA fragments of preferentially 150~200 bp in length, the library fragments were purified with AMPure XP system (Beckman Coulter, Beverly, USA). Then 3 μl USER Enzyme (NEB, USA) was used with size-selected, adaptorligated cDNA at 37 °C for 15 min followed by 5 min at 95 °C before PCR. Then PCR was performed with Phusion High-Fidelity DNA polymerase, Universal PCR primers and Index (X) Primer. At last, PCR products were purified (AMPure XP system) and library quality was assessed on the Agilent Bioanalyzer 2100 system. The clustering of the index-coded samples was performed on a cBot Cluster Generation System using PE Cluster Kit cBot-HS (Illumina) according to the manufacturer's instructions. After cluster generation, the library preparations were sequenced on an Illumina platform and paired-end reads were generated.

RNA-Seq data analysis

Raw data (raw reads) of FASTQ format were firstly processed through fastp. In this step, clean data (clean reads) were obtained by removing reads containing adapter and poly-N sequences and reads with low quality from raw data. At the same time, Q20, Q30 and GC content of the clean data were calculated. All the downstream analyses were based on the clean data with high quality. Reference genome and gene model annotation files were downloaded from genome website browser (NCBI/UCSC/Ensembl) directly. Paired-end clean reads were aligned to the reference genome using the Spliced Transcripts Alignment to a Reference (STAR) software. FeatureCounts was used to count the read numbers mapped of each gene. And then RPKM of each gene was calculated based on the length of the gene and reads count mapped to this gene. Differential expression analysis between two conditions/groups (three biological replicates per condition) was performed using DESeq2 R package. DESeq2 provides statistical routines for determining differential expression in digital gene expression data using a model based on the negative binomial distribution. The resulting P values were adjusted using the Benjamini and Hochberg's approach for controlling the False Discovery Rate (FDR). Genes with an adjusted P value < 0.05 found by DESeq2 were assigned as differentially expressed.

Gene Set Enrichment analysis

GSEA (Subramanian, Tamayo, et al, 2005) was performed by comparing MutuDC1940 VKine (treated with PBS, 4h) RNA-seq data to the corresponding MutuDC1940 EV sample. 4736

differentially expressed gene features for each condition were ranked by the signal to noise metric of GSEA and the analysis was performed using the standard weighted enrichment statistic against human gene sets contained in the Molecular Signatures Database that included all (H) Hallmark gene sets, (C2) curated gene sets, and (C3) motif gene sets. The normalized enrichment score (NES) was calculated using 1000 gene set permutations.

NK cell depletion *in vivo*

For depletion of NK cells, mice were injected i.p. with 50 ug of anti-Asialo-GM1 (Wako Pure Chemical Industries, 100µl/mouse) on days -1, 0, 7, 14 post tumor inoculation.

Cross-presentation assay

MutuDC 1940 were cultured and treated with LPS or PBS control respectively overnight. Next day, the cells were harvested and plated on 96-well round bottom plates: 100,000 cells per plate. DCs were then loaded with OVA peptide 257-264 SINFEKL (3ng/ml) and incubated for 4 hours at 37°C. Cross-presenting MutuDC were then washed with 0.1% PBS-BSA and centrifuged at 800 x g. Next, cells were fixed with 50µl per well of freshly made PBS-glutaraldehyde (GTA) 0.008% (vol/vol) and incubated for 5 minutes on ice. Following that step, 50µl of PBS-glycine 0.4M was added to the PBS-GTA 0.008% solution and cells were centrifuged at 800 x g for 2 minutes at 4°C. Plates were subsequently flicked. Finally, 100 µl of PBS-glycine 0.2M was added to each well and centrifugation of the plates at 800 x g for 2 min at 4°C followed. Fixed cross-presenting DCs were then washed twice with 200 µl/well of T-cell culture medium (RPMI 1640 containing 10% heat inactivated FBS, 100 IU/ml penicillin, 100µg/ml streptomycin, 2mM glutamax, 50µM β-mercaptoethanol, 1xMEM non-essential amino acids, 1x sodium pyruvate) before being resuspended in 100 ul/well of the same medium. 100,000 OT-I T cells per well in 100µl T cell culture medium were added (to a final volume of 200µl). The co-cultured OT-I T cells with the cross-fixed DCs were incubated for 18 h at 37°C. Cell activation cocktail with brefeldin A (PMA/Ionomycin and Brefeldin A Biolegend, #423303) was added to the wells 4 hours before harvesting. At the time of the harvest, plates were spun down at 800 x g for 2 minutes at 4°C and supernatant was kept for subsequent cytokine analysis. They were then washed with 100µl of 0.1% PBS-BSA before proceeding with live/dead staining with fixable viability Ghost 780 dye (Tonbo Biosciences) for 30 min at 4°C in PBS. Cells were then washed with 0.1% PBS-BSA and stained

with a cocktail of 70µl/well of the surface markers (CD8a and CD3) for 40 minutes at 4°C. They were then fixed and permeabilized using the eBiosciences fixation and permeabilization buffer set (eBioscience 88-8824-00) according to the manufacturer's instructions followed by intracellular staining of IFNγ and IL-2 in permeabilization buffer. Finally, cells were washed 2 times with 0.1% PBS-BSA, centrifuged and resuspended in 100µl/well of PBS-BSA and then analyzed by flow cytometry.

Computational Modeling of CD8 T Cell Abundance and Versikine Response

Using the RNA-seq data generated from the versikine response assay a list of genes most strongly associated with BATF3-DC response to versikine were identified and analyzed in the lung cancer cohort of TCGA. Differential expression using DESeq2[4] was performed to identify genes that were differentially expressed between the PBS- EV and LPS- versikine conditions. Genes with a q-value of less than 0.1 were considered significant. To define a versikine response gene set of reasonable size, the significant genes with the 100 highest and lowest log fold-change values were identified and defined as the versikine up- and down-regulated gene sets, respectively. These mouse gene sets were then translated into human gene sets using the HGNC Comparison of Orthology Predictions (HCOP) tool[5]. ssGSEA[1] was then used to measure the signature of these two versikine up- and down-regulated gene sets in the 1017 lung samples in the TCGA cohort. To measure overall versikine response, the versikine down-regulated signature was subtracted from the versikine up-regulated signature. This versikine signature was then compared to the CD8 effector T cell signature using an ordinary least squares linear model including the overall immune infiltration signature as a covariate. P-values of less than 0.05 were considered significant.

Statistical analysis

All statistical analysis was performed using GraphPad Prism software (GraphPad version 9). Statistical significance was determined using unpaired two-tailed Student's t-test or unpaired non-parametric Mann-Whitney test as indicated in figure legends. The log-rank (Mantel-Cox) test was used to determine statistical significance for overall survival in *in vivo* experiments. Data are shown as mean ± SD. Significance was assumed with *$p<0.05$; **$p<0.01$;***$p<0.001$.

Table 1. CyTOF panel

Mouse leukocyte panel tumor tissue

Metal	Target	Clone	Isotype	Cell Type	Subset	Product ID	Company
115In	CD3	145-2C11	Armenian Hamster IgG	T cells		100302	Biolegend
141Pr	Ly6C	HK1.4	Rat IgG2c, κ	myeloid	infl. Mono	128002	Biolegend
142Nd	CD11c	N418		DCs		3142003B	Fluidigm
143Nd	TCRb	H57-597		T cells		3143010B	Fluidigm
148Nd	CD11b	M1/70	Rat IgG2b, κ	myeloid		101202	Biolegend
149Sm	CD19	6D5	Rat IgG2a, κ	B cells		115502	Biolegend
150Nd	CD64	X54-5/7.1	Mouse IgG1, κ	myeloid	Mac	139302	Biolegend
151Eu	CD25	3C7		T cells	Treg	3151007B	Fluidigm
152Sm	Siglec-F	1RNM44N	Mouse IgG2a, κ	myeloid	eosino	14-1702-82	eBio
153Eu	CD8a	53-6.7		T cells	cyto. T cells	3153012B	Fluidigm
155Gd	FR4	TH6	Rat IgG2b, κ	T cells	Treg	125102	Biolegend
156Gd	CD103	2E7	Armenian Hamster IgG	DCs	tolerogenic	121402	Biolegend
158Gd	MERTK	2B10C42	Rat IgG2a, κ	myeloid	Mac	151502	Biolegend
159Tb	TCRg/d	GL3		T cells	g/d T cells	3159012B	Fluidigm
160Gd	B220	RA3-6B2		B cells		3160012B	Fluidigm
161Dy	FCeRI	Mar-1	Armenian Hamster IgG	Mast cells	mast/basophils	134302	Biolegend
162Dy	CD115	AFS98	Rat IgG2a, κ	myeloid	mono	135502	Biolegend
163Dy	CD23	B3B4	Rat IgG2a, κ	B cells	B1/B2	101602	Biolegend
164Dy	NK1.1	PK136	Mouse IgG2a, κ	NK cells		108702	Biolegend
165Ho	CD160	7H1	Rat IgG2a, κ	NKT		143002	Biolegend
166Er	F4/80	BM8	Rat IgG2a, κ	myeloid	Mac	123102	Biolegend
167Er	NKP46	29A1.4		NK cells		3167008B	Fluidigm
168Er	IgE	RME-1	Rat IgG1, κ	myeloid		406902	Biolegend
169Tm	IgM	RMM-1	Rat IgG2a, κ	B cells	B1/B2	406502	Biolegend
170Er	CD138	281-2	Rat IgG2a, κ	B cells	plasma	142502	Biolegend
171Yb	CD43	S11	Rat IgG2b	B cells	B1/B2	143202	Biolegend
172Yb	CD4	RM4-5		T cells	T-helper	3172003B	Fluidigm
173Yb	CD117(c-kit)	2B8		Mast cells		3173004B	Fluidigm
174Yb	MHC-II	M5/114.15.2		DCs		3174003B	Fluidigm
175Lu	Ly6G	1A8	Rat IgG2a, κ	myeloid	granulocytes	127602	Biolegend
89Y	CD45	30-F11		leukocytes		3089005B (89Y)	Fluidigm

Table 2. List of RT-PCR Primers

Primers	Source	Cat. No
CXCL9	Quantitect	QT00097062
CXCL10	Quantitect	QT00093436
IRF8	Quantitect	QT00026026
Batf3	Quantitect	QT00252077
Id2	Quantitect	QT01038870
IL27p28	Quantitect	QT00236250
EBI3	Quantitect	QT01014104
SDHA	Quantitect	QT00265237
Ccl7	Quantitect	QT00171458
IL-15	Quantitect	QT00107653
IL-18	Quantitect	QT00171129
IL-23	Quantitect	QT01663613
IL-12a	Quantitect	QT01048334
IL-12b	Quantitect	QT00153643
CCL5	Quantitect	QT01747165
Flit3L	Quantitect	QT00199430
IFNy	Quantitect	QT01038821
XCL1	Quantitect	QT00095228
CSF2	Quantitect	QT00251286
IFNa2	Quantitect	QT00253092
IFNa4	Quantitect	QT01774353
IFNb	Quantitect	QT00203763

References

1. Wight, T.N., *Versican: a versatile extracellular matrix proteoglycan in cell biology.* Curr Opin Cell Biol, 2002. **14**(5): p. 617-23.
2. Iozzo, R.V., et al., *Mapping of the versican proteoglycan gene (CSPG2) to the long arm of human chromosome 5 (5q12-5q14).* Genomics, 1992. **14**(4): p. 845-51.
3. Naso, M.F., et al., *Expression pattern and mapping of the murine versican gene (Cspg2) to chromosome 13.* Genomics, 1995. **29**(1): p. 297-300.
4. Wu, Y.J., et al., *The interaction of versican with its binding partners.* Cell Res, 2005. **15**(7): p. 483-94.
5. Wight, T.N., *Provisional matrix: A role for versican and hyaluronan.* Matrix Biol, 2017. **60-61**: p. 38-56.
6. Aspberg, A., et al., *The C-type lectin domains of lecticans, a family of aggregating chondroitin sulfate proteoglycans, bind tenascin-R by protein-protein interactions independent of carbohydrate moiety.* Proc Natl Acad Sci U S A, 1997. **94**(19): p. 10116-21.
7. Olin, A.I., et al., *The proteoglycans aggrecan and Versican form networks with fibulin-2 through their lectin domain binding.* J Biol Chem, 2001. **276**(2): p. 1253-61.
8. Isogai, Z., et al., *Versican interacts with fibrillin-1 and links extracellular microfibrils to other connective tissue networks.* J Biol Chem, 2002. **277**(6): p. 4565-72.
9. Touab, M., et al., *Versican is differentially expressed in human melanoma and may play a role in tumor development.* Am J Pathol, 2002. **160**(2): p. 549-57.
10. Yamagata, M., et al., *Chondroitin sulfate proteoglycan (PG-M-like proteoglycan) is involved in the binding of hyaluronic acid to cellular fibronectin.* J Biol Chem, 1986. **261**(29): p. 13526-35.
11. Wijelath, E.S., et al., *Novel vascular endothelial growth factor binding domains of fibronectin enhance vascular endothelial growth factor biological activity.* Circ Res, 2002. **91**(1): p. 25-31.
12. Kawashima, H., et al., *Identification and characterization of ligands for L-selectin in the kidney. I. Versican, a large chondroitin sulfate proteoglycan, is a ligand for L-selectin.* Int Immunol, 1999. **11**(3): p. 393-405.
13. Kawashima, H., et al., *Binding of a large chondroitin sulfate/dermatan sulfate proteoglycan, versican, to L-selectin, P-selectin, and CD44.* J Biol Chem, 2000. **275**(45): p. 35448-56.
14. Nandadasa, S., S. Foulcer, and S.S. Apte, *The multiple, complex roles of versican and its proteolytic turnover by ADAMTS proteases during embryogenesis.* Matrix Biol, 2014. **35**: p. 34-41.
15. Kern, C.B., et al., *Versican proteolysis mediates myocardial regression during outflow tract development.* Dev Dyn, 2007. **236**(3): p. 671-83.
16. Enomoto, H., et al., *Cooperation of two ADAMTS metalloproteases in closure of the mouse palate identifies a requirement for versican proteolysis in regulating palatal mesenchyme proliferation.* Development, 2010. **137**(23): p. 4029-38.
17. Rao, C., et al., *A defect in a novel ADAMTS family member is the cause of the belted white-spotting mutation.* Development, 2003. **130**(19): p. 4665-72.
18. McCulloch, D.R., et al., *ADAMTS metalloproteases generate active versican fragments that regulate interdigital web regression.* Dev Cell, 2009. **17**(5): p. 687-98.
19. Kern, C.B., et al., *Proteolytic cleavage of versican during cardiac cushion morphogenesis.* Dev Dyn, 2006. **235**(8): p. 2238-47.
20. Kern, C.B., et al., *Reduced versican cleavage due to Adamts9 haploinsufficiency is associated with cardiac and aortic anomalies.* Matrix Biol, 2010. **29**(4): p. 304-16.
21. Zhang, Z., L. Miao, and L. Wang, *Inflammation amplification by Versican: the first mediator.* Int J Mol Sci, 2012. **13**(6): p. 6873-82.

22. Wight, T.N., I. Kang, and M.J. Merrilees, *Versican and the control of inflammation.* Matrix Biol, 2014. **35**: p. 152-61.
23. Zheng, P.S., et al., *PG-M/versican binds to P-selectin glycoprotein ligand-1 and mediates leukocyte aggregation.* J Cell Sci, 2004. **117**(Pt 24): p. 5887-95.
24. Vaday, G.G. and O. Lider, *Extracellular matrix moieties, cytokines, and enzymes: dynamic effects on immune cell behavior and inflammation.* J Leukoc Biol, 2000. **67**(2): p. 149-59.
25. Schor, H., G.G. Vaday, and O. Lider, *Modulation of leukocyte behavior by an inflamed extracellular matrix.* Dev Immunol, 2000. **7**(2-4): p. 227-38.
26. Adair-Kirk, T.L. and R.M. Senior, *Fragments of extracellular matrix as mediators of inflammation.* Int J Biochem Cell Biol, 2008. **40**(6-7): p. 1101-10.
27. Arroyo, A.G. and M.L. Iruela-Arispe, *Extracellular matrix, inflammation, and the angiogenic response.* Cardiovasc Res, 2010. **86**(2): p. 226-35.
28. Evanko, S.P., et al., *Hyaluronan and versican in the control of human T-lymphocyte adhesion and migration.* Matrix Biol, 2012. **31**(2): p. 90-100.
29. Fu, Y., et al., *Proteolytic cleavage of versican and involvement of ADAMTS-1 in VEGF-A/VPF-induced pathological angiogenesis.* J Histochem Cytochem, 2011. **59**(5): p. 463-73.
30. Potter-Perigo, S., et al., *Polyinosine-polycytidylic acid stimulates versican accumulation in the extracellular matrix promoting monocyte adhesion.* Am J Respir Cell Mol Biol, 2010. **43**(1): p. 109-20.
31. Hirose, J., et al., *Versican interacts with chemokines and modulates cellular responses.* J Biol Chem, 2001. **276**(7): p. 5228-34.
32. Gill, S., T.N. Wight, and C.W. Frevert, *Proteoglycans: key regulators of pulmonary inflammation and the innate immune response to lung infection.* Anat Rec (Hoboken), 2010. **293**(6): p. 968-81.
33. Wight, T.N., et al., *Versican and the regulation of cell phenotype in disease.* Biochim Biophys Acta, 2014. **1840**(8): p. 2441-51.
34. Wang, W., et al., *Ligation of TLR2 by versican: a link between inflammation and metastasis.* Arch Med Res, 2009. **40**(4): p. 321-3.
35. Holmbeck, K., et al., *MT1-MMP-deficient mice develop dwarfism, osteopenia, arthritis, and connective tissue disease due to inadequate collagen turnover.* Cell, 1999. **99**(1): p. 81-92.
36. Hotary, K., et al., *Regulation of cell invasion and morphogenesis in a three-dimensional type I collagen matrix by membrane-type matrix metalloproteinases 1, 2, and 3.* J Cell Biol, 2000. **149**(6): p. 1309-23.
37. Hotary, K.B., et al., *Membrane type I matrix metalloproteinase usurps tumor growth control imposed by the three-dimensional extracellular matrix.* Cell, 2003. **114**(1): p. 33-45.
38. Malla, N., et al., *In vitro reconstitution of complexes between pro-matrix metalloproteinase-9 and the proteoglycans serglycin and versican.* FEBS J, 2013. **280**(12): p. 2870-87.
39. Masuda, A., et al., *Versican is upregulated in circulating monocytes in patients with systemic sclerosis and amplifies a CCL2-mediated pathogenic loop.* Arthritis Res Ther, 2013. **15**(4): p. R74.
40. Bogen, O., et al., *Dependence of monocyte chemoattractant protein 1 induced hyperalgesia on the isolectin B4-binding protein versican.* Neuroscience, 2009. **159**(2): p. 780-6.
41. Chang, M.Y., et al., *Reprint of: A rapid increase in macrophage-derived versican and hyaluronan in infectious lung disease.* Matrix Biol, 2014. **35**: p. 162-73.
42. Huang, J., et al., *Enhanced proteoglycan deposition in the airway wall of atopic asthmatics.* Am J Respir Crit Care Med, 1999. **160**(2): p. 725-9.
43. Araujo, B.B., et al., *Extracellular matrix components and regulators in the airway smooth muscle in asthma.* Eur Respir J, 2008. **32**(1): p. 61-9.
44. Morales, M.M., et al., *Small airway remodeling in acute respiratory distress syndrome: a study in autopsy lung tissue.* Crit Care, 2011. **15**(1): p. R4.

45. Bensadoun, E.S., et al., *Proteoglycan deposition in pulmonary fibrosis.* Am J Respir Crit Care Med, 1996. **154**(6 Pt 1): p. 1819-28.
46. Andersson-Sjöland, A., et al., *Versican in inflammation and tissue remodeling: the impact on lung disorders.* Glycobiology, 2015. **25**(3): p. 243-51.
47. Pini, L., et al., *Differences in proteoglycan deposition in the airways of moderate and severe asthmatics.* Eur Respir J, 2007. **29**(1): p. 71-7.
48. Nihlberg, K., et al., *Altered matrix production in the distal airways of individuals with asthma.* Thorax, 2010. **65**(8): p. 670-6.
49. Westergren-Thorsson, G., et al., *Correlation between airway responsiveness and proteoglycan production by bronchial fibroblasts from normal and asthmatic subjects.* Int J Biochem Cell Biol, 2002. **34**(10): p. 1256-67.
50. de Medeiros Matsushita, M., et al., *Airway proteoglycans are differentially altered in fatal asthma.* J Pathol, 2005. **207**(1): p. 102-10.
51. Hallgren, O., et al., *Altered fibroblast proteoglycan production in COPD.* Respir Res, 2010. **11**: p. 55.
52. Merrilees, M.J., et al., *Changes in elastin, elastin binding protein and versican in alveoli in chronic obstructive pulmonary disease.* Respir Res, 2008. **9**: p. 41.
53. Merrilees, M.J., et al., *Retrovirally mediated overexpression of versican v3 by arterial smooth muscle cells induces tropoelastin synthesis and elastic fiber formation in vitro and in neointima after vascular injury.* Circ Res, 2002. **90**(4): p. 481-7.
54. Huang, R., et al., *Inhibition of versican synthesis by antisense alters smooth muscle cell phenotype and induces elastic fiber formation in vitro and in neointima after vessel injury.* Circ Res, 2006. **98**(3): p. 370-7.
55. McMahon, M., et al., *ADAMTS5 Is a Critical Regulator of Virus-Specific T Cell Immunity.* PLoS Biol, 2016. **14**(11): p. e1002580.
56. Hanahan, D. and R.A. Weinberg, *Hallmarks of cancer: the next generation.* Cell, 2011. **144**(5): p. 646-74.
57. Kim, S., et al., *Carcinoma-produced factors activate myeloid cells through TLR2 to stimulate metastasis.* Nature, 2009. **457**(7225): p. 102-6.
58. Li, D., et al., *Tumor-produced versican V1 enhances hCAP18/LL-37 expression in macrophages through activation of TLR2 and vitamin D3 signaling to promote ovarian cancer progression in vitro.* PLoS One, 2013. **8**(2): p. e56616.
59. Keire, P.A., et al., *A role for versican in the development of leiomyosarcoma.* J Biol Chem, 2014. **289**(49): p. 34089-103.
60. Xia, L., et al., *Forkhead box Q1 promotes hepatocellular carcinoma metastasis by transactivating ZEB2 and VersicanV1 expression.* Hepatology, 2014. **59**(3): p. 958-73.
61. Bögels, M., et al., *Carcinoma origin dictates differential skewing of monocyte function.* Oncoimmunology, 2012. **1**(6): p. 798-809.
62. Hu, F., et al., *Glioma-derived versican promotes tumor expansion via glioma-associated microglial/macrophages Toll-like receptor 2 signaling.* Neuro Oncol, 2015. **17**(2): p. 200-10.
63. Said, N. and D. Theodorescu, *RhoGDI2 suppresses bladder cancer metastasis via reduction of inflammation in the tumor microenvironment.* Oncoimmunology, 2012. **1**(7): p. 1175-1177.
64. de Lima, C.R., et al., *Changes in glycosaminoglycans and proteoglycans of normal breast and fibroadenoma during the menstrual cycle.* Biochim Biophys Acta, 2012. **1820**(7): p. 1009-19.
65. Kischel, P., et al., *Versican overexpression in human breast cancer lesions: known and new isoforms for stromal tumor targeting.* Int J Cancer, 2010. **126**(3): p. 640-50.

66. Ricciardelli, C., et al., *Regulation of stromal versican expression by breast cancer cells and importance to relapse-free survival in patients with node-negative primary breast cancer.* Clin Cancer Res, 2002. **8**(4): p. 1054-60.
67. Takahashi, Y., et al., *Versican G1 and G3 domains are upregulated and latent transforming growth factor-β binding protein-4 is downregulated in breast cancer stroma.* Breast Cancer, 2012. **19**(1): p. 46-53.
68. Iozzo, R.V., *Tumor stroma as a regulator of neoplastic behavior. Agonistic and antagonistic elements embedded in the same connective tissue.* Lab Invest, 1995. **73**(2): p. 157-60.
69. Pukkila, M.J., et al., *Versican expression in pharyngeal squamous cell carcinoma: an immunohistochemical study.* J Clin Pathol, 2004. **57**(7): p. 735-9.
70. Yeung, T.L., et al., *TGF-β modulates ovarian cancer invasion by upregulating CAF-derived versican in the tumor microenvironment.* Cancer Res, 2013. **73**(16): p. 5016-28.
71. Ricciardelli, C., et al., *Elevated levels of versican but not decorin predict disease progression in early-stage prostate cancer.* Clin Cancer Res, 1998. **4**(4): p. 963-71.
72. Sakko, A.J., et al., *Versican accumulation in human prostatic fibroblast cultures is enhanced by prostate cancer cell-derived transforming growth factor beta1.* Cancer Res, 2001. **61**(3): p. 926-30.
73. Sakko, A.J., et al., *Modulation of prostate cancer cell attachment to matrix by versican.* Cancer Res, 2003. **63**(16): p. 4786-91.
74. Brown, L.F., et al., *Vascular stroma formation in carcinoma in situ, invasive carcinoma, and metastatic carcinoma of the breast.* Clin Cancer Res, 1999. **5**(5): p. 1041-56.
75. Van Bockstal, M., et al., *Differential regulation of extracellular matrix protein expression in carcinoma-associated fibroblasts by TGF-β1 regulates cancer cell spreading but not adhesion.* Oncoscience, 2014. **1**(10): p. 634-48.
76. Onken, J., et al., *Versican isoform V1 regulates proliferation and migration in high-grade gliomas.* J Neurooncol, 2014. **120**(1): p. 73-83.
77. Oktem, G., et al., *Cancer stem cell differentiation: TGFβ1 and versican may trigger molecules for the organization of tumor spheroids.* Oncol Rep, 2014. **32**(2): p. 641-9.
78. Kodama, J., et al., *Prognostic significance of stromal versican expression in human endometrial cancer.* Ann Oncol, 2007. **18**(2): p. 269-74.
79. Gao, D., et al., *Myeloid progenitor cells in the premetastatic lung promote metastases by inducing mesenchymal to epithelial transition.* Cancer Res, 2012. **72**(6): p. 1384-94.
80. Gao, D., et al., *Microenvironmental regulation of epithelial-mesenchymal transitions in cancer.* Cancer Res, 2012. **72**(19): p. 4883-9.
81. Senda, M., R. Fukuyama, and T. Nagasaka, *Kinetics of versican-expressing macrophages in bone marrow after cord blood stem cell transplantation for treatment of acute myelogenous leukaemia.* J Clin Pathol, 2016. **69**(10): p. 906-11.
82. Hope, C., et al., *TPL2 kinase regulates the inflammatory milieu of the myeloma niche.* Blood, 2014. **123**(21): p. 3305-15.
83. Yang, B.L., et al., *Cell adhesion and proliferation mediated through the G1 domain of versican.* J Cell Biochem, 1999. **72**(2): p. 210-20.
84. Du, W.W., et al., *Versican G3 promotes mouse mammary tumor cell growth, migration, and metastasis by influencing EGF receptor signaling.* PLoS One, 2010. **5**(11): p. e13828.
85. Zhang, Y., et al., *The G3 domain of versican enhances cell proliferation via epidermial growth factor-like motifs.* J Biol Chem, 1998. **273**(33): p. 21342-51.
86. Zhang, Y., et al., *Promotion of chondrocyte proliferation by versican mediated by G1 domain and EGF-like motifs.* J Cell Biochem, 1999. **73**(4): p. 445-57.

87. Du, W.W., et al., *The role of versican in modulating breast cancer cell self-renewal.* Mol Cancer Res, 2013. **11**(5): p. 443-55.
88. Evanko, S.P., J.C. Angello, and T.N. Wight, *Formation of hyaluronan- and versican-rich pericellular matrix is required for proliferation and migration of vascular smooth muscle cells.* Arterioscler Thromb Vasc Biol, 1999. **19**(4): p. 1004-13.
89. Evanko, S.P., et al., *Platelet-derived growth factor stimulates the formation of versican-hyaluronan aggregates and pericellular matrix expansion in arterial smooth muscle cells.* Arch Biochem Biophys, 2001. **394**(1): p. 29-38.
90. Schönherr, E., M.G. Kinsella, and T.N. Wight, *Genistein selectively inhibits platelet-derived growth factor-stimulated versican biosynthesis in monkey arterial smooth muscle cells.* Arch Biochem Biophys, 1997. **339**(2): p. 353-61.
91. Igney, F.H. and P.H. Krammer, *Death and anti-death: tumour resistance to apoptosis.* Nat Rev Cancer, 2002. **2**(4): p. 277-88.
92. LaPierre, D.P., et al., *The ability of versican to simultaneously cause apoptotic resistance and sensitivity.* Cancer Res, 2007. **67**(10): p. 4742-50.
93. Cattaruzza, S., et al., *The globular domains of PG-M/versican modulate the proliferation-apoptosis equilibrium and invasive capabilities of tumor cells.* FASEB J, 2004. **18**(6): p. 779-81.
94. Wu, Y., et al., *beta 1-Integrin-mediated glioma cell adhesion and free radical-induced apoptosis are regulated by binding to a C-terminal domain of PG-M/versican.* J Biol Chem, 2002. **277**(14): p. 12294-301.
95. Wu, Y., et al., *Versican protects cells from oxidative stress-induced apoptosis.* Matrix Biol, 2005. **24**(1): p. 3-13.
96. Asano, K., et al., *Stromal Versican Regulates Tumor Growth by Promoting Angiogenesis.* Sci Rep, 2017. **7**(1): p. 17225.
97. Zheng, P.S., et al., *Versican/PG-M G3 domain promotes tumor growth and angiogenesis.* FASEB J, 2004. **18**(6): p. 754-6.
98. Yang, W. and A.J. Yee, *Versican V2 isoform enhances angiogenesis by regulating endothelial cell activities and fibronectin expression.* FEBS Lett, 2013. **587**(2): p. 185-92.
99. Birbrair, A., et al., *Type-2 pericytes participate in normal and tumoral angiogenesis.* Am J Physiol Cell Physiol, 2014. **307**(1): p. C25-38.
100. Diefenderfer, D.L. and C.T. Brighton, *Microvascular pericytes express aggrecan message which is regulated by BMP-2.* Biochem Biophys Res Commun, 2000. **269**(1): p. 172-8.
101. Ricciardelli, C., et al., *The biological role and regulation of versican levels in cancer.* Cancer Metastasis Rev, 2009. **28**(1-2): p. 233-45.
102. Ricciardelli, C., et al., *Elevated stromal chondroitin sulfate glycosaminoglycan predicts progression in early-stage prostate cancer.* Clin Cancer Res, 1997. **3**(6): p. 983-92.
103. Ricciardelli, C., et al., *Elevated levels of peritumoral chondroitin sulfate are predictive of poor prognosis in patients treated by radical prostatectomy for early-stage prostate cancer.* Cancer Res, 1999. **59**(10): p. 2324-8.
104. Suwiwat, S., et al., *Expression of extracellular matrix components versican, chondroitin sulfate, tenascin, and hyaluronan, and their association with disease outcome in node-negative breast cancer.* Clin Cancer Res, 2004. **10**(7): p. 2491-8.
105. Ang, L.C., et al., *Versican enhances locomotion of astrocytoma cells and reduces cell adhesion through its G1 domain.* J Neuropathol Exp Neurol, 1999. **58**(6): p. 597-605.
106. Ricciardelli, C., et al., *Formation of hyaluronan- and versican-rich pericellular matrix by prostate cancer cells promotes cell motility.* J Biol Chem, 2007. **282**(14): p. 10814-25.

107. Skandalis, S.S., et al., *The greatly increased amounts of accumulated versican and decorin with specific post-translational modifications may be closely associated with the malignant phenotype of pancreatic cancer.* Biochim Biophys Acta, 2006. **1760**(8): p. 1217-25.
108. Kusumoto, T., et al., *Clinical significance of syndecan-1 and versican expression in human epithelial ovarian cancer.* Oncol Rep, 2010. **23**(4): p. 917-25.
109. Gorter, A., et al., *Versican expression is associated with tumor-infiltrating CD8-positive T cells and infiltration depth in cervical cancer.* Mod Pathol, 2010. **23**(12): p. 1605-15.
110. Hanekamp, E.E., et al., *Consequences of loss of progesterone receptor expression in development of invasive endometrial cancer.* Clin Cancer Res, 2003. **9**(11): p. 4190-9.
111. Hernández, D., et al., *Role of versican V0/V1 and CD44 in the regulation of human melanoma cell behavior.* Int J Mol Med, 2011. **27**(2): p. 269-75.
112. Ween, M.P., et al., *Versican induces a pro-metastatic ovarian cancer cell behavior which can be inhibited by small hyaluronan oligosaccharides.* Clin Exp Metastasis, 2011. **28**(2): p. 113-25.
113. Mitsui, Y., et al., *Versican Promotes Tumor Progression, Metastasis and Predicts Poor Prognosis in Renal Carcinoma.* Mol Cancer Res, 2017. **15**(7): p. 884-895.
114. Luo, J.L., et al., *Inhibition of NF-kappaB in cancer cells converts inflammation- induced tumor growth mediated by TNFalpha to TRAIL-mediated tumor regression.* Cancer Cell, 2004. **6**(3): p. 297-305.
115. Tracey, K.J., et al., *Shock and tissue injury induced by recombinant human cachectin.* Science, 1986. **234**(4775): p. 470-4.
116. Spranger, S., et al., *Tumor-Residing Batf3 Dendritic Cells Are Required for Effector T Cell Trafficking and Adoptive T Cell Therapy.* Cancer Cell, 2017. **31**(5): p. 711-723.e4.
117. Noy, R. and J.W. Pollard, *Tumor-associated macrophages: from mechanisms to therapy.* Immunity, 2014. **41**(1): p. 49-61.
118. Fu, C. and A. Jiang, *Dendritic Cells and CD8 T Cell Immunity in Tumor Microenvironment.* Front Immunol, 2018. **9**: p. 3059.
119. Tang, M., J. Diao, and M.S. Cattral, *Molecular mechanisms involved in dendritic cell dysfunction in cancer.* Cell Mol Life Sci, 2017. **74**(5): p. 761-776.
120. Tang, M., et al., *Toll-like Receptor 2 Activation Promotes Tumor Dendritic Cell Dysfunction by Regulating IL-6 and IL-10 Receptor Signaling.* Cell Rep, 2015. **13**(12): p. 2851-64.
121. Bailur, J.K., et al., *Early alterations in stem-like/resident T cells, innate and myeloid cells in the bone marrow in preneoplastic gammopathy.* JCI Insight, 2019. **5**.
122. Arana, P., et al., *High-Throughput Characterization and New Insight into the Role of Tumor Associated Macrophages (TAMs) in Multiple Myeloma (MM).* Blood, 2016. **128**(22): p. 482-482.
123. Pappas, A.G., et al., *Versican modulates tumor-associated macrophage properties to stimulate mesothelioma growth.* Oncoimmunology, 2019. **8**(2): p. e1537427.
124. Dhakal, B., et al., *Versican proteolysis predicts immune effector infiltration and post-transplant survival in myeloma.* Leuk Lymphoma, 2019: p. 1-5.
125. Hope, C., et al., *Immunoregulatory roles of versican proteolysis in the myeloma microenvironment.* Blood, 2016. **128**(5): p. 680-5.
126. Hope, C., et al., *Versican-Derived Matrikines Regulate Batf3-Dendritic Cell Differentiation and Promote T Cell Infiltration in Colorectal Cancer.* J Immunol, 2017. **199**(5): p. 1933-1941.
127. Grajales-Reyes, G.E., et al., *Batf3 maintains autoactivation of Irf8 for commitment of a CD8alpha(+) conventional DC clonogenic progenitor.* Nat Immunol, 2015. **16**(7): p. 708-17.
128. Murphy, K.M., *Transcriptional control of dendritic cell development.* Adv Immunol, 2013. **120**: p. 239-67.
129. Pukkila, M., et al., *High stromal versican expression predicts unfavourable outcome in oral squamous cell carcinoma.* J Clin Pathol, 2007. **60**(3): p. 267-72.

130. Tanaka, Y., et al., *Sharpin promotes hepatocellular carcinoma progression via transactivation of Versican expression.* Oncogenesis, 2016. **5**(12): p. e277.
131. Suhovskih, A.V., et al., *Proteoglycans as potential microenvironmental biomarkers for colon cancer.* Cell Tissue Res, 2015. **361**(3): p. 833-44.
132. Voutilainen, K., et al., *Versican in epithelial ovarian cancer: relation to hyaluronan, clinicopathologic factors and prognosis.* Int J Cancer, 2003. **107**(3): p. 359-64.
133. Pan, S., et al., *Quantitative proteomics analysis integrated with microarray data reveals that extracellular matrix proteins, catenins, and p53 binding protein 1 are important for chemotherapy response in ovarian cancers.* OMICS, 2009. **13**(4): p. 345-54.
134. Mushtaq, M.U., et al., *Tumor matrix remodeling and novel immunotherapies: the promise of matrix-derived immune biomarkers.* J Immunother Cancer, 2018. **6**(1): p. 65.
135. Papadas, A., et al., *Versican and Versican-matrikines in Cancer Progression, Inflammation, and Immunity.* J Histochem Cytochem, 2020. **68**(12): p. 871-885.
136. Maquart, F.X., et al., *An introduction to matrikines: extracellular matrix-derived peptides which regulate cell activity. Implication in tumor invasion.* Crit Rev Oncol Hematol, 2004. **49**(3): p. 199-202.
137. Gaggar, A. and N. Weathington, *Bioactive extracellular matrix fragments in lung health and disease.* J Clin Invest, 2016. **126**(9): p. 3176-84.
138. Bonnans, C., J. Chou, and Z. Werb, *Remodelling the extracellular matrix in development and disease.* Nat Rev Mol Cell Biol, 2014. **15**(12): p. 786-801.
139. Wang, K. and M. Karin, *Tumor-Elicited Inflammation and Colorectal Cancer.* Adv Cancer Res, 2015. **128**: p. 173-96.
140. Bupathi, M. and C. Wu, *Biomarkers for immune therapy in colorectal cancer: mismatch-repair deficiency and others.* J Gastrointest Oncol, 2016. **7**(5): p. 713-720.
141. Lynch, D. and A. Murphy, *The emerging role of immunotherapy in colorectal cancer.* Ann Transl Med, 2016. **4**(16): p. 305.
142. Westdorp, H., et al., *Opportunities for immunotherapy in microsatellite instable colorectal cancer.* Cancer Immunol Immunother, 2016. **65**(10): p. 1249-59.
143. Sichien, D., et al., *IRF8 Transcription Factor Controls Survival and Function of Terminally Differentiated Conventional and Plasmacytoid Dendritic Cells, Respectively.* Immunity, 2016.
144. Broz, M.L., et al., *Dissecting the tumor myeloid compartment reveals rare activating antigen-presenting cells critical for T cell immunity.* Cancer Cell, 2014. **26**(5): p. 638-52.
145. Salmon, H., et al., *Expansion and Activation of CD103(+) Dendritic Cell Progenitors at the Tumor Site Enhances Tumor Responses to Therapeutic PD-L1 and BRAF Inhibition.* Immunity, 2016. **44**(4): p. 924-38.
146. Spranger, S., R. Bao, and T.F. Gajewski, *Melanoma-intrinsic beta-catenin signalling prevents anti-tumour immunity.* Nature, 2015. **523**(7559): p. 231-5.
147. Ruffell, B., et al., *Macrophage IL-10 blocks CD8+ T cell-dependent responses to chemotherapy by suppressing IL-12 expression in intratumoral dendritic cells.* Cancer Cell, 2014. **26**(5): p. 623-37.
148. Spranger, S., et al., *Tumor-Residing Batf3 Dendritic Cells Are Required for Effector T Cell Trafficking and Adoptive T Cell Therapy.* Cancer Cell, 2017. **31**(5): p. 711-723 e4.
149. Lavin, Y., et al., *Innate Immune Landscape in Early Lung Adenocarcinoma by Paired Single-Cell Analyses.* Cell, 2017. **169**(4): p. 750-765 e17.
150. Laoui, D., et al., *The tumour microenvironment harbours ontogenically distinct dendritic cell populations with opposing effects on tumour immunity.* Nat Commun, 2016. **7**: p. 13720.
151. Sánchez-Paulete, A.R., et al., *Cancer Immunotherapy with Immunomodulatory Anti-CD137 and Anti-PD-1 Monoclonal Antibodies Requires BATF3-Dependent Dendritic Cells.* Cancer Discov, 2016. **6**(1): p. 71-9.

152. Brasel, K., et al., *Generation of murine dendritic cells from flt3-ligand-supplemented bone marrow cultures.* Blood, 2000. **96**(9): p. 3029-39.
153. Mayer, C.T., et al., *Selective and efficient generation of functional Batf3-dependent CD103+ dendritic cells from mouse bone marrow.* Blood, 2014. **124**(20): p. 3081-91.
154. Gajewski, T.F., *The Next Hurdle in Cancer Immunotherapy: Overcoming the Non-T-Cell-Inflamed Tumor Microenvironment.* Semin Oncol, 2015. **42**(4): p. 663-71.
155. Ochoa de Olza, M., et al., *Turning up the heat on non-immunoreactive tumours: opportunities for clinical development.* Lancet Oncol, 2020. **21**(9): p. e419-e430.
156. Garris, C.S. and J.J. Luke, *Dendritic Cells, the T-cell-inflamed Tumor Microenvironment, and Immunotherapy Treatment Response.* Clin Cancer Res, 2020. **26**(15): p. 3901-3907.
157. Gajewski, T.F. and K.R. Cron, *cDC1 dysregulation in cancer: An opportunity for intervention.* J Exp Med, 2020. **217**(8).
158. Binnewies, M., et al., *Understanding the tumor immune microenvironment (TIME) for effective therapy.* Nat Med, 2018. **24**(5): p. 541-550.
159. Merad, M., et al., *The dendritic cell lineage: ontogeny and function of dendritic cells and their subsets in the steady state and the inflamed setting.* Annu Rev Immunol, 2013. **31**: p. 563-604.
160. Bodder, J., et al., *Harnessing the cDC1-NK Cross-Talk in the Tumor Microenvironment to Battle Cancer.* Front Immunol, 2020. **11**: p. 631713.
161. Peterson, E.E. and K.C. Barry, *The Natural Killer-Dendritic Cell Immune Axis in Anti-Cancer Immunity and Immunotherapy.* Front Immunol, 2020. **11**: p. 621254.
162. Huntington, N.D., J. Cursons, and J. Rautela, *The cancer-natural killer cell immunity cycle.* Nat Rev Cancer, 2020. **20**(8): p. 437-454.
163. Mittal, D., et al., *Interleukin-12 from CD103(+) Batf3-Dependent Dendritic Cells Required for NK-Cell Suppression of Metastasis.* Cancer Immunol Res, 2017. **5**(12): p. 1098-1108.
164. Barry, K.C., et al., *A natural killer-dendritic cell axis defines checkpoint therapy-responsive tumor microenvironments.* Nat Med, 2018.
165. Bottcher, J.P., et al., *NK Cells Stimulate Recruitment of cDC1 into the Tumor Microenvironment Promoting Cancer Immune Control.* Cell, 2018. **172**(5): p. 1022-1037 e14.
166. Sorokin, L., *The impact of the extracellular matrix on inflammation.* Nat Rev Immunol, 2010. **10**(10): p. 712-23.
167. Bejarano, L., M.J.C. Jordao, and J.A. Joyce, *Therapeutic Targeting of the Tumor Microenvironment.* Cancer Discov, 2021. **11**(4): p. 933-959.
168. Rossi, G.R., E.S. Trindade, and F. Souza-Fonseca-Guimaraes, *Tumor Microenvironment-Associated Extracellular Matrix Components Regulate NK Cell Function.* Front Immunol, 2020. **11**: p. 73.
169. Schaefer, L., *Complexity of danger: the diverse nature of damage-associated molecular patterns.* J Biol Chem, 2014. **289**(51): p. 35237-45.
170. Schaefer, L. and R.V. Iozzo, *Small leucine-rich proteoglycans, at the crossroad of cancer growth and inflammation.* Curr Opin Genet Dev, 2012. **22**(1): p. 56-7.
171. Hynes, R.O. and A. Naba, *Overview of the matrisome--an inventory of extracellular matrix constituents and functions.* Cold Spring Harb Perspect Biol, 2012. **4**(1): p. a004903.
172. Papadas, A., et al., *Versican and Versican-matrikines in Cancer Progression, Inflammation, and Immunity.* J Histochem Cytochem, 2020: p. 22155420937098.
173. Papadas, A. and F. Asimakopoulos, *Versican in the Tumor Microenvironment.* Adv Exp Med Biol, 2020. **1272**: p. 55-72.
174. Wight, T.N., et al., *Versican-A Critical Extracellular Matrix Regulator of Immunity and Inflammation.* Front Immunol, 2020. **11**: p. 512.
175. Wight, T.N., et al., *Versican and the regulation of cell phenotype in disease.* Biochim Biophys Acta, 2014.

176. Islam, S. and H. Watanabe, *Versican: A Dynamic Regulator of the Extracellular Matrix.* J Histochem Cytochem, 2020. **68**(11): p. 763-775.
177. Mjaatvedt, C.H., et al., *The Cspg2 gene, disrupted in the hdf mutant, is required for right cardiac chamber and endocardial cushion formation.* Dev Biol, 1998. **202**(1): p. 56-66.
178. Du, W.W., et al., *Versican G3 domain modulates breast cancer cell apoptosis: a mechanism for breast cancer cell response to chemotherapy and EGFR therapy.* PLoS One, 2011. **6**(11): p. e26396.
179. Du, W.W., W. Yang, and A.J. Yee, *Roles of versican in cancer biology--tumorigenesis, progression and metastasis.* Histol Histopathol, 2013. **28**(6): p. 701-13.
180. Fujii, K., et al., *Versican upregulation in Sézary cells alters growth, motility and resistance to chemotherapy.* Leukemia, 2015. **29**(10): p. 2024-32.
181. Emmerich, P., et al., *VCAN accumulation and proteolysis as predictors of T lymphocyte-excluded and permissive tumor microenvironments.* Journal of Clinical Oncology, 2020. **38**(15_suppl): p. 3127-3127.
182. Han, C.Y., et al., *Adipocyte-Derived Versican and Macrophage-Derived Biglycan Control Adipose Tissue Inflammation in Obesity.* Cell Rep, 2020. **31**(13): p. 107818.
183. Hattori, N., et al., *Pericellular versican regulates the fibroblast-myofibroblast transition: a role for ADAMTS5 protease-mediated proteolysis.* J Biol Chem, 2011. **286**(39): p. 34298-310.
184. Foulcer, S.J., A.J. Day, and S.S. Apte, *Isolation and purification of versican and analysis of versican proteolysis.* Methods Mol Biol, 2015. **1229**: p. 587-604.
185. Waight, J.D., et al., *Myeloid-derived suppressor cell development is regulated by a STAT/IRF-8 axis.* J Clin Invest, 2013. **123**(10): p. 4464-78.
186. Wen, Z., et al., *Expression of NrasQ61R and MYC transgene in germinal center B cells induces a highly malignant multiple myeloma in mice.* Blood, 2021. **137**(1): p. 61-74.
187. Schiavoni, G., L. Gabriele, and F. Mattei, *The dual role of IRF8 in cancer immunosurveillance.* Oncoimmunology, 2013. **2**(8): p. e25476.
188. Fuertes Marraco, S.A., et al., *Novel murine dendritic cell lines: a powerful auxiliary tool for dendritic cell research.* Front Immunol, 2012. **3**: p. 331.
189. Conejo-Garcia, J.R., M.R. Rutkowski, and J.R. Cubillos-Ruiz, *State-of-the-art of regulatory dendritic cells in cancer.* Pharmacol Ther, 2016. **164**: p. 97-104.
190. Morante-Palacios, O., et al., *Tolerogenic Dendritic Cells in Autoimmunity and Inflammatory Diseases.* Trends Immunol, 2021. **42**(1): p. 59-75.
191. Suryawanshi, A., et al., *Wnt Signaling Cascade in Dendritic Cells and Regulation of Anti-tumor Immunity.* Front Immunol, 2020. **11**: p. 122.
192. Manicassamy, S., et al., *Activation of beta-catenin in dendritic cells regulates immunity versus tolerance in the intestine.* Science, 2010. **329**(5993): p. 849-53.
193. Zhang, M., et al., *CCL7 recruits cDC1 to promote antitumor immunity and facilitate checkpoint immunotherapy to non-small cell lung cancer.* Nat Commun, 2020. **11**(1): p. 6119.
194. Mirlekar, B. and Y. Pylayeva-Gupta, *IL-12 Family Cytokines in Cancer and Immunotherapy.* Cancers (Basel), 2021. **13**(2).
195. Hewitt, S.L., et al., *Durable anticancer immunity from intratumoral administration of IL-23, IL-36gamma, and OX40L mRNAs.* Sci Transl Med, 2019. **11**(477).
196. Lopez-Yglesias, A.H., et al., *T-bet-dependent ILC1- and NK cell-derived IFN-gamma mediates cDC1-dependent host resistance against Toxoplasma gondii.* PLoS Pathog, 2021. **17**(1): p. e1008299.
197. Kingston, D., et al., *The concerted action of GM-CSF and Flt3-ligand on in vivo dendritic cell homeostasis.* Blood, 2009. **114**(4): p. 835-43.
198. Greter, M., et al., *GM-CSF controls nonlymphoid tissue dendritic cell homeostasis but is dispensable for the differentiation of inflammatory dendritic cells.* Immunity, 2012. **36**(6): p. 1031-46.

199. Medina, B.D., et al., *Oncogenic kinase inhibition limits Batf3-dependent dendritic cell development and antitumor immunity.* J Exp Med, 2019. **216**(6): p. 1359-1376.
200. Victorino, F., et al., *Tissue-Resident NK Cells Mediate Ischemic Kidney Injury and Are Not Depleted by Anti-Asialo-GM1 Antibody.* J Immunol, 2015. **195**(10): p. 4973-85.
201. Netherby, C.S., et al., *The Granulocyte Progenitor Stage Is a Key Target of IRF8-Mediated Regulation of Myeloid-Derived Suppressor Cell Production.* J Immunol, 2017. **198**(10): p. 4129-4139.
202. Spranger, S., et al., *Tumor and Host Factors Controlling Antitumor Immunity and Efficacy of Cancer Immunotherapy.* Adv Immunol, 2016. **130**: p. 75-93.
203. Corrales, L., et al., *Direct Activation of STING in the Tumor Microenvironment Leads to Potent and Systemic Tumor Regression and Immunity.* Cell Rep, 2015. **11**(7): p. 1018-30.
204. Jarnicki, A.G., et al., *Suppression of antitumor immunity by IL-10 and TGF-beta-producing T cells infiltrating the growing tumor: influence of tumor environment on the induction of CD4+ and CD8+ regulatory T cells.* J Immunol, 2006. **177**(2): p. 896-904.
205. Lu, C., et al., *Type I interferon suppresses tumor growth through activating the STAT3-granzyme B pathway in tumor-infiltrating cytotoxic T lymphocytes.* J Immunother Cancer, 2019. **7**(1): p. 157.
206. Woo, S.R., et al., *STING-dependent cytosolic DNA sensing mediates innate immune recognition of immunogenic tumors.* Immunity, 2014. **41**(5): p. 830-42.
207. Corrales, L. and T.F. Gajewski, *Molecular Pathways: Targeting the Stimulator of Interferon Genes (STING) in the Immunotherapy of Cancer.* Clin Cancer Res, 2015. **21**(21): p. 4774-9.
208. Sharma, P. and J.P. Allison, *Dissecting the mechanisms of immune checkpoint therapy.* Nat Rev Immunol, 2020. **20**(2): p. 75-76.
209. Waldman, A.D., J.M. Fritz, and M.J. Lenardo, *A guide to cancer immunotherapy: from T cell basic science to clinical practice.* Nat Rev Immunol, 2020. **20**(11): p. 651-668.
210. Havel, J.J., D. Chowell, and T.A. Chan, *The evolving landscape of biomarkers for checkpoint inhibitor immunotherapy.* Nat Rev Cancer, 2019. **19**(3): p. 133-150.
211. Butt, A.Q. and K.H. Mills, *Immunosuppressive networks and checkpoints controlling antitumor immunity and their blockade in the development of cancer immunotherapeutics and vaccines.* Oncogene, 2014. **33**(38): p. 4623-31.
212. Chow, A., B.D. Brown, and M. Merad, *Studying the mononuclear phagocyte system in the molecular age.* Nat Rev Immunol, 2011. **11**(11): p. 788-98.
213. Chen, D.S. and I. Mellman, *Oncology meets immunology: the cancer-immunity cycle.* Immunity, 2013. **39**(1): p. 1-10.
214. Chen, D.S. and I. Mellman, *Elements of cancer immunity and the cancer-immune set point.* Nature, 2017. **541**(7637): p. 321-330.
215. Le Naour, J., et al., *Trial watch: STING agonists in cancer therapy.* Oncoimmunology, 2020. **9**(1): p. 1777624.
216. Flood, B.A., et al., *STING pathway agonism as a cancer therapeutic.* Immunol Rev, 2019. **290**(1): p. 24-38.